REFACTORING THE RETINA WITH CONNECTOMICS

by

James Scott Lauritzen

A dissertation submitted to the faculty of
The University of Utah
in partial fulfillment of the requirements for the degree of

Doctor of Philosophy

in

Neuroscience

Interdepartmental Program in Neuroscience

The University of Utah

May 2013

The University of Utah Graduate School

STATEMENT OF DISSERTATION APPROVAL

The dissertation of **James Scott Lauritzen**

has been approved by the following supervisory committee members:

Robert E. Marc	, Chair	**5/15/2012** Date Approved
John A. White	, Member	**5/15/2012** Date Approved
David Krizaj	, Member	**5/15/2012** Date Approved
F. Edward Dudek	, Member	**5/15/2012** Date Approved
Bradley E. Greger	, Member	**5/15/2012** Date Approved

and by **Kristen A. Keefe** , Chair of

the Department of **Interdepartmental Program in Neuroscience**

and by Donna M. White, Interim Dean of The Graduate School.

ABSTRACT

It is imperative to obtain a complete network graph of at least one representative retina if we are to fully understand vertebrate vision. Synaptic connectomics endeavors to construct such graphs. Though previously prevented by hardware and software limitations, the creation of customized viewing and analysis software, affordable data storage, and advances in electron imaging platform control now permit connectome assembly and analysis. The optimal strategy for building complete connectomes utilizes automated transmission electron imaging with 2 nm or better resolution, molecular tags for cell identification, open access data volumes for navigation, and annotation with open source tools to build three-dimensional cell libraries, complete network diagrams, and connectivity databases. In a few years, the first retinal connectome analyses reveal that many well-studied cells participate in much richer networks than expected. Collectively, these results impel a refactoring of the inner plexiform layer, while providing proof of concept for connectomics as a game-changing approach for a new era of scientific discovery.

To my parents, Pamela and Charles, my brother, Michael, and my wife, Melanie, without whose undying love, encouragement, and support I would not have accomplished this goal.

TABLE OF CONTENTS

Chapter

LIST OF TABLES

LIST OF FIGURES

CHAPTER 1

INTRODUCTION

Connectomics Discovery

No complete subnetwork is known for any retinal neuron. If we are to obtain a complete understanding of the nervous system, neuroanatomy and electrophysiology must concert their efforts. New electron imaging technologies now have the potential to reconstruct complete networks: connectomes. Reported herein are specific analyses and results conducted in the first retinal connectome ever assembled, Rabbit Retinal Connectome 1 (RC1), demonstrating the power of connectomes as analytical tools for scientific discovery not achievable by other means. In a few short years, connectomics analysis of a canonical sample of retinal tissue has reframed our understanding of network complexity in the retina, and discovered a neural substrate responsible for mesopic vision; a problem that has eluded scientists for over forty years. New cell classes breaking the retinal inner plexiform layer (IPL) stratification rules with unpredicted network motifs emerge, neural substrates analogous to winner-take-all networks in cortex are discovered, and a refactoring of the IPL unfolds. The results force us to reconsider long-held assumptions regarding the neural retina used in model construction and interpretation of physiological data. A discussion of the impact of connectomes on our scientific knowledge of specific retinal neural networks is included, along with proof of concept that connectomics is a necessary (though insufficient) component of the path toward complete understanding of plexiform layers throughout the brain.

Connectomics tools delineate complex, sparse networks by systematically tracing cellular partners across complex synaptic chains (Sporns et al., 2005).

They can also serve a hypothesis testing role. Often, scientists attempt to infer the subnetworks and networks accounting for functional results, and often, they are incorrect despite heroic effort and clever experimental design. This is largely because there are so many possible neural configurations (see Neural Network Complexity Section below) that could generate any specific observable phenomena that is impractical if not impossible to derive from neural behavior alone.

New analyses not possible with previous ultrastructural techniques become manageable with high-resolution connectomics. Any cell can be traced repeatedly, even concurrently, and an event history stored. From any starting point in a canonical volume, a synapse nexus can be traced back to its sources. Concurrently, coordinates (locations) and relational properties (links) are captured for every cell (parent structure) or part (child structure), used for automatically populating statistical tables, and building network graphs, data navigation maps, and three-dimensional renderings. All attributes are stored as queryable databases, all forms of data query tools are enabled, and all data can be shared. Distinct from traditional anatomy, the data collected and analyzed in a connectomics format is fully transparent. Further, synaptic identification can approach 100% with high-resolution automated transmission electron microscope-based (ATEM) connectomics (Anderson et al., 2011a). With traditional single-section imaging, vast numbers of synapses are missed (Marc and Liu, 2000), giving rise to underestimates of even simple motifs such as serial synapses. More importantly, every potential synapse can be flagged, assigned a

certainty or query status, assessed by other analysts, reviewed in its full network context, reimaged goniometrically at higher resolution if necessary, and have its identity finalized (Anderson et al., 2011b; Anderson et al., 2011a). This was never possible with manual TEM, including serial section TEM.

Neural Network Complexity

Retinal and brain networks are so complex that we turn to graph theory (Diestel, 2005; Harary and Palmer, 1973) to gain traction. In this context, cells are represented as vertices, synaptic connections become edges connecting vertices, and the edges can be unidirectional or directional. Thus, we can construct multiedge digraphs (directed graphs) to understand neural networks. The number of possible graphs N_n constructed from n vertices is incredibly large, even with aggressive constraints (Figure 1.1). Even the simplest three-vertex labeled digraph creates $N_3 = 64$ possible networks. The human retina has at least 70 classes of cells (Marc, 2010), the human brain has no fewer than 250 regions ($\approx$ 200 for cortex alone (Van Essen et al., 2011)) and >1000 expected neuronal classes. Topologic complexities such as diverse cell copy numbers and coverages (Reese, 2008), molecular connection types, and synaptic weights exponentially expand this universe of possible networks. Attempting to infer correct neural networks based on physiological response properties alone is not a realistic solution. Indeed, no provable mappings of physiologic transfer functions onto unique graph topologies exist (Aster et al., 2005). Computational modelers have a name for the process of *attempting* to discover network motifs,

it is called the subgraph isomorphism problem (Karp, 1972). There is no current solution to this problem as the answer is either incredibly difficult or impossible to compute. Moreover, definitive proof of a specific network motif's functional role is impossible. Other "-omics" fields, such as genomics and proteomics, suffer the same problem, as the complexity of relational properties quickly becomes unmanageable with any system operating as a multiedge digraph (Wong et al., 2012). The solution lies in obtaining network ground truth (Anderson et al., 2011b), not inference. It is imperative that we reconstruct the proper wiring diagram for representative networks so physiologists and modelers can then correctly parameterize them.

Specific Connectomics Techniques

<u>Connectome Approaches</u>

Connectomics approaches span macroscopic analyses such as the Human Connectome Project (Marcus et al., 2011), other large-scale projects (Sporns et al., 2005; van den Heuvel and Sporns, 2011), and microscopic analyses of synaptic networks in specific tissues (e.g., the vertebrate retina) (Anderson et al., 2011a; Briggman et al., 2011). Conventional TEM fixation and postfixation are optimal for connectomics. Image segmentation with molecular or functional markers can be achieved by registering optical imagery to TEM image fields. Excitation mapping with the channel-permeant organic ion 1-amino-4-guanidobutane (AGB) (Anderson et al., 2011a; Anderson et al., 2009) embeds small-molecule light-mediated response histories into a retinal sample. Briggman

et al. (2011) and Bock et al. (2011) computational aligned optical calcium imaging data onto ultrastructural imagery to pre-identify neuron classes for targeted annotation. TEM-based connectomes could also utilize genetic markers (Gaietta et al., 2002; Hoffmann et al., 2010; Lichtman and Smith, 2008; Shu et al., 2011). Molecular tags used for cell classification in a feature space independent from morphology and connectivity are key components for complete connectomics, and thus far, only ATEM-based schemes are compatible with them (Anderson et al., 2009; Jones et al., 2011; Jones et al., 2003; Marc and Liu, 2000; Micheva and Bruchez, 2011; Micheva et al., 2010; Micheva and Smith, 2007).

The tissue section used for connectome datasets are obtained either by ablation of a block surface or capturing sections. Ablation methods include in vacuo serial block-face (SBF) sectioning (Briggman and Denk, 2006; Denk and Horstmann, 2004) or ion beam milling (Knott et al., 2008), then scanning electron microscopy (SEM) or scanning transmission electron microscopy (STEM) imaging measures backscattered secondary electrons. Ablation methods obligatorily have limited depth profiles and require very thin sections for tracking. In contrast, manually captured ultramicrotomy sections (Anderson et al., 2009; Bourne and Harris, 2011) onto electron-transparent film supports followed by conventional staining and ATEM imaging (Anderson et al., 2009) produces primary electron projection images through the section thickness, optimally at 50–70 nm. Manual section capture obligatorily requires tile registration on a large scale, but that problem is solved (Tasdizen et al., 2010). Finally, automated

sectioning onto electron-opaque films has been developed for STEM imaging (Kleinfeld et al., 2011), but the required hardware is rare and expensive.

<u>Wide Analyses and Deep Analyses</u>

In the RC1 volume, assembled with manually captured ultramicrotomy sections captured with a high-throughput automated TEM (ATEM), we searched for synaptic chains spanning ON and OFF cone bipolar cell networks, and rod and cone bipolar cell networks, using Viking annotation and Viz network analysis (Anderson et al., 2009). We hereafter refere to ON and OFF cone bipolar cells as CBbs and CBas, respectively, to adhere to the MacNeil et al. (2004) rabbit bipolar cell classification scheme described in more detail in Chapter 1. We utilized combinations of *wide analysis* (querying many copies of a cell class for shared features) and *deep analysis* (mapping a connection cohort of a cell to saturation) on patches of bipolar cells to define their connections with amacrine cells. All cells were classified in independent molecular, morphologic, and connectivity feature spaces as detailed in the methods and previous publications (Anderson et al., 2011b; Anderson et al., 2011a; Anderson et al., 2009). This combination of deep and wide connectomics of the rod BC cohort revealed incredibly rich networks and subnetworks with direct functional significance. Moreover, the topologies underlying these functional motifs force us to reconsider legacy functional schema.

<u>Network Concatenation</u>

We systematically concatenate several independently discovered subnetworks into larger networks to establish the interconnectivity of specialized processing streams throughout the retina. For any question of interest, we start with the cell classes suspected to contribute, then annotate the immediately connected subnetworks. Often serendipidously, the subnetworks collide which we concatenate to create increasingly larger networks.

Specific Connectomics Discoveries

Have connectomics advanced our knowledge base? The oversimplicity of many long-held beliefs is now crystallizing with the ability to better scrutinize neural connectivity in the retina. Many key findings are summarized here. We use the following conventions to represent synaptic chains and their associated gains: >, high-gain sign-conserving (e.g., mediated by ionotropic glutamate receptors); $>_m$, high-gain sign-inverting (mediated by mGluR6 glutamate receptors); $>_i$, low-gain sign-inverting (ionotropic glycine and GABA receptors). High-gain excitatory transfers are assigned a gain of n and low-gain inhibitory transfers are assigned a separate gain of p, based on evidence that most excitatory gains are >>1 (Copenhagen et al., 1990; Yang and Wu, 2004), whereas inhibitory gains are fractional (Maltenfort et al., 1998; Wu, 1991). The latter is not necessarily true in all cases and requires further investigation, which further justifies treating classical ionotropic inhibition as a separate parameter. Coupling is also a separate parameter, here treated as ~1 for notational

simplicity, although it is certainly attenuating. Gains achieved via synaptic chains are multiplicative. For instance, a chain of cone $>_m$ CBb > AC $>_i$ GC has a total gain of n^2p and a net sign-conserving polarity (i.e., the chain copies the cone polarity into the target GC).

Cone Bipolar Cell Cross-Inhibition Motifs

Crossover inhibition is currently a high-profile topic in retinal electrophysiology. The key concept is that polarity-matched ON $\rightarrow$ OFF and OFF $\rightarrow$ ON crossover pathways, dominated by GAC signaling, fine tune signaling throughout the retina (Hsueh et al., 2008; Werblin, 2010, 2011). The exact functional roles of crossover are currently debated, with conflicting evidence for rectification compensation (Werblin, 2010) versus rectification enhancement (Liang and Freed, 2010). Essentially, diffusely-stratified GACs are believed to cross the ON-OFF border to mediate, for example, [CBb > GAC $>_i$ OFF GC] chains where the GAC input provides an appropriate OFF polarity via an anionic current to compensate for AMPA receptor rectification. Importantly (Werblin, 2010), refactoring of bipolar cell outputs in the inner plexiform layer shows that CBb axonal ribbons provide an ON $\rightarrow$ OFF crossover topology to monostratified GACs in the OFF layer directly. Moreover, there are also [CBb > γAC $>_i$ OFF GC] chains in the OFF layer (Lauritzen et al., 2013). Because the latter are deeply embedded in both feedback and feedforward motifs, they have not yet been pharmacologically isolated. Additionally, none of the CBb axonal output crossover elements involve the A_{II} AC. Indeed, the bulk of the synaptic

output of A_{II} ACs is onto CBa cells of all classes, which means the net gain from the [A_{II} >$_i$ CBa > OFF GC] chain is np and likely rectifying. There is extensive direct A_{II} synaptic drive to α- and δ- OFF GCs, which are both strongly rectified GCs, but the net gain will only be p counterbalanced by even more numerous CBa2 drive with gain of np. Therefore, the A_{II} AC is not likely a major source of rectification correction for the OFF layer. Other GACs likely are.

Many of the specific network motifs discovered tell us about the capacity of individual cells, and therefore the spatial extent of an individual cell and cell class's influence (i.e., one GAC can inject ON-OFF signals that spread at least up to 200-250 um away).

Photopic-Scotopic Cross-Inhibition Motifs

Crossover networks between rod and cone pathways have not been discovered despite decades of electron microscopy. Indeed visualizing retinal crossover networks (Molnar et al., 2009; Werblin, 2010) and, in particular, those inhibitory connections between demonstrably dissimilar channels, requires wide-scale 3D ultrastructural tracing at synaptic resolution.

We chose to unravel rod-cone pathway interactions by starting at individual rod BCs and mining their contacts outward across wide fields of the inner plexiform layer. We mined RC1 for synaptic chains spanning rod and cone BC networks. We performed *wide analysis* (querying many copies of a cell class for shared features) on 104 adjacent rod bipolar cells, and *deep analysis* (mapping a connection cohort of a cell to saturation) on a central patch of 5 rod

BCs to define all their connections with amacrine cells, including those that connect to surrounding cone bipolar cell networks. All cells were classified in independent molecular, morphological, and network feature spaces as detailed in the methods and previous publications (Anderson et al., 2011a; Lauritzen et al., 2013).

A major attribute of mammalian vision is rapid switching between rod- and cone-dominated operations, especially during extended crepuscular periods where both rods and cones operate. Psychophysical analyses, including over three decades of work by Ulf and Bjorn Stabell, reveal powerful rod–cone interactions, including mutually suppressive regimes (Brill, 1990; Buck, 2004; Frumkes and Eysteinsson, 1988; Goldberg et al., 1983; Lange et al., 1997; Stabell and Stabell, 1998; Thomas and Buck, 2006; Trezona, 1970, 1973), but the mechanisms have remained unknown. The notion that horizontal cells mediate such interactions is complicated by the lack of evidence for axonal signaling in mammalian horizontal cells. Connectomics reveals at least seven unique instances of high-gain mediated cone suppression of rod signaling. Deep and wide connectomics of the rod BC cohort reveal that every rod BC gets direct inhibitory input from CBb-driven ON γACs and GACs and that ~25% of AC synapses on rod BC terminals come from ON cone ACs with a cone $\rightarrow$ rod suppression of n^2p. Further, both A_I and A_{II} ACs receive extensive cone pathway inhibition. A_I ACs receive inhibition (~100 inhibitory synapses/cell) on their proximal dendrites in the OFF layer via selective CBa > γAC >$_i$ A_I AC motifs, and A_{II} ACs receive cone-driven inhibition at every level of the inner plexiform layer,
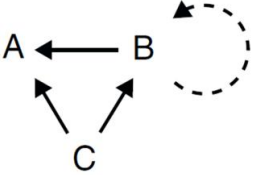
including a highly selective inhibitory input from ON GACs that target rod BC, A_{II} AC, and A_I AC. Three pathways mediate rod suppression of cone signaling. Certain wide-field γACs (different from the cone → rod suppressors) collect sparse rod BC inputs and are both presynaptic and postsynaptic to CBb cells, forming a selective [RB > γAC $>_i$ CBb] suppression chain with a rod → cone suppression of n^2p. However, the most powerful motif is the [rod $>_m$ RB > A_{II} ACs::CBb > γAC $>_i$ CBb] chain with a rod → cone suppression of n^3p. Because A_{II} cells are narrow-field elements (<100 μm), whereas the γACs are wide-field (>250 μm), each patch of rods can inhibit a vast field of surrounding cones.

Proof of Concept and Generalization

The following three chapters elucidate the ability of connectomics to unravel the daunting neural networks of the retina, and illustrate how results obtained in the past three years are already refactoring our legacy of retinal structure-function relationships. Specific cell-class relationships are emerging to clarify source-target distributions, the multiplexing capacity of individual cells is now more clear, and elusive network substrates responsible for psychophysical phenomena unexplainable for over a century are becoming accessible. These results not only solve previously unanswerable questions, but advance new sets of testable hypotheses in the process. Finally, the lessons learned in the IPL of the retina will yield important insight into the structure-function relationships of plexiform layers throughout the brain. With the technological scaffolding now in

place for connectomics analysis of neural architectures everywhere in the central

nervous system, we can embark on a new era of scientific discovery.

Figure 1.1. Graph enumeration for networks. A three vertex (n = 3) network (ABC) can form different numbers of motifs if the connections are undirected U(n), directed D(n) (solid arrows), or directed with re-entrant loops R(n) (dotted arrows). Networks can be limited to vertex clusters of size k [C(n,k)]. Directed (D) and combinatoric (C) networks in retina (n = 70), brain regions (n = 250), and brain neurons (n = 1000) were calculated using the Wolfram Alpha engine.

$$U(n) = 2^{(n(n-1))/2}$$

$$D(n) = 2^{n(n-1)}$$

$$R(n) = 2^n D(n)$$

$$C(n,k) = \binom{n}{k}$$

Retina $D(70) = 9 \times 10^{1453}$

$$C(70,10) = 4 \times 10^{11}$$

Brain areas $D(250) = 1 \times 10^{18739}$

$$C(250, 10) = 2 \times 10^{17}$$

Brain neurons $D(1000) = 9 \times 10^{300728}$

$$C(1000, 10) = 2 \times 10^{23}$$

Current Opinion in Neurobiology

References

Anderson, J.R., Grimm, B., Mohammed, S., Jones, B.W., Spaltenstein, J., Koshevoy, P., Tasdizen, T., Whitaker, R., Marc, R.E. 2011b. The Viking Viewer: Scalable multiuser annotation and summarization of large connectomics datasets. J Microscopy 241:13-28.

Anderson, J.R., Jones, B.W., Watt, C.B., Shaw, M.V., Yang, J., DeMill, D., Lauritzen, J.S., Lin, Y., Rapp, K., Mastronarde, D., Koshevoy, P., Grimm, B., Tasdizen, T., Whitaker, R., Marc, R.E., 2011a. Exploring the retinal connectome. Mol Vision 17:355-379.

Anderson, J.R., Jones, B.W., Yang, J.-H., Shaw, M.V., Watt, C.B., Koshevoy, P., Spaltenstein, J., Jurrus, E., Kannan, U.V., Whitaker, R., Mastronarde, D., Tasdizen, T., Marc, R.E. 2009. A computational framework for ultrastructural mapping of neural circuitry. PLoS Biol 7:e1000074.

Aster, R., Borchers, B., Thurber, C. 2005. Parameter Estimation and Inverse Problems. Academic Press, NY.

Bock, D.D., Lee, W.-C.A., Kerlin, A.M., Andermann, M.L., Hood, G., Wetzel, A.W., Yurgenson, S., Soucy, E.R., Kim, H.S., Reid, R.C. 2011. Network anatomy and in vivo physiology of visual cortical neurons. Nature 471:177-182.

Bourne, J.N., Harris, K.M. 2011. Nanoscale analysis of structural synaptic plasticity. Current Opinion in Neurobiology 22:1-11.

Briggman, K.L., Denk, W. 2006. Towards neural circuit reconstruction with volume electron microscopy techniques. Current Opinion in Neurobiology 16:562-570.

Briggman, K.L., Helmstaedter, M., Denk, W. 2011. Wiring specificity in the direction-selectivity circuit of the retina. Nature 471:138-188.

Brill, M.H. 1990. Mesopic color matching: some theoretical issues. J Opt Soc Am A 7:2048-2051.

Buck, S.L. 2004. Rod-cone interactions in human vision, in: Chalupa, L.M., Werner, J. (Eds.), Visual Neurosciences. MIT Press, Cambridge, MA, pp. 863-878.

Copenhagen, D.R., Hemilä, S., Reuter, T. 1990. Signal transmission through the dark-adapted retina of the toad (Bufo marinus). Gain, convergence, and signal/noise. J Gen Physiol 95:717-732.

Denk, W., Horstmann, H. 2004. Serial block-face scanning electron microscopy to recon-struct three-dimensional tissue nanostructure. PLoS Biol 2:e329

Diestel, R. 2005. Graph Theory, 3 ed. Springer-Verlag, Heidelberg.

Frumkes, T.E., Eysteinsson, T. 1988. The cellular basis for suppressive rod-cone interaction. Vis Neurosci 1:263-273.

Gaietta, G., Deerinck, T.J., Adams, S.R., Bouwer, J., Tour, O., Laird, D.W., Sosinsky, G.E., Tsien, R.Y., Ellisman, M.H. 2002. Multicolor and electron microscopic imaging of connexin trafficking. Science 296:503-507.

Goldberg, S.H., Frumkes, T.E., Nygaard, R.W. 1983. Inhibitory influence of unstimulated rods in the human retina: evidence provided by examining cone flicker. Science 221:180-182.

Harary, F., Palmer, E.M. 1973. Graphical Enumeration. Academic Press, New York.

Hoffmann, C., Gaietta, G., Zürn, A., Adams, S.R., Terrillon, S., Ellisman, M.H., Tsien, R.Y., Lohse, M.J. 2010. Fluorescent labeling of tetracysteine-tagged proteins in intact cells. Nat Protoc 5:1666-1677.

Hsueh, H.A., Molnar, A., FS., W. 2008. Amacrine-to-amacrine cell inhibition in the rabbit retina. J Neurophysiol 100:2077-2088.

Jones, B.W., Kondo, M., Terasaki, H., Watt, C.B., Rapp, K., Anderson, J., Lin, Y., Shaw, M.V., Yang, J.-H., Marc, R.E. 2011. Retinal degenerative disease and remodeling in a large eye model. J Comp Neurol 519:2713-2733.

Jones, B.W., Watt, C.B., Frederick, J.M., Baehr, W., Chen, C.K., Levine, E.M., Milam, A.H., LaVail, M.M., Marc, R.E. 2003. Retinal remodeling triggered by photoreceptor degenerations. Journal of Comparative Neurology 464:1-16.

Karp, R.M., 1972. Reducibility Among Combinatorial Problems, in: Miller, R.E., Thatcher, J.W. (Eds.), Complexity of Computer Computations. Plenum, New York, pp. 85–103.

Kleinfeld, D., Bharioke, A., Blinder, P., Bock, D.D., Briggman, K.L., Chklovskii, D.B., Denk, W., Helmstaedter, M., Kaufhold, J.P., Lee, W.C., Meyer, H.S., Micheva, K.D., Oberlaender, M., Prohaska, S., Reid, R.C., Smith, S.J., Takemura, S., Tsai, P.S., Sakmann, B. 2011. Large-Scale Automated Histology in the Pursuit of Connectomes. J Neurosci 31:16125-16138.

Knott, G., Marchman, H., Wall, D., Lich, B. 2008. Serial section scanning electron microscopy of adult brain tissue using focused ion beam milling. J Neurosci 28:2959-2964.

Lange, G., Denny, N., Frumkes, T.E. 1997. Suppressive rod-cone interactions: evidence for separate retinal (temporal) and extraretinal (spatial) mechanisms in achromatic vision. J Opt Soc Am A Opt Image Sci Vis 14:2487-2498.

Lauritzen, J.S., Watt, C.B., Anderson, J.R., Jones, B.W., Marc, R.E. 2013. ON Cone Bipolar Cell Axonal Ribbons in the OFF Inner Plexiform Layer of the Rabbit Retina. J Comp Neurol 521:977-1201.

Liang, Z., Freed, M.A. 2010. The ON pathway rectifies the OFF pathway of the mammalian retina. J Neurosci 30:553-543.

Lichtman, J.W., Smith, S.J. 2008. Seeing circuits assemble. Neuron 60:441-448.

MacNeil, M.A., Heussy, J.K., Dacheux, R.F., Raviola, E., Masland, R.H. 2004. The population of bipolar cells in the rabbit retina. Journal of Comparative Neurology 472:73-86.

Maltenfort, M.G., Heckman, C.J., Rymer, W.Z. 1998. Decorrelating actions of Renshaw interneurons on the firing of spinal motoneurons within a motor nucleus: a simulation study. J Neurophysiol 80:309-323.

Marc, R.E. 2010. Synaptic Organization of the Retina, in: Levin, L.A., Nilsson, S.F.E., Ver Hoeve, J., Wu, S.M., Kaufman, P.L., Alm, A. (Eds.), Adler's Physiology of the Eye. Elsevier, pp. 443-458.

Marc, R.E., Liu, W. 2000. Fundamental GABAergic amacrine cell circuitries in the retina: nested feedback, concatenated inhibition, and axosomatic synapses. Journal of Comparative Neurology 425:560-582.

Marcus, D.S., Harwell, J., Olsen, T., Hodge, M., Glasser, M.F., Prior, F., Jenkinson, M., Laumann, T., Curtiss, S.W., Van Essen, D.C. 2011. Informatics and Data Mining Tools and Strategies for the Human Connectome Project. Front Neuroinform 5:4.

Micheva, K.D., Bruchez, M.P. 2011. The gain in brain: novel imaging techniques and multiplexed proteomic imaging of brain tissue ultrastructure. Current Opinion in Neurobiology 22(1):94-100.

Micheva, K.D., Busse, B., Weiler, N.C., O'Rourke, N., Smith, S.J. 2010. Single-synapse analysis of a diverse synapse population: proteomic imaging methods and markers. Neuron 68:639-653.

Micheva, K.D., Smith, S.J. 2007. Array Tomography: A New Tool for Imaging the Molecular Architecture and Ultrastructure of Neural Circuits. Neuron 55:25-36.

Molnar, A., Hain-Ann, H., Roska, B., Werblin, F.S. 2009. Crossover inhibition in the retina: circuitry that compensates for nonlinear rectifying synaptic transmission. J Comput Neurosci 27:569-590.

Reese, B. 2008. Mosaics, tiling and coverage by retinal neurons, in: Masland, R.H., Albright, T. (Eds.), The Senses: A comprehensive reference. Vision. Elsevier, Amsterdam.

Shu, X., Lev-Ram, V., Deerinck, T.J., Qi, Y., Ramko, E.B., Davidson, M.W., Jin, Y., Ellisman, M.H., Tsien, R.Y. 2011. A genetically encoded tag for correlated light and electron microscopy of intact cells, tissues, and organisms. PLoS Biol 9:e1001041.

Sporns, O., Tononi, G., K√∂tter, R. 2005. The Human Connectome: A Structural Description of the Human Brain. PLoS Computational Biology 1:e42.

Stabell, B., Stabell, U. 1998. Chromatic rod-cone interaction during dark adaptation. J Opt Soc Am A Opt Image Sci Vis 15:2809-2815.

Tasdizen, T., Koshevoy, P., Grimm, B., Anderson, J.R., Jones, B.W., Whitaker, R., Marc, R.E. 2010. Automatic mosaicking and volume assembly for high-throughput serial-section transmission electron microscopy J Neuroscience Methods 193:132-144.

Thomas, L.P., Buck, S.L. 2006. Foveal and extra-foveal influences on rod hue biases. Vis Neurosci 23:539-542.

Trezona, P.W. 1970. Rod participation in the 'blue' mechanism and its effect on colour matching. Vision Res 10:317-332.

Trezona, P.W. 1973. The tetrachromatic colour match as a colorimetric technique. Vision Res:13, 9-25.

Van den Heuvel, M.P., Sporns, O. 2011. Rich-Club Organization of the Human Connectome. The Journal of Neuroscience 31:15775-15786.

Van Essen, D.C., Glasser, M.F., Dierker, D.L., Harwell, J., Coalson, T. 2011. Parcellations and Hemispheric Asymmetries of Human Cerebral Cortex Analyzed on Surface-Based Atlases. Cerebral Cortex 22(10):2241-2262.

Werblin, F.S. 2010. Six different roles for crossover inhibition in the retina: correcting the nonlinearities of synaptic transmission. Vis Neurosci 27:1-8.

Werblin, F.S. 2011. The retinal hypercircuit: a repeating synaptic interactive motif underlying visual function. J Physiol 589:3691-3702.

Wong, E., Baur, B., Quader, S., Huang, C.-H. 2012. Biological network motif detection: principles and practice. Briefings in Bioinformatics 13(2):202-215.

Wu, S.M. 1991. Input-output relations of the feedback synapse between horizontal cells and cones in the tiger salamander retina. J Neurophysiol 65:1197-1206.

Yang, X.L., Wu, S.M. 2004. Signal transmission from cones to amacrine cells in dark- and light-adapted tiger salamander retina. Brain Res 1029:155-161.

CHAPTER 2

ON CONE BIPOLAR CELL AXONAL SYNAPSES

IN THE OFF INNER PLEXIFORM LAYER

Abstract

Analysis of the rabbit retinal connectome RC1 (Figure 2.1) reveals that the division between the ON and OFF inner plexiform layer (IPL) is not structurally absolute. ON cone bipolar cells (ON CBCs) make noncanonical axonal synapses onto specific targets and receive amacrine cell synapses in the nominal OFF layer, creating novel motifs, including inhibitory crossover networks. Automated transmission electron microscope (ATEM) imaging, molecular tagging, tracing, and rendering of ≈ 400 bipolar cells reveals axonal ribbons in 36% of ON CBCs, throughout the OFF IPL. The targets include GABA-positive amacrine cells (γACs), glycine-positive amacrine cells (GACs), and ganglion cells. Most ON CBC axonal contacts target GACs driven by OFF cone bipolar cells (OFF CBCs), forming new architectures for generating ON-OFF amacrine cells. Many of these ON-OFF GACs target ON CBC axons, ON γACs, and/or ON-OFF ganglion cells, representing widespread mechanisms for OFF to ON crossover inhibition. Other targets include OFF γACs presynaptic to ON CBCs, forming γAC-mediated crossover motifs. ON cone bipolar cell axonal ribbons drive bistratified ON-OFF ganglion cells in the OFF layer and provide ON drive to polarity-appropriate targets such as bistratified diving ganglion cells (bsdGCs). The targeting precision of ON CBC axonal synapses shows that this drive incidence is necessarily a joint distribution of cone bipolar cell axonal frequency and target cell trajectories through a given volume of the OFF layer. Such joint distribution sampling is likely common when targets are sparser than sources and when sources are coupled, as are ON CBCs.

Introduction

Structure-function relationships have been explored in the retina for over a century. Ramón y Cajal observed differential bipolar cell stratification in the inner plexiform layer (IPL) and suspected direct structure-function correlations (Ramón y Cajal, 1892). Indeed, it has long since been established that ON and OFF channels occupy distinct domains within the mammalian IPL, with OFF cells that depolarize to light decrements stratified in the distal 40% of the IPL and ON cells that depolarize to light increments stratified in the proximal 60% of the IPL (Famiglietti et al., 1977; Famiglietti and Kolb, 1976; MacNeil et al., 2004; Wässle et al., 2009; Werblin and Dowling, 1969). Nevertheless, examples of nominal cone bipolar cells breaking the mammalian IPL stratification rules were recently reported (Anderson et al., 2011a; Dumitrescu et al., 2009; Hoshi et al., 2009). Type 6, and possibly type 7 or 8, ON cone bipolar cells in mouse, and calbindin-positive layer 4/5 stratifying ON cone bipolar cells in rabbit, have been demonstrated targeting tyrosine hydrdoxylase-positive cells (TH1s), M1-type intrinsically photosensitive retinal ganglion cells (ipRGCs), and bsdGCs in stratum one of the IPL (Dumitrescu et al., 2009; Hoshi et al., 2009), thus representing an accessory ON input to the OFF IPL layers. These ribbon contacts appear in two varieties: *en passant*, occurring inside the main bipolar cell descending axons, and branched, occurring from small processes that branch off the main descending axon (Figure 2.2). (Anderson et al., 2011a) demonstrated by ATEM that presynaptic ribbon and postsynaptic conventional

synaptic ultrastructures existed at axonal ribbon locations, but characterization of their cognate networks was incomplete.

Indirect evidence exists to suspect that different ON cone bipolar cell types might communicate in the OFF IPL. First, in previous confocal imaging studies (Hoshi et al., 2009), only 23% of bsdGCs were apposed to calbindin positive bipolar cells, but most bsdGC spines were apposed to ribeye puncta. This indicates the remaining ribbons must be associated with other BC types. Also, many nonmammalian bipolar cell classes are multistratified, with axonal outputs in both the OFF and ON sublayers (Kolb, 1982; Pang et al., 2004; Ramon y Cajal, 1892; Scholes, 1975; Scholes and Morris, 1973; Sherry and Yazulla, 1993; Wong and Dowling, 2005) Moreover, infrequent reports of mammalian bistratified bipolar cells exist (Calkins et al., 1998; Famiglietti, 1981; Jeon and Masland, 1995; Kolb et al., 1990; Kolb et al., 1992; Linberg et al., 1996; Mariani, 1982; McGuire et al., 1984). These results impelled us to comprehensively classify ON cone bipolar cells that synapse in the OFF sublayer of the IPL.

In addition to the previously identified axonal ribbon targets, unknown targets with distinctive morphologies and ultrastructural elements were observed in retinal connectome RC1 (Anderson et al., 2011a). This strongly suggested additional cell types as targets. Axonal cisterns associated with postsynaptic densities were also discovered in the axons of ON cone bipolar cells (Anderson et al., 2011a), and are thus possible contributors to accessory ON networks. Sparse reports of rod bipolar cell axonal ribbons exist, implicating them as

candidates for providing the ON input to ipRGCs, yet we demonstrate that rod bipolar cell axonal ribbons are not spatially coincident with ipRGCs and so cannot be responsible for ipRGC ON drive.

Electrophysiology with pharmacological blockade has revealed glycinergic crosstalk between ON and OFF channels at every synaptic tier in the retina, referred to as crossover inhibition (Chavez and Diamond, 2008; Chen et al., 2011; Liang and Freed, 2010; Manookin et al., 2008; Molnar et al., 2009; Roska et al., 2006; Werblin, 2010). Multistratified GACs are implicated as the source, yet the network topologies responsible remain speculative. Crossover inhibition has been posited to achieve a range of functions, including fidelity restoration of photic drive distorted by glutamate synapse nonlinearities, which would otherwise constrain OFF channels to negative contrast processing (Liang and Freed, 2010; Molnar et al., 2009; Werblin, 2010). Given that some of the targets of axonal ribbon synapses are GACs, ON-OFF crossover is one possible function of this accessory input. We show that crossover inhibition can definitely arise from accessory ON bipolar cell networks.

γACs mediate feedback, nested feedback, and feedforward networks throughout the retina, yet the reasons for the great diversity of types (wide-field, narrow-field, mono-, and multistratified) remain a mystery (Marc and Liu, 2000; Wagner and Wagner, 1988). We show examples of wide-field, OFF layer, monostratified γAC processes postsynaptic to ON cone bipolar cell axonal ribbons and presynaptic to both ON and OFF cone bipolar cells, arguing for the existence of γAC-mediated within- and cross channel inhibition in addition to

GAC-mediated within- and crosschannel inhibition. Many instances of GAC-mediatedand γAC-mediated crossover inhibition motifs have been identified in RC1 that do not involve axonal ribbons (data not shown), but that will be the subject of future papers.

In summary, ON cone bipolar cells participate in accessory ON input throughout the OFF sublayer of IPL, targeting not only the previously characterized ipRGCs and bsdGCs, but also newly identified targets. As yet unknown targets exist in RC1, some of which which may be sparse TH1 axonal cell dendrites reported by Dumitrescu et al. (2009) and Hoshi et al. (2009). Additionally, preliminary data reveal that sixty-eight of ninety-seven (70.1%) measured ON cone bipolar cells contain one or more postsynaptic densitites (PSDs) to amacrine cell input in the OFF IPL, and recently discovered axonal cisterns appear in 55 of 113 (48.7%) ON cone bipolar cell axons measured thus far. This specificity enhances the likelihood that accessory ON networks are evolved strategies rather than systemic oddities. Further, such networks are not readily predicted with physiological techniques. ON cone bipolar cell axonal ribbons inject both convergent and divergent ON input to several ganglion cell, GAC, and γAC networks, thus constructing ON-OFF amacrine cells and ganglion cells, and mediating within- and crosschannel inhibition. We show that both monad and dyad versions of axonal ribbons can involve single-ribbon or multiribbon forms. Some rod bipolar cells possess axonal ribbons, but they are very close to their initial axon terminal branches, only contact A_I (A17) and A_{II} ACs, and do not supply the rod signals discovered in ipRGCs. Ultimately,

analysis of axonal ribbons yields a refactoring of the mammalian inner plexiform layer where the OFF layer contains precisely multiplexed ON cone bipolar cell inputs.

Methods

<u>Tissue</u>

Connectome volume RC1 was assembled from a light-adapted female Dutch Belted rabbit (Oregon Rabbitry, OR) after *in vivo* excitation mapping as described in Anderson et al. (2011a) in accord with Institutional Animal Care and Use protocols of the University of Utah, the ARVO Statement for the Use of Animals in Ophthalmic and Visual Research, and the Policies on the Use of Animals and Humans in Neuroscience Research of the Society for Neuroscience.

<u>Computational Molecular Phenotyping (CMP)</u>

Retinal neurons in RC1 were classified by CMP per Marc and Jones (2002) by using an array of small-molecule signatures (4-aminobutyrate [GABA], glycine, L-glutamate, L-glutamine, taurine, and the activity marker 1-amino-4-guanidobutane [AGB]). Briefly, the isolated rabbit eye was hemisected and immersion-fixed overnight in 1% paraformaldehyde, 2.5% glutaraldehyde, 3% sucrose, 0.01% $CaCl_2$, in 0.1 M phosphate buffer, pH 7.4. Tissues were then dehydrated in graded methanols and acetone and embedded in epoxy resin. Tissues were then serial sectioned at 70-90 nm onto 12-spot Teflon-coated slides (Cel Line, Fisher Scientific, Waltham, MA). Antibody exposure and silver

intensification is described below under antibody characterization. Incubation of all antibodies generated against small-molecular targets was performed overnight at room temperature, and visualization was with goat anti-rabbit secondary IgG coated with 1.4 nm gold (Amersham, Arlington Heights, IL) and silverintensified (Kalloniatis and Fletcher, 1993).

Small-Molecular Antibody Characterization

Anti-hapten IgGs from Signature Immunologics (Salt Lake City, UT; Table 2.1) have been extensively characterized in prior publications (Marc et al., 1995; Marc,1999a, b; Marc and Cameron, 2002; Marc and Jones, 2002). Each is an IgG isotype (determined by affinity chromatography and immunoblotting) produced in rabbit hosts immunized with glutaraldehyde-amino acid conjugates to bovine serum albumin (BSA), as described in Marc et al. (1995). Five analysis types were used to characterize the specificity and detectivity of each anti-hapten IgG: 1) dependence on target molecule trapping; 2) immunodot assays against cognate small molecule–protein conjugates; 3) competition assays against free and bis-conjugates of small molecules (Table 2.2); 4) binding curves on quantitative artificial antigen stacks; and 5) cluster analysis (Marc et al., 1995).

RC1 Assembly, Analysis, and Sharing

Bipolar cell networks in the ultrastructural rabbit retinal connectome RC1 (Anderson et al., 2011a) were annotated with the Viking viewer (Anderson et al., 2011b), and explored via three-dimensional rendering and graph visualization of

connectivity (Anderson et al., 2011b). Small molecule signals embedded in RC1 for computational molecular phenotyping (CMP) include 4-aminobutyrate, glycine, L-glutamate, L-glutamine, taurine, and the activity marker 1-amino-4-guanidobutane (AGB). Combined with morphological reconstruction, CMP permits robust bipolar cell classification (Anderson et al., 2011a). RC1 was acquired by ATEM at 2.18 nm resolution and assembled into a volume with the NCRToolset (Anderson et al., 2009). Molecular-ultrastructural registrations were generated with ir-tweak (Anderson et al., 2011a; Anderson et al., 2009; Anderson et al., 2011b). Three-dimensional renderings are built from disk annotations in Vikingplot (Anderson et al., 2011b), allowing rendering of surfaces and characterization of areas and volumes. Table 2.3 lists the synaptic color scheme applied to all renderings. All cells rendered in this paper are publicly available as Google Collada *.dae files via the Connectome Viz application. These can be imported into 3D visualization tools such as Collada or Blender (http://www.blender.org). One defect in converting disk topologies to volumes for rendering of tapered processes sometimes led to somas or varicose neurites with vertically peaked shapes. These anomalies will be repaired in future code sets. Networks were visualized as directed multigraphs with Connectome Viz, and topologies explored with Structure Viz (Anderson et al., 2011b). The RC1 dataset and these associated analytical tools are publically available at connectomes.utah.edu. Quantitative features of connections (numbers of synapses, axon dimensions, etc.) can be queried within these various tools and with Microsoft SQL.

Identification of IPL Layers

The ON-OFF border of the IPL is not absolute and we adopted a structural reference to define the transition between zones dominated by OFF and ON cone bipolar cells. In practice, the axial location of the ON-OFF border was set as the most proximal surface of the A_{II} AC lobule nearest a given bipolar cell. The OFF layer was defined as the region between the most distal GABA+ (γ+) processes and the ON-OFF border. Similarly, the ON layer was defined as the region between the most proximal γ+ processes and the ON-OFF border. For simplicity, we refer to these regions as the ON and OFF layers, corresponding to the older but less descriptive sublamina a and sublamina b, respectively. As in previous work, we define the amacrine cell layer - IPL border as level 0 and the ganglion cell layer - IPL border as level 100 (Marc, 1986).

Cell Classification

All cells were classified using three criteria: molecular signatures, synaptic connectivity, and morphology. Bipolar cells were further subclassified according to their stratifications within the IPL, compared to the rabbit bipolar cell classification scheme outlined by MacNeil et al. (2004). An itemization of the rules required for cell identity follows. Table 2.4 lists cell abbreviations used throughout this manuscript.

Rules for bipolar cells. Their somas reside in the inner nuclear layer (INL) and they are glutamate-positive. Glycine-positive (G+) bipolar cells coupled to A_{II} AC arboreal dendrites via gap junctions and stratified in the proximal 60% of the

IPL were classified as ON cone bipolar cells with their precise level of stratification used to further refine their class memberships (CBb3, CBb3n, CBb3-4, CBb4, CBb5, CBb6, wide-field cone bipolar cell, and rod bipolar cell). Anderson et al. (2011a) showed that quantitative G+ signatures are an absolute discriminator of bipolar cell :: A_{II} AC coupling. Glycine-negative (G-) bipolar cells that stratified in the distal 40% of the IPL and were both presynaptic and postsynaptic to A_{II} AC appendages were defined as OFF cone bipolar cells, with their precise level of stratification used to further refine their class (CBa1, CBa1w, CBa1-2, CBa1-2n). Bipolar cells with G- signatures stratified in the most proximal IPL, presynaptic to A_{II} AC arboreal dendrites, neither postsynaptic nor coupled to them, and presynaptic and postsynaptic to γ+ A_I ACs were classified as rod bipolar cells. There are 104 rod bipolar cells in RC1. These independent classifiers are, collectively, errorless (Anderson et al., 2011a). There are instances where CBa and CBb terminals (never rod bipolar cells) make synaptic contacts lacking classical synaptic ribbons. We call these bipolar cell conventional synapses, and they occur in terminals with numerous ribbons at other sites. One glutamate-positive bipolar cell class (CBa1w) is presynaptic and postsynaptic to A_{II} ACs but lacks ribbons and only makes bipolar cell conventional synapses. These cells are not discussed in this paper as they are not involved with the characterization of axonal synapses.

Rules for amacrine cells. Amacrine cells possessed conventional synapses only (not ribbon synapses) with somas residing in the INL, except for ON starburst amacrine cells whose somas reside in the ganglion cell layer. G

and γ signals further refined their classification as GACs and γACs. Cells with moderate glycine signals, presynaptic lobular appendages in the OFF IPL, and coupled and postsynaptic arboreal dendrites in the ON IPL were defined as A_{II} ACs.

Rules for ganglion cells. Ganglion cells discussed in this paper were glutamate-positive, lacked presynaptic specializations, were never postsynaptic to rod bipolar cells and had somas placed in the GCL or processes that traversed the entire volume. Based on cone bipolar cell input patterns they were further classified as ON, OFF, or ON-OFF. Some classes were also γ+ to differing extents (Marc and Jones, 2002) due to amacrine cell coupling.

Axonal ribbon synapses. Axonal ribbon synapses were defined by presynaptic and postsynaptic form in all cases, with the presynaptic ribbon itself surrounded by a halo or cluster of synaptic vesicles, a dense presynaptic membrane, complete glial withdrawal from the contact site, an evenly spaced synaptic cleft, and an unambiguous postsynaptic density on the target process. Synaptic clefts of synapses sectioned at oblique angles were often obscured, but were recaptured via goniometric re-imaging at higher resolution when necessary. Axonal ribbon synapses were defined as residing distal to the first branch point of each bipolar cell's primary axonal arborization. While this criterion is formally arbitrary, it distinguishes pure axonal ribbons from those in the thin branches between terminal swellings in the axonal arborization.

<u>Image Preparation</u>

As described in our prior papers on connectomics (Anderson et al., 2009), display TEM images in this paper were produced by remapping RC1 volume tiles to gamma 1.3. Optical and TEM overlays used the TEM greyscale brightness combined with the hue, and saturation from the optical image as described in Anderson et al. (2011a). 3D versions and network maps of annotated cells were generated in Vikingplot and Viz applications (Anderson et al., 2011b).

Results

The rabbit retinal connectome volume RC1 is a serial section, 2 nm resolution, 16.4 terabyte TEM image collection assembled into a cylindrical data volume ≈ 0.25 mm wide and ≈ 0.025 mm high spanning the mid-inner nuclear layer through the GC layer (Figure 2.1 A), augmented by molecular channels capping and intercalated every 30 sections through it (Anderson et al., 2011a; Anderson et al., 2009; Anderson et al., 2011b). The CMP channels include aspartate, glutamate, 4-aminobutyrate (GABA), glycine, glutamine, taurine, and AGB as a marker of light-driven activity. These channels permit robust classification of cells (Anderson et al., 2011a; Anderson et al., 2009; Anderson et al., 2011b; Marc and Jones, 2002; Marc et al., 1995) and form an analytic statistic independent of network motif measures. The 0.25 mm wide volume disc represents a mixture of sampling domains, including complete, semicomplete, and partial architectures (Figure 2.1 B). The complete architectures include ≈ 360 bipolar cells and ≈ 50 narrow-field amacrine cells. The semicomplete

architectures include ≈ 40 bipolar cells, ≈ 50 medium to wide-field amacrine cells, and 15 ganglion cells with somas in the volume and dendrites extending beyond it. The partial architectures include large numbers (hundreds) of traversing amacrine cell and ganglion cell dendrites and axonal amacrine cell fields arising from somas outside the volume. This in no way invalidates use of partial architectures. Many of these traversing elements are still identifiable from their molecular signatures and corresponding network motifs. The size of the volume is limited by storage and time. The 2 nm resolution essential for mapping small synapses and the gap junctions that provide diverse coupling topologies in retinal networks and serve as network identity signatures for specific neurons requires 16.5 terabytes (Tb) of raw data and ≈ 50 Tb total, and required 5 months to image. A volume containing complete wide-field amacrine cells would require many years of capture time to produce. Even so, the network motifs that emerge from deep analyses of partial elements such as crossing ganglion cell dendrites still accurately capture the native structure of the source cells, especially since no evidence exists for (and much against) network anisotropy in individual GC and amacrine cell dendrites. Finally, the connectivity map of any volume is a compromise between intrinsic connections arising from cells completely inside the volume and extrinsic connections arising from cells outside the volume. Forexample, cortical connectome volumes contain far more extrinsic than intrinsic elements (Briggman and Bock, 2011). For the purposes of this manuscript, we mined the axons of all bipolar cells for the presence of axonal ribbons and reconstructed the targets of these ribbons. Table 2.3 contains a

legend for the color scheme used to represent synapse types in all 3D reconstructions displayed throughout this manuscript. All cell identification numbers used in this manuscript are identifiers that can be invoked in Viking, VikingPlot, and Viz tools (Anderson et al., 2011a) to validate all of the ultrastructural features, network motifs and statistics we report here. RC1 is an open-source, open-access, open-data resource.

ON Cone Bipolar Cell Axonal Ribbons Throughout the

OFF IPL form Accessory ON Pathways

ON cone bipolar cells make numerous axonal ribbon contacts throughout the OFF IPL: 175 of 398 (44%) bipolar cells in RC1 are ON cone bipolar cells. Thirty-four of these bipolar cells are semi-complete, with incomplete descending axons, thus we cannot determine the frequency of axonal ribbons in this subset. Fifty-four of the remaining complete 141 ON cone bipolar cells possess axonal ribbons (Figure 2.2). Thus 38% of the measurable ON cone bipolar cells make accessory ON axonal synapses. Three of these contain axonal ribbons only in the ON IPL, the remaining 51 of 141 bipolar cells (36%) contain one or more axonal ribbons in the OFF IPL. Importantly, most of these make multiple contacts through the OFF IPL and, on average, each ON cone bipolar cell that makes axonal synapses will do so at three different instances. For clarity we will use the MacNeil et al. (2004) rabbit bipolar cell morphological classification scheme to describe bipolar cells throughout this manuscript.   Briefly, the MacNeil et al. (2004) scheme abbreviates "cone bipolar" as "CB", OFF laminae of the IPL as

"a", ON laminae of the IPL as "b", with numbers representing the specific IPL sublaminae within which bipolar cell axons primarily arborize. For instance, an OFF cone bipolar cell that primarily arborizes in sublamina 1 is referred to as "CBa1", and an ON cone bipolar cell that primarily arborizes in sublamina 5 is referred to as "CBb5", etc. Wide-field bipolar cells and rod bipolar cells are simply stated as such. Further cone bipolar cell subsets deemed as narrow and wide are additionally labeled with "n" or "w", respectively, as in "CBb3n" or "CBa1w." We introduce two newly discovered morphological bipolar cell classes, CBb5w and CBb6, which make axonal ribbons. Moreover, all major classes of ON cone bipolar cell (CBb3, CBb3n , CBb3-4, CBb4, CBb5, CBb5w, CBb6, Wide-field cone bipolar cell) make axonal ribbons, five of which are highlighted throughout this manuscript (Figure 2.3). CBb5w cells costratify with CBb5 cells, yet they possess axonal arbor field diameters ≈ 40-55 μm versus the 25-30 μm field diameters of most cone bipolar cells. CBb6s are non-wide-field bipolar cells that stratify alongside rod bipolar cells, more deeply than any other class of cone bipolar cell.

Previous studies indicated that the functional IPL stratification schemes require amendment to include an accessory ON layer at the most distal portion of IPL stratum one, and perhaps throughout the entire OFF IPL (Dumitrescu et al., 2009; Hoshi et al., 2009). Our data are consistent with mixed ON-OFF processing throughout levels 0-45% of the IPL, consistent with bipolar cell stratification patterns in nonmammalians.

Rod Bipolar Cell Axonal Ribbons Do Not Provide

Accessory ON Drive

In contrast to CBbs, 61 of 105 (58%) rod BCs also make *bona fide* axonal ribbon synapses (synapses in the axon above the primary branch point), but these are virtually all within the upper part of the ON IPL with only a few breaking into the nominal OFF IPL (Figure 2.4). Further, virtually all of these (>90%) are contacts with identified A_I or A_{II} ACs. Every rabbit rod bipolar cell axon branches into 2 or 3 trunks as soon as it enters the ON IPL and immediately makes both pre- and postsynaptic specializations. The location of every axonal ribbon distal to the branch was mapped and we found that 89% were exclusively in sublamina b while 11% weakly breached the a/b border by an average of 600 nm. Over 90% of the traced targets of rod bipolar cell ribbons were verified as processes of A_I or A_{II} ACs. Indeed, all the A_{II} AC processes were arboreal dendrites and never lobules.

CBb axonal ribbon frequency is approximately three times greater than rod axonal ribbons, and CBb axonal ribbon frequency (122 axonal ribbons) in sublamina a is approximately eight times greater than rod axonal ribbons (15 axonal ribbons), for fewer bipolar cells. Further, the IPL ON-OFF border is not distinct but is rather a blend of CBa and CBb terminals. The distribution of CBb axonal ribbons represents a unique accessory pathway in the OFF channel, whereas the distribution of rod bipolar cell axonal ribbons reflects the targeting of normal ON pathway amacrine cells near the a/b border.

The upper 80% of the OFF IPL displays no rod bipolar cell axonal ribbons. We posited that this might be due to the heavy layer of Müller cell processes that ensheath the rod bipolar cells. This may be partly correct, but clearly depends on the nature of the target. For example, arboreal dendrites of A_{II} ACs readily induce desheathing of rod bipolar cell axons, but lobular processes never do, leading to an obvious bias for forming axonal ribbons in the ON IPL. However, A_I ACs, which are both presynaptic and postsynaptic to rod bipolar cells in the ON IPL, effectively induce desheathing in the OFF IPL and were presynaptic to rod bipolar cell axons (this network will be the subject of other papers), but were never postsynaptic. Thus, the formation of axonal ribbons is both site- and function-specific. The comparison of rod bipolar cell and ON cone bipolar cell ribbons shows that their roles are very different.

Finally, though ipRGCs receive rod signals (Aggelopoulos and Meissl, 2000; Dacey et al., 2005; Wong et al., 2007), the network pathway for this transmission remains unclear. The primary and secondary scotopic pathways and rod bipolar cell axonal ribbon pathways have all been implicated, so we examined the relationship between rod bipolar cell axonal ribbons and M1 ipRGCs in the RC1 volume. We discovered that rod bipolar cell axonal ribbons are not cospatial with an M1 ipRGC dendrite present in the RC1 volume (Figure 2.5); hence, this pathway cannot provide rod signals to M1 ipRGCs in the rabbit retina. Though ipRGC 12208's identity cannot be absolutely confirmed because there was no melanopsin immunolabeling in RC1, it monostratifies at the IPL/INL border, sparsely branches, accepts axonal ribbon input from every ON cone

bipolar cell it contacts (wide-field cone bipolar cell 6156 and wide-field cone bipolar cell 5283), and refuses input from two OFF cone bipolar cells (Figure 2.4. G-H). All of the above are consistent with M1-type ipRGCs (Dumitrescu et al., 2009; Graham et al., 2008; Hoshi et al., 2009). Henceforth, we shall simply refer to it as ipRGC 12208.

<u>Ganglion Cell Targets</u>

We identified axonal ribbons from CBbs in the OFF IPL targeting bistratified diving ganglion cells (bsdGCs), multistratified ganglion cells, intrinsically photosensitive ganglion cells (ipRGCs), and other ON-OFF multistratified and OFF layer monostratified ganglion cell processes (Figure 2.6). Unexpectedly, a chain of coupled ON cone bipolar cells provides axonal ribbon input to the bsdGC. Furthermore, multiple ON cone bipolar cell classes synaptically converge to common targets, and individual ON cone bipolar cells diverge to multiple targets, via axonal ribbons.

First, CBb4 3116 forms an axonal ribbon dyad onto bsdGC 15796 and a currently unidentified target (Figure 2.6 A,E). bsdGCs were identified in rabbit with dendrites that rise through the ON layer to stratify in the OFF IPL, where they receive CBb axonal ribbon input before re-entering the ON IPL (Hoshi et al., 2009). Our bsdGCs may be the same as the G9 ganglion cell identified by (Roska and Werblin, 2003), with depolarizing responses to light blocked by L-APB and enhanced by glycine and GABA receptor antagonists, and thus appear to be directly excited by ON cone bipolar cell input despite multistratification in

both the ON and OFF IPL. Note the ganglion cell target process ascends to the OFF sublaminae where it receives the axonal ribbon input, then more distally returns to approximately the same IPL depth as the primary axonal arborization of the CBb4 that provides the axonal input. No OFF cone bipolar cell input to this ganglion cell has been found, despite abundant contact opportunities. Interestingly, CBb4 3116 participates in a chain of coupled CBbs across classes (CBb3 and CBb4). Moreover, none of these other CBbs, except CBb4 3116, have been discovered to synapse onto bsdGC 15796 despite costratification of their primary axonal arbors with it. CBb4 3116 only provides input to bsdGC 15796 at the axonal ribbon location in the OFF IPL. Furthermore, the descending axon of CBb4 4569, one of the chain of coupled CBbs, passes within 0.25 μm of the axonal ribbon input to bsdGC 15796 by CBb4 3116 and does not form an axonal ribbon. These results are consistent with and extend those of Hoshi et al. (2009) by validating the selective input from CBb cells in the OFF layer.

Second, an axonal ribbon contact from CBb5 400 drives multistratified ganglion cell 5118. We cannot currently verify whether this ganglion cell is a bsdGC or ON-OFF ganglion cell, as its OFF layer-stratifying processes exit the volume without descending to ON layers and no OFF inputs have been discovered as of yet. That said, ganglion cell 5118 appears morphologically distinct from bsdGC 15796, thus is likely a different ganglion cell class.

Third, CBb5w 6156 and wide-field cone bipolar cell 5283 convergently drive M1 ipRGC 12208 with axonal ribbons, a single-ribbon monad and four-ribbon monad, respectively (Figure 2.6 C,G,H). This convergent input from two

CBb classes presumably indicates fusion of different CBb response profiles to extend the functional range of the ipRGC. This is concrete evidence for convergent axonal ribbon input from multiple bipolar cell classes onto ganglion cells.

Fourth, CBb6 447 and CBb6 353 converge axonal ribbon synapses onto OFF layer monostratified ganglion cell process 21779, and CBb6 447 diverges its output across the OFF and ON IPL via another axonal ribbon synapse in the ON layer to multistratified ganglion cell process 34336 (Figure 2.6 D,J,K,L). Both ganglion cell processes branch sparsely or not at all as they traverse nearly the entire width of the RC1 volume (257 μm) with no evidence of somata, indicating dendritic arbor radii of $\geq$ 250 μm and, thus, diameters $\geq$ 500 μm. Therefore, ganglion cell 21779 could belong to one of several classes of OFF layer-stratifying ganglion cells, but is unlikely to be an M1 ipRGC for two reasons. First, it monostratifies closer to the primary branch points of CBb3s than expected for an ipRGC. Second, it receives ribbon input from a partial trace of an OFF cone bipolar cell axonal arbor (data not shown), further inconsistent with M1 ipRGC electrophysiology. Ganglion cell 34336 could belong to any number of multistratified ganglion cell classes. This constitutes the first evidence that axonal ribbons in a single ON cone bipolar cell divergently drive targets in both the ON and OFF IPL. Importantly, all three of the axonal ribbons (across both CBb6s) form dyads onto a ganglion cell and amacrine cell targets, and both the amacrine cell targets of CBb6 447 conventionally synapse onto the ganglion cell target, thus forming CBb > amacrine cell $\geq$ ON-OFF ganglion cell feedforward motifs

(Figure 2.6 I, J, K, L). Furthermore, amacrine cell 32273 provides feedback onto a finger-like projection from CBb 447 in addition to the feedforward to ganglion cell 21779, thus regulating both presynaptic bipolar cell release and postsynaptic ganglion cell membrane potential (Figure 2.6 J, right subpanel).

Combined, these results demonstrate that axonal ribbons from multiple CBb classes convergently and divergently drive multiple classes of ganglion cells across OFF and ON sublayers, and inject both ON excitation and ON inhibition to ON-OFF ganglion cells.

GAC Targets

Axonal ribbons from at least two CBb classes target both mono- and multistratified GACs (Figure 2.7). The first demonstrated reciprocal synapse at an axonal ribbon location appears between CBb6 4570 and monostratified GAC 906 (Figure 2.7 A, E), revealing axonal ribbons as sites of potential input as well as output. GAC 906 receives both ON and OFF inputs via monostratification in the overlapping region of ON-OFF processing in the mid-IPL described above. ON-OFF cells in the IPL are generally believed to be multistratified, yet this GAC, and ganglion cell 18693 described below, highlight ON-OFF comingling in the IPL as fundamental topology. This reinforces the fact that bipolar cells can multistratify to facilitate crosschannel communication; that they do not constrain their synaptic communication to discrete ON-OFF territories. GAC 5507 is currently a partial trace, so it is possibly multi-, rather than monostratified (Figure 2.7 C, G). Multistratified GAC 5575 is particularly interesting, as it extends a dendrite off its

main trunk directly toward the descending axon of CBb5w 6156, where it receives axonal ribbon input (Figure 2.7 D, H). GAC 5575 divergently drives both ON cone bipolar cell ≥ ON ganglion cell (bsdGC) and ON cone bipolar cell ≥ ON-OFF ganglion cell inhibition, described in the text below. The combination of mono- and multistratified GAC targets suggests differential sign-inverting distribution of the CBb glutamatergic drive, but that will be explored in separate manuscripts.

γAC Targets Mediate Within- and Cross-Channel Inhibition

Three classes of ON cone bipolar cell were discovered to form γAC-mediated within- (Figure 2.8 A) and cross-channel (Figure 2.8 B-C) inhibitory motifs with axonal ribbons. First, CBb5 5562 drives multistratified γAC 5294 with an axonal ribbon (Figure 2.8 A, D, F). γAC 5294 forms a conventional synapse onto the primary telodendria of CBb5 5645 (Figure 2.8 A inset,G), completing a within channel inhibition motif. This within-channel inhibition is consistent with formation of the inhibitory surround of a center surround receptive field for CBb5 5645, yet this is the first report of such surround inhibition arising from axonal ribbon drive. Second, CBb6 5536 divergently drives a pair of amacrine cells, one of which is γ+ (Figure 2.8 E), at a branched axonal ribbon dyad site (Figure 2.8 B-C, H). Target amacrine cell 20537 is the γAC dendrite, and it spans most of the width of the RC1 volume without attachment to its soma, indicating a dendritic arbor radius ≥ 250 um, and therefore a dendritic arbor diameter ≥ 500 um. Thus, γAC 20537 is a wide-field γAC. Target amacrine cell 19571 does not cross an

immunolabeled section of the RC1 volume, and cannot be confirmed as γ+, but it is glycine negative (data not shown), and possesses the characteristic light cytoplasm (clear varicosities) of γACs. Furthermore, the two amacrine cell targets form a nested feedback architecture onto CBb6 5536 (Figure 2.8 H, right subpanel), a γAC network motif previously demonstrated in teleosts (Marc and Liu, 2000). Wide-field γAC 20537 also receives branched axonal ribbons from wide-field cone bipolar cell 16026 (Figure 2.8 B, C left inset, I), which combined with input from CBb6 5536 forms a CBb > γAC convergent motif. The second amacrine cell target of the divergence from the CBb6 5536 branched axonal ribbon creates a CBb > γAC ≥ CBa crossover inhibition motif (Figure 2.8 B, C right inset,J).

Axonal Cisterns Appear in Accessory ON Networks

Axonal cisterns, reported by (Anderson et al., 2011a), are characterized by a cistern adjacent to the plasma membrane of the nominal presynaptic cell, desheathed glia, an evenly spaced cleft similar to a synaptic cleft, and a definitive postcisternal density (PCD) indistinguishable from classic postsynaptic densities. As an example, some targets collect from multiple cisterns. In addition to its axonal ribbon input, γAC 20537 contacts axonal cisterns from CBb5 176 and wide-field cone bipolar cell 5283 (Figure 2.8 B, K; Figure 2.5 H). The convergent axonal ribbon input to ipRGC 12208 described previously is linked to this γAC axonal ribbon network via the axonal cistern and axonal ribbons in the same plane of section by wide-field cone bipolar cell 5283. Taken together, this partial

network of axonal ribbons and cisterns illuminate the complexity of axonal communication. The simultaneous divergence and convergence illustrated by the branched axonal ribbon dyad and monad from CBb6 5536 and wide-field cone bipolar cell 16026, respectively, spotlights the efficient design inherent in these networks.

Divergent ON-OFF GAC Inhibition to CBbs and

ON-OFF Ganglion Cells

We explored identified GAC axonal ribbon targets as possible crossover candidates. Axonal ribbon-driven GACs can distribute ON-OFF inhibition to both CBbs and ON-OFF ganglion cells (Figure 2.9). Specifically, the following network motifs exist: CBa > ON-OFF GAC ≥ CBb, CBa > ON-OFF GAC ≥ ON-OFF ganglion cell, and CBb > ON-OFF GAC ≥ ON-OFF ganglion cell, all three of which constitute ON-OFF cross-inhibition.

First, CBa2 424 and CBa2w 478 (a new CBa class discovered in RC1) drive monostratified GAC 906 with ribbon synapses (Figure 2.9 A, E, F). GAC 906 forms a conventional synapse onto CBb6 4570, reciprocal to an axonal ribbon (Figure 2.9 A, Figure 2.6 E), thus bestowing ON-OFF properties to GAC 906, and constructing a CBa > monostratified ON-OFF GAC ≥ CBb crossover inhibition motif. ON-OFF GAC 906 also synaptically diverges this ON-OFF inhibition to monostratified ON-OFF ganglion cell 18693. This is the first example of one GAC divergently distributing ON-OFF inhibition to both CBb and ON-OFF ganglion cell targets.

Next, CBb5w 6156 forms axonal ribbon synapses onto multistratified GAC 5575, (Figure 2.9 B, Figure 2.7 H), and GAC 906 and GAC 5575 cross inhibit each other (data not shown). GAC 906 therefore injects its ON-OFF properties to GAC 5575. Some ON-OFF amacrine cells are known to receive ON-OFF inhibition (Chen et al., 2011), and we add that the excitatory drive for this can arise from axonal ribbons. Each of the above ON-OFF GACs makes conventional synapses onto mid-IPL monostratified ON-OFF ganglion cell 18693 (Figure 2.9 B, G, H, I), forming parallel CBb > ON-OFF GAC ≥ ON-OFF ganglion cell motifs via two morphologically distinct GAC classes, thus blurring classical ideas of structure-function relationships. Clearly, the relationships are complex. The OFF input to GAC 906 from the above two CBas further constructs a CBa > ON-OFF GAC ≥ ON-OFF ganglion cell motif. Examples of GAC-mediated crossover inhibition motifs via axonal ribbons from ON to pure OFF targets remain to be discovered in RC1.

Divergent ON-OFF GAC Inhibition to ON-OFF Ganglion Cells
and bsdGCs

bsdGCs obtain ON polarity response properties via direct synaptic drive from CBbs, some of which arises from axonal ribbons (Hoshi et al., 2009; Roska and Werblin, 2003). Here, we report that axonal ribbons also drive ON-OFF inhibition to bsdGCs via one branch of a divergent inhibitory pathway. ON-OFF GAC 5575, introduced above, not only mediates CBb > ON-OFF GAC ≥ ON-OFF ganglion cell inhibition, it also synaptically diverges its signals to bsdGC 15796

(Figure 2.9 B, C, D, H, I, J). This constitutes the first reported evidence that a single narrow-field multistratified GAC can disperse sign-inverted axonal ribbon excitatory signals to both ON-OFF ganglion cells and ON ganglion cells (bsdGCs), and emphasizes the inherently multiplexed nature of GACs.

ON Cone Bipolar Cell Axon Tangency without

Axonal Ribbon Synapses

Thirty-eight percent of CBbs in RC1 make axonal ribbons, which raises the question of why the other 60% do not. This requires some new terminology. Most neurites in the retina directly appose those of other neurons without forming any specialization such as a synapse, gap junction, or adherens junction (Anderson et al., 2011a). We refer to such neurite pairs as *tangent* processes. In some cases, a single descending axon simply bypasses a cell to which it is tangent without forming an axonal ribbon (Figure 2.10 A, C). More intriguing, two ON cone bipolar cell axons may be tangent to the same cell, with differential connectivity to it. For example, CBb4 3116 forms an axonal ribbon dyad onto a bsdGC 15796 and an unknown target, and CBb4 4569 is tangent to the same unknown process, without forming an axonal ribbon synapse (Figure 2.10 B, D). In the first case, the potential but unconsummated target is an OFF layer monostratified ganglion cell that may be a pure OFF ganglion cell, as we have identified only OFF cone bipolar cell input to this ganglion cell. Thus, it may not be an appropriate target. In the second case, three interesting points arise: 1) the CBb without axonal ribbons in the figure does not make *any* axonal ribbons,

2) the CBbs are of the same class (CBb4), and 3) the CBbs are coupled by gap junctions and therefore share signaling attributes. One possibility for the differential connectivity is that ON cone bipolar cell coupling obviates the need for axonal ribbon input from both CBbs. That said, coupled CBbs do drive common targets from their telodendria, but never at the same locus. This topic will be addressed in future papers.

Discussion

The analysis of RC1 and noncanonical ON cone bipolar cell axonal ribbon synapses in the OFF layer exposes new organizational concepts in retina and leads to a refactoring of the IPL. We first address the existence of mixed signaling strata and new network access schemas; the distinction between simple tangency and functional contact; and the importance of joint distributions for interpreting synaptic statistics. Then we will review key signaling features of specific targets of axonal ribbons. Since bipolar cell nomenclatures differ across species and we will now be discussing many of them, and since all cone bipolar cell classes in rabbit make axonal ribbons, we periodically depart from the McNeil et al. (2004) rabbit scheme for the discussion and simply refer to cone bipolar cells as ON cone bipolar cells and OFF cone bipolar cells.

First, why do ON cone bipolar cells target the OFF layer of IPL at all? The answer is partly evolutionary: the OFF layer of the IPL has been a mixed ON-OFF stratum throughout vertebrate descent. Every nonmammalian vertebrate class harbors multistratified ON bipolar cells, (Kolb, 1982; Pang et al., 2004;

Ramon y Cajal, 1892; Scholes, 1975; Scholes and Morris, 1973; Sherry and Yazulla, 1993; Wong and Dowling, 2005) and their discovery in the mammalian retina demonstrates that no evolutionary mechanism has ever "purified" the OFF layer. But more concretely, mixed strata reflect important network access properties. Axonal ribbons provide ON inputs to unique monostratified cells such as TH1 axonal cells and M1 ipRGCs (Dumitrescu et al., 2009; Hoshi et al., 2009) that send their dendrites to the most distal layer of the IPL. That is an incomplete explanation since the very same ON cone bipolar cells also have outputs in the ON layer. The question should be reframed in future work: why do the target ON cells invade the OFF layer at all. We have preliminary data to show that, in addition to ON inputs, these cells seek inputs from CBa1-driven OFF γACs accessible only in the OFF layer. Ultimately, there is no unique distal ON stratum in the IPL. Indeed, the entire OFF layer is a stack of mixed ON-OFF strata with cone bipolar cell axonal ribbons distributed throughout (Figure 2.2, 2.3, 2.4). We propose that ON signals in the OFF layer provide unique network opportunities for crossover signaling and loci for mixing ON excitation with polarity-matched OFF inhibition.

Analysis of axonal ribbon sites reveals that specific rules control their incidence, though we clearly have a poor idea of the molecular mechanisms. ON cone bipolar cell axons are sheathed by three facing Müller cells throughout their transit of the OFF layer except at sites of potential target contact, where the Müller cells are parted by unknown mechanisms. As described by Anderson et al. (2011a), many neural processes are apposed without intervening glia but

never make synapses, gap junctions, or even adherens junctions. We, noted above, refer to such lack of functional contact as tangency. Many processes somehow induce unsheathing of Müller cells around CBb cells in the OFF layer yet remain simply tangent. Another important point is that ribbon synapses, whether in the axon or axon terminal, never appear at the membrane without an associated postsynaptic density. This suggests that complete synaptic contacts are induced by the target or source-target interactions, but that unsheathing to expose the source seems to be under the control of the target.

Finally, not all ON cone bipolar cells in a given class form axonal synapses, but members of all classes do form OFF layer axonal synapses. Using a very strict criterion, 36% of all identified ON cone bipolar cells in RC1 engage the OFF IPL with axonal ribbon synapses. Our analysis of sources and targets for these and other synaptic pairings suggests that the retina routinely invokes such partial motifs. Such sampling schemes conflict with our traditional expectations and methods of tabulating synaptic contacts (e.g., counting the percent of outputs onto a target). That approach to network analysis would lead us to ask: If most ON cone bipolar cells do not form axonal synapses, how can we argue that they are functional and not some statistical anomaly? We can approach this problem via graph theory, with cells represented as vertices and synaptic connections represented as edges. Every vertex in a directed graph represents a point of signal transfer between a source and target. In a multidigraph like the retina (Marc et al., 2012), each vertex represents the source or target for multiple edges. And given that the copy numbers for each class of

vertices (i.e., each *ultimate* cell class, Marc and Jones (2002)) varies, as do their coverages and Hausdorff dimensions, one cannot optimize a complex biological system to give smooth statistics or provide 100% source contacts for all cells. Figure 2.11 provides a geometric proof of this. The white dots in Figure 2.11 represent the projection of 15 ON cone bipolar cell axons through a sampling plane of the IPL. In Figure 2.11 A, a set of cells from a single class (with individual cells in different colors) with a high coverage contacts every cone bipolar cell axon. Indeed, the overlap of individual cells leads to multiple edges. The outflow efficiency *appears* to be 100%, with a mean contact number of 2.67 ± 0.7 (standard deviation). However, it is important to grasp that these are meaningless metrics, especially the variance. The only metric that matters is the efficiency of *target* sampling, which is also 100%. This becomes clearer in Figure 2.11 B, where two different, sparse cell classes send dendrites through the axonal field. Only 6 of 15 axons are hit for an output efficiency of 40%. Indeed, the output efficiency is even lower for each class. Yet, from the perspective of the targets, the two cells make synapses with 100% of the axons they encounter. This is critical for cells with low coverages such as ganglion cells. Their target sampling is perfect. Not all axons are hit because there is an oversupply of sources. The target does not "know" that there are excess source axons since they are not needed. Thus, the partial incidence of axonal synapses in ON cone bipolar cell axons reflects the spatial needs of the targets, not the sources. It does not represent any imprecision: QED. The key descriptor for such networks

is the joint density distribution of source and target, expressed as a metric of signal transfer sites per unit area or volume of neural space.

Two ON Cone Bipolar Cell Classes Converge onto ipRGCs

The putative ipRGC identified in RC1 receives axonal ribbon input from every ON cone bipolar cell it encounters, wide-field cone bipolar cell 5283 and CBb5w 6156. It further refuses input from two OFF cone bipolar cells to which it is tangent (data not shown). Neural structure-function correspondence is widely agreed upon, and every *tested* class of bipolar cell identified based on unique morphology has thus far proven to possess unique physiological response properties (Masland, 2001). Thus, wide-field cone bipolar cell 5283 and CBb5w 6156 contribute their presumably differential responses properties via sign conserving synapses to the ipRGC, thereby increasing the complexity or range of the ipRGC responses. This could represent convergence of different spectral sensitivities and/or flux range fractionation.

Coupled Bipolar Cell Input to bsdGCs

bsdGC 15796 is one target of an axonal ribbon dyad from CBb4 3116 (Figure 2.6 A), which belongs to a cluster of seven coupled ON cone bipolar cells that likely represent a patch in a larger sheet of coupled cone bipolar cells, similar to the coupled clusters of ON cone bipolar cells discovered in teleosts (Umino et al., 1994). It is striking that none of the other members of the coupled chain provide input to the bsdGC, despite a second axon from CBb4 4569 very

close to the axonal ribbon input by CBb4 3116 (Figure 2.6 A; Figure 2.10 B-C), and costratification of ON cone bipolar cell primary axonal arbors with ON layer bsdGC arbors. Again, this reflects the concept of joint distributions where a limited bsdGC target architecture samples inputs from an array of excess sources. This would be especially true when sampling from coupled arrays since a single sampled input would provide some weighted mean output from a patch. Teleost coupled bipolar cells appear to receive variable input from cones, which introduces noise into the system, and modeling coupled bipolar cells as hexagonal arrays of isopotential units indicates that coupling increases the input signal to noise ratio without significantly sacrificing resolution (Umino et al., 1994). bsdGCs receive most of their ribbon input in the ON layer (Hoshi et al., 2009), and the need for axonal ribbon input remains a mystery. As noted above, it is likely that the primary function of OFF stratification in nominal ON cells is accessing OFF amacrine cell inputs.

γAC Targets, GAC Targets, and Crossover Inhibition

Physiological analyses show that ON and OFF channels cross-inhibit each other via glycinergic synapses at every tier of the IPL (Chen et al., 2011; Molnar et al., 2009; Roska and Werblin, 2003; Werblin, 2010). Functional reasons for this include possible restoration of linearity to rectified currents driven by AMPA and NMDA receptors, expanding photopic dynamic range into the scotopic domain, luminance-contrast distinction, better impedence matching in postsynaptic neurons, OFF cone bipolar cell gain and high frequency response

increase, and limitation of OFF channels to negative contrast processing (Liang and Freed, 2010; Molnar et al., 2009; Werblin, 2010). We add evidence that ON cone bipolar cell axonal ribbons mediate crossover inhibition via synapses with both γACs and GACs, revealing network topologies not predicted from electrophysiology.

The GAC and γAC targets are both mono- and multistratified (Figures 2.7 and 2.8). Both GAC and γAC targets form feedback and feedforward motifs, and γAC targets also form nested feedback to axonal ribbons. Given the extensive γAC networks at bipolar cell axon terminals, it is not surprising they engage axonal ribbons as well. γAC feedback and nested feedback onto bipolar cells fine-tunes bipolar cell presynaptic release (Marc and Liu, 2000), and is implicated in axonal ribbon release as well (Figures 2.7 and 2.9).

γAC-mediated crossover inhibition via axonal ribbons (Figure 2.8 B, C right inset) extends the functional repertoire of γACs, demanding dissection of the potentially differential functional role of glycinergic and GABAergic crossover inhibition. Two nonexclusive functional implications arise. First, glycine receptor (glyR)-mediated, GABA receptor (GABAR)-mediated inhibition of bipolar cells may manifest different kinetics that combine with amacrine cell presynaptic release, such that GABA$_A$R- and glyR-mediated inhibition predominantly control the magnitude of bipolar cell glutamate release, whereas GABA$_C$-mediated inhibition controls the timing of bipolar cell glutamate release by increasing its transiency (Eggers and Lukasiewicz, 2011; Eggers and Lukasiewicz, 2006a, 2006b, 2010; Eggers et al., 2007). Crossover inhibition networks may appropriate

these kinetic differences to increase the range and complexity of bipolar cell and ganglion cell responses. Second, dual transmitters may optimize crossover inhibition by preventing synaptic occlusion, which occurs when two or more adjacent presynaptic terminals release the same neurotransmitter onto a shared postsynaptic target (Fatima-Shad and Barry, 1992; Gold and Martin, 1984). Since the postsynaptic cell detects these multiple GABAergic synaptic inputs via the same type of GABA$_A$Rs, for example, adjacent GABAergic inputs cross-desensitize. Introduction of multiple neurotransmitters at these locations discretizes the signals, which may be necessary to properly effect crossover inhibition.

We now consider the functional role of dual transmitter-mediated crossover inhibition for the CBb > γAC ≥ CBa motif (Figure 2.8 B, C right inset). Most OFF cone bipolar cells receive ON inhibition (Molnar and Werblin, 2007). Further, OFF cone bipolar cells are dominated by glyR-mediated inhibition, though they also receive some GABA$_A$R-mediated inhibition, but little GABA$_C$R-mediated inhibition (Eggers and Lukasiewicz, 2011). This is quantitatively inconsistent with the dominance of γAC inputs to CBa cells, but qualitatively matches observed higher GAC convergence on CBa as opposed to CBb cells. Given the similarites between glyR- and GABA$_A$R-mediated OFF cone bipolar cell response kinetics in response to natural stimuli, there is no obvious kinetic advantage to the utilization of both to cross-inhibit OFF cone bipolar cells. Thus, dual γAC-mediated and GAC-mediated bipolar cell > amacrine cell ≥ bipolar cell crossover inhibition networks may reduce synaptic occlusion, rather than control

OFF cone bipolar cell peak release. That said, examples of axonal ribbon-involved adjacent γAC and GAC processes sharing postsynaptic targets remain to be found. Though axonal ribbon-mediated OFF $\geq$ ON GABAergic crossover inhibition has not been discovered in the OFF layer, it has been found in the ON layer between OFF cone bipolar cell telodendria and ON cone bipolar cells, and is the topic of future papers.

Predicting the function of OFF $\geq$ ON, dual transmitter crossover inhibition is less clear, due to some slight discrepancies in the literature. Eggers and Lukasiewicz (2011) report that murine ON cone bipolar cells possess similar levels of $GABA_AR$- and $GABA_CR$-mediated inhibition, and little to no glyR-mediated inhibition, whereas others report glycine-mediated crossover inhibition of ON cone bipolar cells (Molnar et al., 2009; Werblin, 2010). Presuming that glyR-, $GABA_AR$-, and $GABA_CR$-mediated inhibition all occur in rabbit ON cone bipolar cells, which is consistent with amacrine cell networks in RC1, dual glycine- and GABA-mediated crossover inhibition would afford control of both the peak amplitude and the degree of prolonged release in ON cone bipolar cells. Synaptic occlusion reduction could be an additional benefit of dual-transmitter crossover inhibition in these cells as well, but more analysis is needed to determine the frequency of adjacent γAC and GAC inputs to common targets.

GAC- versus γAC-Mediated Cross-Channel Feedback

and Feedforward Inhibition

Many networks described in this manuscript constitute axonal ribbon-mediated cross-channel feedback inhibition (CBb > γAC ≥ CBa and CBa > GAC ≥ CBb motifs), and cross-channel feedforward inhibition (CBb > GAC ≥ ganglion cell and CBa > GAC ≥ ganglion cell motifs). These motifs could also subserve kinetically appropriate ON-OFF response properties in polarity-opposite targets. Axonal ribbon reciprocal synapses can inject OFF components into ON channels, inject ON components into OFF channels, and construct ON-OFF target cells. GAC and γAC feedforward motifs discovered thus far are different. γACs feedforward to targets also directly driven by axonal ribbons by the CBb, whereas GACs feedforward to targets not directly driven by those axonal ribbons. We refer to these as in-class and cross-class feedforward motifs, respectively. One common form of glycinergic ON $\geq$ OFF crossover is provided by A_{II} AC lobular dendrite synapses onto OFF cone bipolar cells and extensive input to OFF α and δ ganglion cells. Importantly, neither A_{II} ACs nor OFF α / δ ganglion cells are targeted by ON cone bipolar cell axonal synapses, despite abundant opportunities.

The diversity of inputs to ON-OFF amacrine cells aligns with the complexity of amacrine cell/ganglion cell response properties. We show that an anatomical framework exists to support glycine- and GABA-mediated control of ON cone bipolar cell release at axonal ribbon locations, which may subserve

both crossover inhibition and ON-OFF GAC regulation of ON cone bipolar cell axonal ribbon synapse release kinetics.

Rod Bipolar Cell Axonal Ribbons Are Distinct from

ON Cone Bipolar Cell Axonal Ribbons

Despite the fact that multiple laboratories have reported very few, if any, axonal ribbons in rod bipolar cells (Chun et al., 1993; Ghosh et al., 2001; Tsukamoto et al., 2001), our results are more consistent with those of Strettoi et al. (1990), in which they reported occasional instances of output synapses along the descending axons of rod bipolar cells. Nonetheless, the rod bipolar cell axonal ribbons all occur en passant, with no evident branching, and are concentrated in the ON IPL (Figure 2.4). Those that breach the ON-OFF boundary do so marginally; they comprise ON drive to polarity-matched targets, distinct from ON-OFF crosstalk achieved by ON cone bipolar cell axonal ribbons in the rabbit retina. The absence of rod bipolar cell axonal ribbons in the distal OFF layer is significant since M1 ipRGCs exhibit rod responses (Aggelopoulos and Meissl, 2000; Dacey et al., 2005; Wong et al., 2007). Possible sources include the primary A_{II}-mediated scotopic pathway, the secondary rod::cone coupling scotopic pathway, or direct rod bipolar cell axonal synapses with M1 ipRGCs, as suggested by Ostergaard et al. (2007). Our data demonstrate that rod input to M1 cells absolutely does not arise from rod bipolar cell axonal ribbons. Moreover, we have found no evidence of rod bipolar cell synapses onto ganglion cells of any type, and the rod bipolar cell axonal ribbons discovered thus

far target only A_I and A_{II} ACs, both typical ON layer targets of rod bipolar cell ribbons. A_I AC rod bipolar cell axonal ribbon targets are further consistent with previous work demonstrating that A_I AC dendrites sometimes immediately appose GABA receptors on descending rod bipolar cell axons in the ON IPL sublaminae, expected for reciprocal synapses observed between A_I ACs and rod bipolar cell ribbons (Wässle et al., 1991; Zhang et al., 2002).

Multiple Axonal Synaptic and Network Topologies

Distribute Functionality

Axonal ribbons routinely construct convergent and divergent synaptic motifs. The synaptic topologies vary across these examples, including all combinations of single- versus multiribbon, and monadic versus dyadic synapses (Figures 2.6, 2.7, 2.8, 2.9). Axonal ribbons also tend to be smaller than ribbons in the primary ON cone bipolar cell arbors. Distinct synaptic topologies are considered here.

First, wide-field cone bipolar cell 6156 forms single-ribbon, monadic axonal synapses to drive an ipRGC and a narrow-field, diffusely stratified GAC employed for divergent within- and cross-channel inhibition motifs (Figure 2.6 C, G; Figure 2.7 D, H). Second, wide-field cone bipolar cell 5283 drives the ipRGC targeted by CBb5w 6156 with a multiribbon, monadic axonal synapse, demonstrating different synaptic topological input to a common target, albeit from two classes of ON cone bipolar cell. Third, CBb6 5536 displays a single-ribbon, branched axonal synapse dyad to drive a pair of OFF layer, monostratified

amacrine cell processes, which provide nested feedback to the CBb6, and one of which mediates CBb > γAC ≥ CBa crossover inhibition (Figure 2.8 C right inset, H). Finally, CBb5 400 forms a multiribbon, dyadic axonal synapse onto ganglion cell 5118 and a currently unidentified process (Figure 2.6 B, F).

No clear pattern emerges as to the rules governing axonal ribbon synaptic topologies, but we can eliminate two possibilities. First, the target cell does not govern axonal ribbon count, as evidenced by the ipRGC recipient to convergent input from two axonal ribbon monads with different numbers of ribbons. Second, cone bipolar cell class does not govern axonal ribbon synaptic topology, given that ON cone bipolar cells of the same class can instantiate different axonal synaptic topologies, and ON cone bipolar cells of different classes can share synaptic topologies. More source-target analysis is needed on this topic.

Monostratification Achieves ON-OFF Crosstalk

via Axonal Ribbons

It is generally thought that ganglion cells acquire ON-OFF responses via bistratification across the ON and OFF IPL, yet in WT mice, 11% of ganglion cells establish ON-OFF properties by P33 via monostratification of one thick band of dendrites in the middle IPL (Tian, 2008). Ganglion cell process 18693, targeted in CBb > ON-OFF GAC ≥ ON-OFF ganglion cell crossover inhibition (Figure 2.9 B, C, D), is one such monostratified ganglion cell. Unfortunately, this ganglion cell process exits RC1, so we cannot verify that it lacks another stratum of arborization. However, its annotated processes costratifiy in the mid-IPL with

GAC 906 from which it receives crossover inhibition, driven by an axonal ribbon (Figure 2.9 B). This example of co-monostratification of a GAC and ganglion cell in the same crossover inhibition network demonstrates that multistratified bipolar cells can mediate ON-OFF crosstalk. Moreover, since it is now established that the entire OFF layer of the IPL contains mixed ON-OFF signal processing, it follows that almost any monostratified cell could develop ON-OFF responses.

<u>Axonal Cisterns</u>

Though the function of axonal cisterns is unknown, they are not randomly distributed and appear as well-ordered accessory ON network elements to common target cells (Figure 2.8 B, K; Figure 2.6 H). They are often in close proximity to axonal ribbon synapses (Figure 2.6 H), converge onto common targets (Figure 2.8 B), and have been observed reciprocal to conventional synapses (data not shown), suggesting that they are real structural or communicative elements of accessory ON networks. Indeed, preliminary analyses reveal that 55 of 113 (48.7%) measured cone bipolar cells contain one or more axonal cisterns. More complete analyses will be conducted in future manuscripts.

<u>Axonal Ribbons Are Routine Network Elements</u>
<u>Throughout the IPL</u>

Ten axonal ribbon-mediated network motifs have been discovered in RC1 thus far spanning all IPL sublaminae (Figure 2.12), emphasizing their routinity in

cone bipolar cell signaling. It is highly likely that additional motifs exist, as many axonal ribbon targets and networks remain to be identified. The excitatory motifs provide direct axonal ribbon drive to an array of ganglion cell classes. The inhibitory motifs comprise both   feedback and feedforward as they target GACs and γACs, which in turn form synapses onto CBas, CBbs, and several classes of ganglion cell.

Figure 2.12 collapses the network motifs reported in this manuscript onto one representative cone bipolar cell for clarity. As such two features that occur in a minority of cells are included, branched axonal ribbons in the canonical OFF IPL and bifurcated descending axons. It is important to distinguish between a bifurcated axon and the primary branch point of the telodendria. ON cone bipolar cell descending axon bifurcations occur in sublaminae 3-5, distinctly distal to the primary arborization of the cell. In such cases, the descending axon typically bifurcates into major (Figure 2.12, right branch) and minor (Figure 2.12, left branch) axons before each primarily arborizes. The major branch diameter remains comparable to the descending axon diameter distal to the bifurcation, while the minor branch point adopts a smaller diameter. Each branch retains axonal features such as predominant microtubule bundles and a scarcity of vescicles, except for vesicle clouds concentrated near axonal ribbons. In cases of clearly bifurcated descending axons distal to the primary arborization of the cell, such as that shown in Figure 2.12, ribbon synapses in both the major and minor axons were still classified as "axonal".

Note that in addition to abundant axonal ribbon output, cone bipolar descending axons are frequently postsynaptic to amacrine cell inputs, both reciprocal and nonreciprocal to axonal ribbons.

Acknowledgments

Table 2.1. Primary antibodies used in this study

Antibody	Immunogen, Host Species	Source	Dilution Used
AGB	BSA-glutaraldehyde- (1-amino-4-guanidobutane) conjugate, rabbit	Signature Immunologics B100/rabbit-polyclonal	1:4,000
GABA	BSA-glutaraldehyde- (4-aminobutyrate) conjugate, rabbit	Signature Immunologics YY100/rabbit-polyclonal	1:32,000
Glycine	BSA-glutaraldehyde (glycine) conjugate, rabbit	Signature Immunologics G100/rabbit-polyclonal	1:4,000
L-glutamate	BSA-glutaraldehyde- (L-glutamate), conjugate, rabbit	Signature Immunologics E100/rabbit-polyclonal	1:32,000
L-glutamine	BSA-glutaraldehyde- (L-glutamine) conjugate, rabbit	Signature Immunologics Q100/rabbit-polyclonal	1:4,000
Taurine	BSA-glutaraldehyde- (taurine) conjugate, rabbit	Signature Immunologics TT100/rabbit-polyclonal	1:16,000

Legend. Abbreviations: AGB 1-Amino-4-guanidobutane, GABA γ-Aminobutyric acid.

Table 2.2. IgG competitive sensitivities computed from inhibition assays

Bis-conjugate	γ	G	E	Q	τ
γ	0	8	5	7	6
G	6	0	5	7	6
E	4	9	0	5	6
Q	6	9	5	0	6
τ	5	10	5	7	0

Legend. IgG competitive sensitivities computed from inhibition assays and expressed as log differential inhibition: log [C]/[T], where [C] and [T] are the concentrations of any conjugate (C) or the cognate target conjugate (T) required for 100% binding block. γ GABA, G glycine, E glutamate, Q glutamine, τ taurine.

Table 2.3. Synapse color scheme – 3D reconstructions

Synapse Type	Color
Ribbon	Green
Conventional	Blue
Postsynaptic Density	Red
Gap Junction	Yellow
Adherens Junction	White
Cistern Contact	Grey

Table 2.4. Abbreviations

INL	Inner Nuclear Layer
IPL	Inner Plexiform Layer
GCL	Ganglion Cell Layer
GAC	Glycine-positive Amacrine Cell
γAC	GABA-positive Amacrine Cell
A_I AC	A_I Amacrine Cell = A17 Amacrine Cell
A_{II} AC	A_{II} Amacrine Cell
ipRGC	Intrinsically Photosensitive Retinal Ganglion Cell
bsdGC	Bistratified Diving Ganglion Cell
>	Sign-Conserving Synapse
≥	Sign-Inverting Synapse
$GABA_AR$	$GABA_A$ Receptor
$GABA_CR$	$GABA_C$ Receptor
glyR	Glycine Receptor

Figure 2.1. RC1 overview. **A.** The RC1 volume with its top section (001) beginning in mid-INL and ending in the GCL at section 371, shown in a mirror image below. RC1 is a short cylinder ≈ 250 μm in diameter and ≈ 30 μm high containing 341 TEM sections and 11 intercalated CMP sections. The cylinder is capped at top and bottom with 10-section CMP series allowing molecular segmentation. TEM section 001 is a near-horizontal plane section through the INL visualized with GABA.glycine.glutamate → red.green.blue transparency mapping and a dark gold alpha channel (ANDed taurine + glutamine channels) described in Anderson et al. 2011a. Similarly, TEM section 371 is a near-horizontal plane section through the GCL visualized with GABA.AGB.glutamate → red.green.blue transparency mapping. **B.** Representative cells contained in RC1 are rendered in 3D onto the volume. Many complete copies of small cells exist (tens to hundreds) such as rod bipolar cells (cells 1, 2) and A_{II} ACs (cell 3). A few semicomplete copies (5-10) of medium-diameter cell classes have their somas and much of their arbors within RC1, but extend outside it, such as interstitial γACs (cell 4) and A_I amacrine cells (cell 5). Finally, RC1 contains many processes from partial cells: large cells such as wide-field amacrine cells or OFF α ganglion cells (cell 6) with somas outside the volume and often fully traversing it.
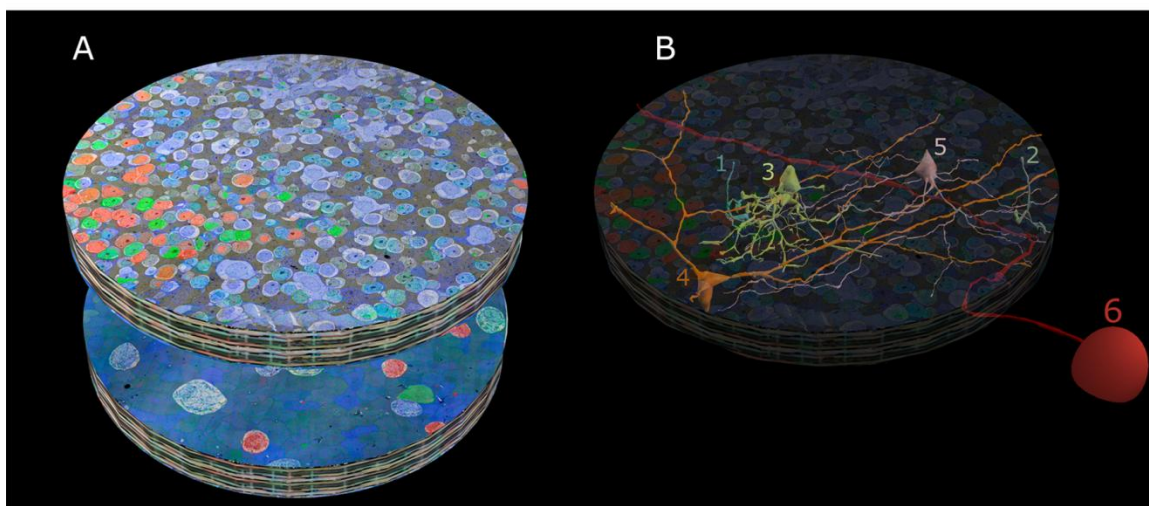
Figure 2.2. Subsets of CBbs make en passant and branched axonal ribbons. **A.** Vertically oriented renderings of 53 CBbs (neutral and warm colors) with axonal ribbons in the OFF IPL plotted against 48 CBas (cool colors). Cone bipolar cell color corresponds to depth of IPL stratification as follows: CBa1, sage; CBa2, green; CBb3, tan; CBb3-4, dark mustard; CBb4, silver; CBb5, mustard; CBb6, bright red; wide-field cone bipolar cell, deep red. Arrows, somas of CBbs referenced in B-P. Scale bar, 25 µm. **B-K.** CBbs indicated in A are confirmed as glycine-positive (B-F, TEM of CBb somas; G-K, glycine-positive labeling of corresponding somas in B-F). Scale bars, 5 µm. **L-P.** TEM of gap junctions between CBbs indicated in A and A_{II} ACs**.** White arrows delineate gap junctions; A-II, A_{II} amacrine cell; WF BC, wide-field bipolar cell; scale bars, 0.5 µm. **A, B, G, L.** CBb3 1637 rendering (A), TEM of soma (B), corresponding glycine-positive signature (G), and indirect A_{II} AC coupling via a gap junction with CBb3-4 1724 (L, left subpanel) which is couple to A_{II} AC 514 (L, right subpanel). **A, C, H, M.** CBb4 593 rendering (A), TEM of soma (C), corresponding glycine-positive signature (H), and gap junction with A_{II} AC 3679 (M). **A, D, I, N.** CBb5w 6156 rendering (A), TEM of soma (D), corresponding glycine-positive signature (I), and gap junction with A_{II} AC 476 (N). **A, E, J, O.** CBb6 4570 rendering (A), TEM of soma (E), corresponding glycine-positive signature (J), and gap junction with A_{II} AC 3257 (O). **A, F, K, P.** Wide-field cone bipolar cell 5283 rendering (A), TEM of soma (F), corresponding glycine-positive signature (K), and gap junction with A_{II} AC 3679 (P). **Q.** CBb4 485 (silver) and CBb5w 180 (copper) form *en passant* axonal ribbon synapses (circles) among CBa1 and CBa2 arbors. Scale bar, 5 µm. **R.** Wide-field cone bipolar cell 16026 (red) forms branched axonal ribbon synapses (circle) among CBa1 and CBa2 arbors. Scale bar, 5 µm.
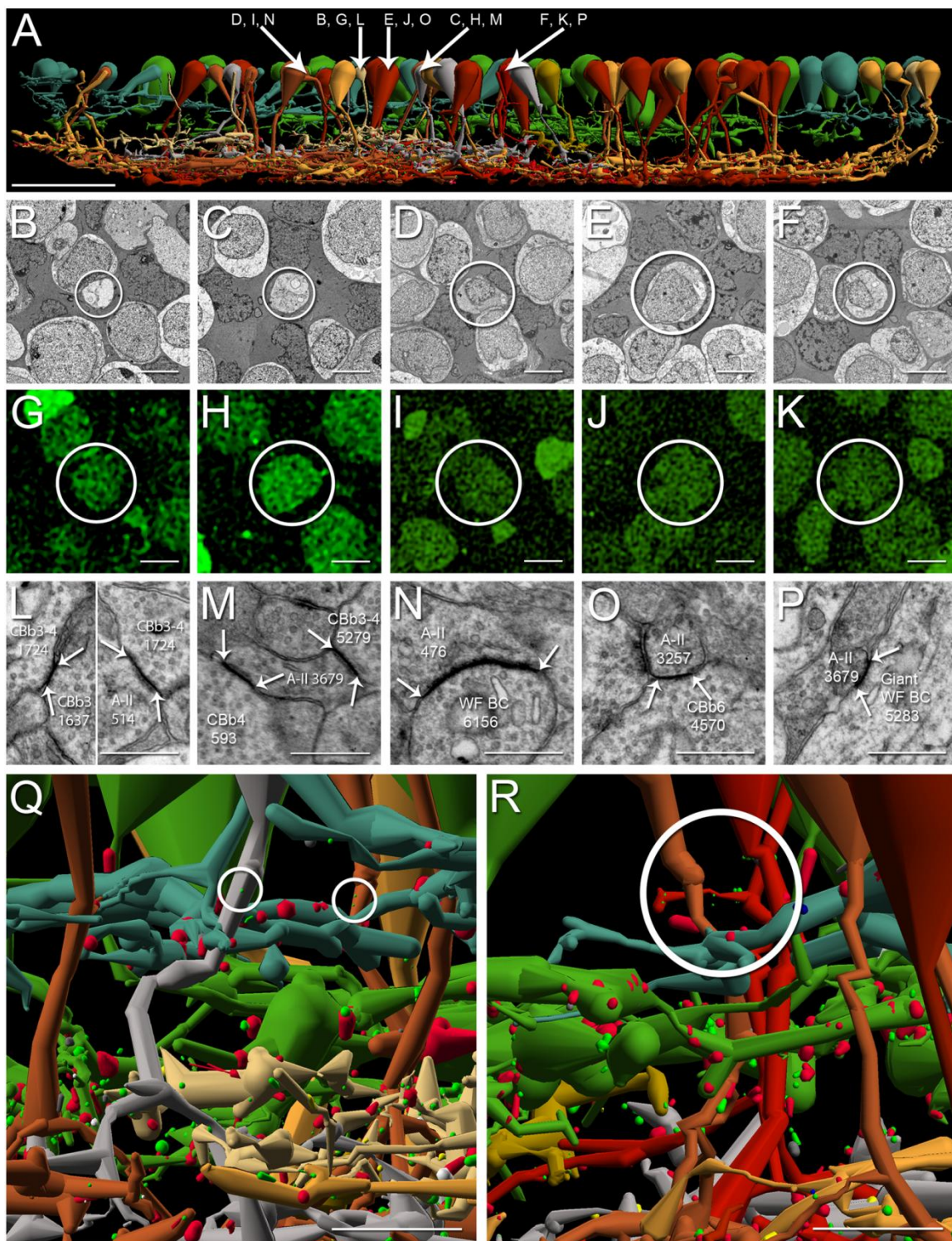
Figure 2.3. All major classes of CBbs possess axonal ribbons, stereogram. The five CBbs highlighted in Figure 2.2 are displayed in isolation for clarity. Varied numbers of axonal ribbons across CBb classes span the IPL. Cone bipolar cell color corresponds to depth of IPL stratification. Specific cone bipolar cell colors as follows: CBb3, tan; CBb4, silver; CBb5w, copper; CBb6, bright red (left); wide-field cone bipolar cell, deep red (right). Note the class-specific arborization thickness, pattern of varicosities, and axonal arbor diameters.   Spatial relationships are preserved. Scale bar,10 µm.
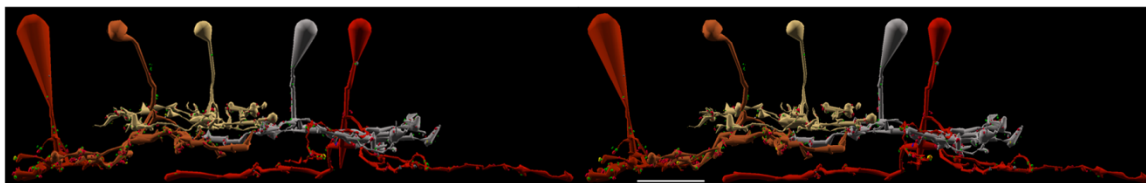
Figure 2.4. CBb versus rod bipolar cell axonal ribbon depths. The distribution of 160 axonal ribbons in 54 CBbs and 63 ribbons in 63 of 104 rod bipolar cells in RC1. Ribbon positions are measured relative to the sublamina a/b border, defined as the proximal face of the nearest A$_{II}$ amacrine cell lobule. CBb axonal ribbons are distributed throughout sublamina a. Rod bipolar cell axonal ribbons are excluded from 80% of sublamina a. ACL, amacrine cell layer; Rod BC, rod bipolar cell.
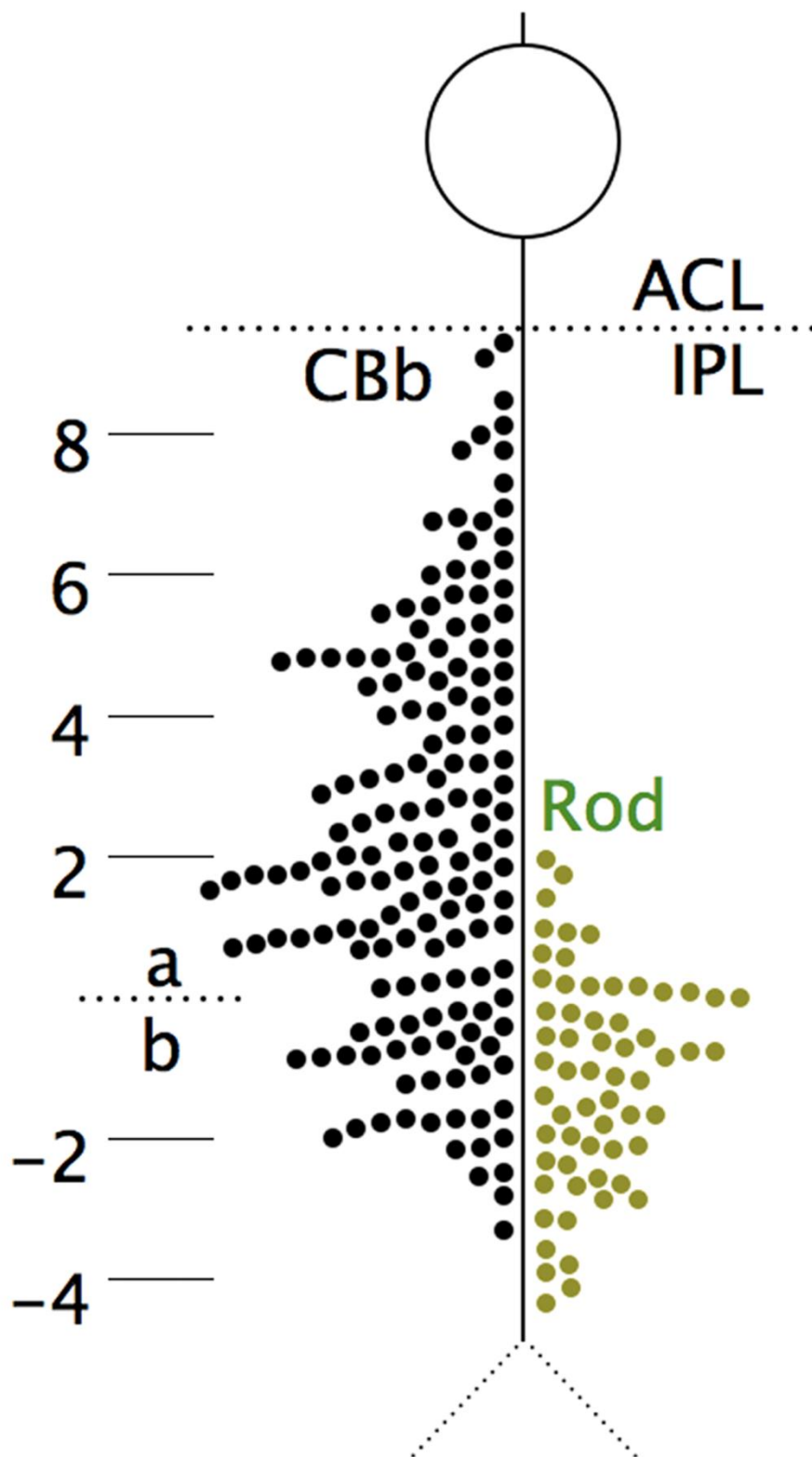
Figure 2.5. Rod bipolar cell axonal ribbons cannot drive M1 ipRGCs. All 63 rod bipolar cells (ghosts) with axonal ribbons in RC1 are displayed against ipRGC 12208 (sand). Note that all ribbon synapses (bright green dots), including the axonal ribbons, are too proximal in the IPL to form synapses with the ipRGC. Scale bar, 20 μm.
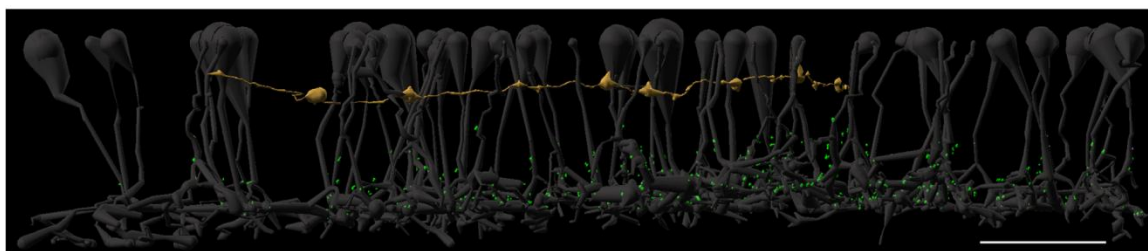
Figure 2.6. Ganglion cell axonal ribbon targets. **A-D.** Renderings of five CBb classes forming axonal ribbons onto multiple ganglion cell classes, vertical orientation. Circles indicate location of synapses shown in E-L. Scale bars (A-B), 25 μm; scale bars (C-D), 20 μm. **E-L.** TEM of synapses indicated in A-D. White arrows indicate synapse directionality. GC, ganglion cell; WF BC, wide-field bipolar cell; AC, amacrine cell; r, ribbons; c, cistern; pcd, postcisternal density; scale bars, 0.5 μm;. **A,E.** CBb4 3116 (left cell of the silver pair that intersect ganglion cell 15796 (red)) forms an axonal single-ribbon dyad with bsdGC 15796 and an unknown cell. CBb4 3116 participates in a chain of seven coupled CBb3s (tan) and CBb4s (silver). The bsdGC 15796 dendritic target of the axonal ribbon abruptly ascends to the OFF IPL where it receives the input before returning to the ON IPL distally (far right of panel A). **B,F.** CBb5 400 (mustard) forms an axonal multiribbon dyad with ON-OFF ganglion cell 5118 (red) and an unknown cell. **C,G,H.** CBb5w 6156 (copper) and wide-field cone bipolar cell 5283 (red) converge an axonal single-ribbon monad and axonal multiribbon monad, respectively, onto ipRGC 12208 (off white). Note the omega figure in the right subpanel of panel G. Wide-field cone bipolar cell 5283 forms an axonal cistern onto γAC 20537 (not shown in C, see Fig. 2.8, B-C) in the same plane of section as the four-ribbon axonal monad onto ipRGC 12208. **D,I,J,K,L.** CBb6 353 (red, left cell) and CBb6 447 (red, right cell) both form multiribbon axonal dyads (I,J) onto OFF-layer monostratified ganglion cell 21779 (silver) and another amacrine cell, amacrine cell 22210 (not shown inD for clarity,I) and amacrine cell 32273 (upper bright green cell in D, D inset,J), respectively. Amacrine cell 32273 creates both feedback (J, right subpanel) and feedforward (K) inhibition motifs via conventional synapses onto CBb6 447 and ganglion cell 21779, respectively. CBb6 447 also forms a single-ribbon axonal dyad in the ON IPL onto multistratified ganglion cell process 34336 (beige in D, D inset,L left subpanel) and amacrine cell 34337 (lower bright green cell in D, D inset,L left subpanel). Amacrine cell 34337 forms a conventional synapse onto ganglion cell 34336 (L right subpanel), thus completing a feedforward inhibition motif.
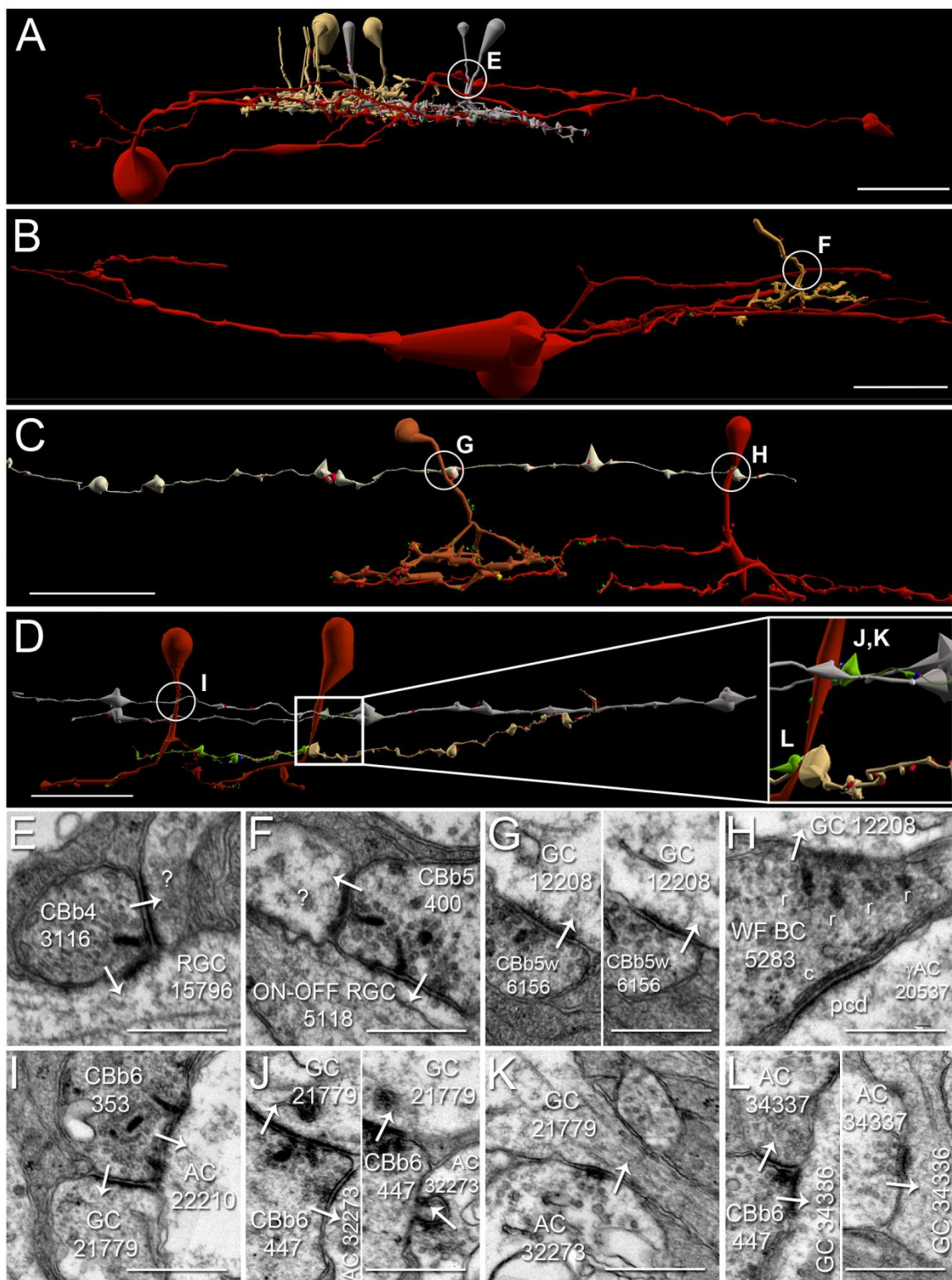
Figure 2.7. GAC axonal ribbon targets. **A-D**. Renderings of CBbs targeting both mono- and multistratified GACs with axonal ribbons, vertical orientation. Circles indicate locations of synapses shown in E-H. Scale bars, 10 μm**. E-H.** TEM of axonal synapses at locations indicated A-D. White arrows indicate synapse directionality. r, ribbons; scale bars, 0.5 μm**. I-L**. TEM of GAC somas. Scale bars, 5 μm. **M-P.** Glycine-positive signatures of the corresponding GAC somas in I-L. Scale bars, 5 μm. **A, E.** CBb6 4570 (red) forms a single-ribbon monadic reciprocal synapse with GAC 906 (patina). **B,F.** CBb5w 309 (copper) forms a single-ribbon monadic synapse onto GAC 310 (patina). **C,G.** CBb5w 6997 (copper) forms a single-ribbon axonal monad with GAC 5507. The ribbon is very light, but possesses the characteristic halo of clear vesicles, and both pre- and postsynaptic densities are visible. **D,H.** CBb5w 6156 (copper) forms a single-ribbon axonal monad with GAC 5575 (patina).
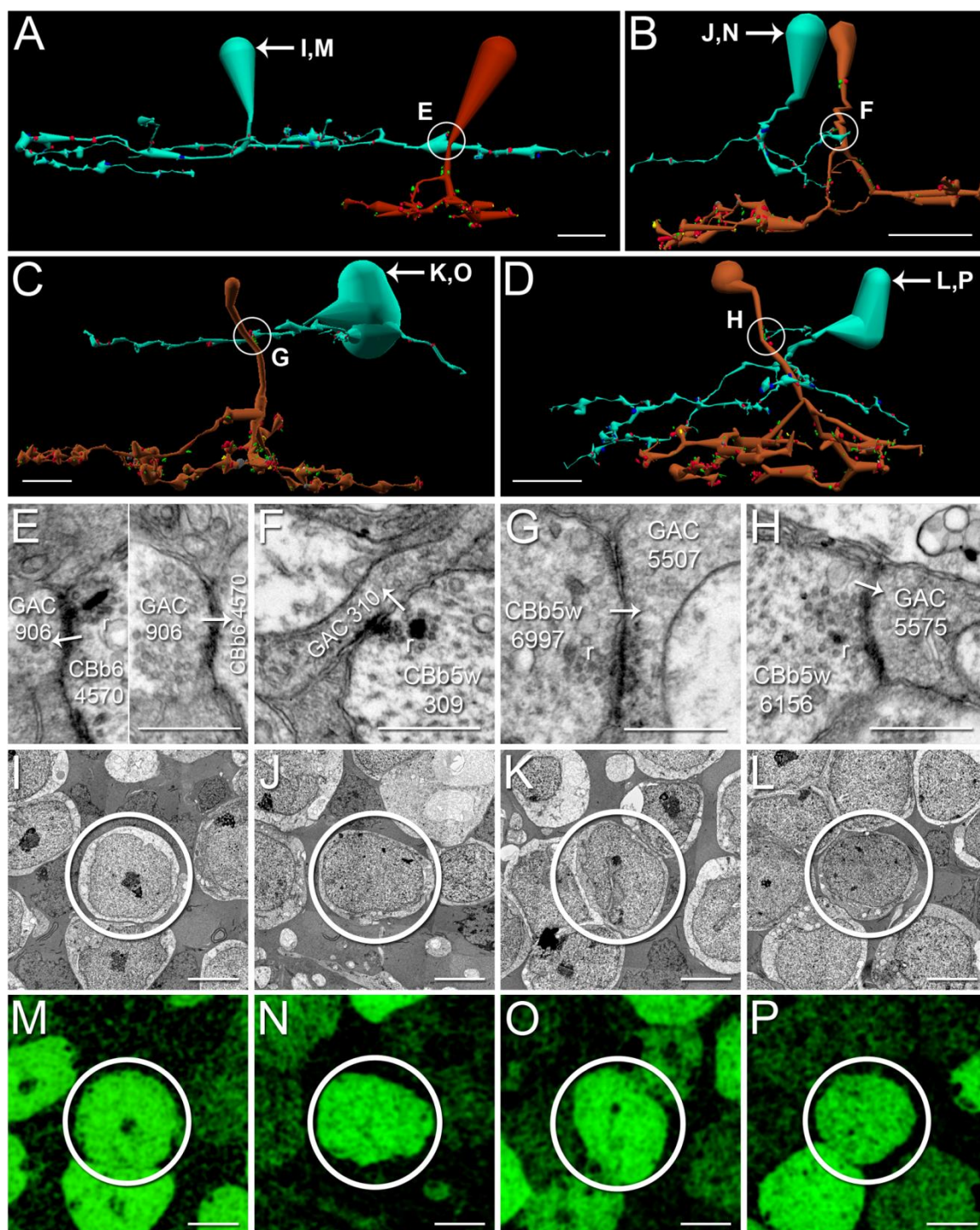
Figure 2.8. γAC axonal ribbon targets and axonal cisterns. **A-C.** Renderings of axonal-ribbon driven γACs mediating within- and cross-channel, divergent and convergent, inhibitory networks, vertical orientation (A-B), horizontal orientation (C). Arrows, locations of γ+ signatures shown in D-E; circles, locations of synapses shown in F-K; scale bars, 20 μm. **D-E.** TEM of γACs in A-C with corresponding γ+ signatures. Scale bar (D), 5 μm; scale bar (E), 0.5 μm. **F-K.** TEM of synapses indicated in A-C. White arrows indicate synapse directionality. AC, amacrine cell; WF BC, wide-field bipolar cell; r, ribbons; c, cistern; pcd, post-cisternal density; scale bars, 0.5 μm. **A.** CBb5 5562 (mustard, left) forms an axonal single ribbon monad onto multistratified γAC 5294 (silver, F). γAC 5294 forms a conventional synapse (A inset, G) onto CBb5 5645 (mustard, right), thus completing an axonal ribbon-mediated within channel inhibition motif. 5294's soma is γ+ (D). **B.** A chain of five CBbs converge and diverge axonal ribbon and cistern contacts onto common γAC and ganglion cell targets, vertical orientation. CBb6 5536 (red, right) provides divergent input to amacrine cell 19571process (silver) and wide-field γAC 20537(silver) with an axonal ribbon dyad (H) at locations indicated in C insets. Wide-field γAC 20537 is γ+ (E). Amacrine cell 19571 cannot be confirmed as γ+, but is glycine negative, and participates in nested feedback with γAC 20537 (H, right subpanel). CBb5 176 (mustard) and wide-field cone bipolar cell 5283 (deep red, center) converge axonal cistern contacts onto γAC 20537 (K, Fig. 2.6 H, respectively). In the same plane of section wide-field cone bipolar cell 5283 drives ipRGC 12208 with a four-ribbon axonal monad (Fig. 2.6 H). This ipRGC receives convergent axonal ribbon input from CBb5w 6156 (copper, Fig. 2.5 G). **C.** Horizontal view of B. Scale bar, 20 μm. (Left inset): Rotated and zoomed-in vertical view of the circled area in the main panel (some cells removed for clarity). CBb6 5536 (red) and wide-field cone bipolar cell 16026 (sand) provide convergent, branched axonal ribbon input to γAC 20537 (H left subpanel & I, respectively). This view looks down the length of γAC 20537 (silver) between wide-field cone bipolar cell 16026 in the right foreground and CBb6 5536 in the left background. Wide-field cone bipolar cell 5283 (red, right) can be seen close to wide-field cone bipolar cell 16026. Scale bar, 2.5 μm. (Right inset): Rotated and zoomed-in vertical view of CBb > γAC ≥ CBa crossover inhibition. CBb6 5536 (red) provides a branched axonal ribbon dyad onto amacrine cell 19571 (H, left subpanel). amacrine cell 19571 forms a conventional synapse (J) onto CBa2 5539 (green) nearby, thus completing the crossover inhibition motif. Scale bar, 5 μm.
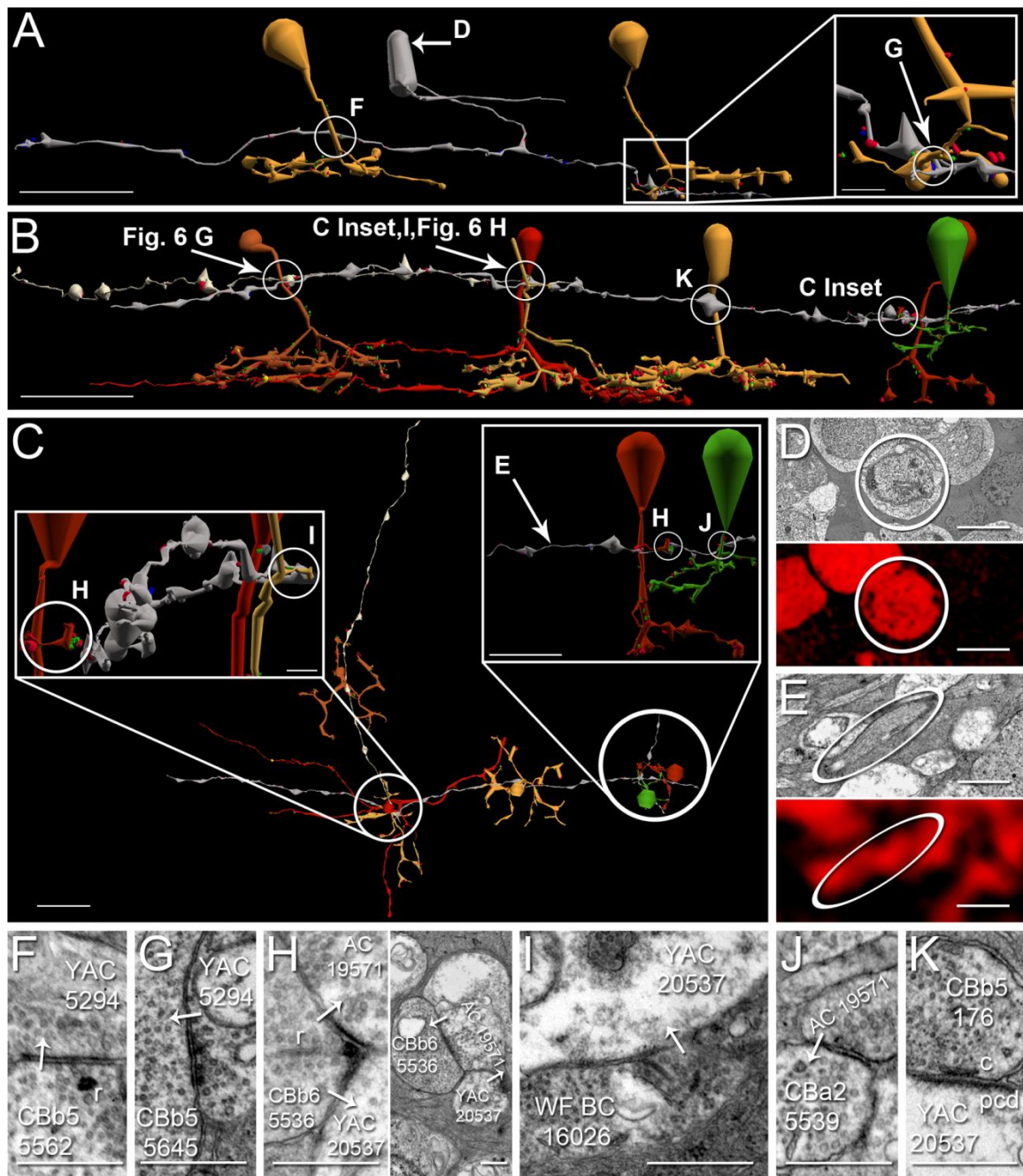
Figure 2.9. Novel network topologies mediate within- and cross-channel inhibition. **A-D.** Vertically orientated enderings of ON-OFF GAC construction and CBa > GAC ≥ CBb crossover inhibition (A), and CBb > GAC ≥ ganglion cell within- and crosschannel (crossover) inhibition motifs (B-D). Circles, location of synapses shown in E-J; scale bar (A), 10 µm; scale bar (A inset), 5 µm; scale bar (B-C), 20 µm; scale bar (D), 10 µm. **E-J.** TEM of synapses indicated by circles in A-D. White arrows indicate synapse directionality; GC,ganglion cell; scale bars, 0.5 µm. **A,E-F.** Axonal ribbon topologies employed for construction of a *monostratified*, ON-OFF GAC and CBa > GAC ≥ CBb crossover inhibition motifs. (**A Inset):** Rotated and zoomed in horizontal view of CBa2 424 (green), CBa2 478 (sage), GAC 906 (silver), and CBb6 4570 (red). CBa2 424 and CBa2 478 converge a single-ribbon monad and single-ribbon dyad onto GAC 906 (E & F, respectively). GAC 906 forms a conventional synapse onto CBb6 4570 (red), reciprocal to an axonal ribbon (Fig. 2.6 E) . **B,G-J.** Parallel CBb > GAC ≥ ON-OFF ganglion cell crosschannel inhibition, and divergent within- (CBb > GAC ≥ bsdGC) and crosschannel (CBb > GAC ≥ ON-OFF ganglion cell) inhibition. CBb6 4570 (red) drives GAC 906 (green) at the axonal synapse described in A. GAC 906 forms a conventional synapse onto monostratified ON-OFF ganglion cell 18693 (off-white, G). CBb5w 6156 (copper) drives narrow-field multistratified GAC 5575 (patina) with an axonal ribbon (Fig. 2.6 H). GAC 5575 forms conventional synapses onto monostratified ON-OFF ganglion cell 18693 at two locations (H,I). The above two synaptic chains thus form parallel CBb > GAC ≥ ON-OFF ganglion cell motifs that converge onto the same ganglion cell target. GAC 5575 also forms a conventional synapse onto bsdGC 15796 (sand, J), thereby creating divergent inhibitory motifs from CBb5w 6156 to two distinct classes of ganglion cell. **C,H-J.** Rotated zoom-in and isolation of divergent inhibition shown in B. Multistratified, narrow-field GAC 5575 (patina) receives axonal ribbon input from CBb5w 6156 (copper) at an OFF-layer branch (Fig. 2.7 H, not circled for anatomical clarity), and forms conventional synapses with ganglion cell 18693 (off-white,H-I) and bsdGC 15796 (sand, J). **D,H-J.** Zoom-in of GAC 5575 divergent inhibition in B-C for anatomical clarity and detail, better appreciation of network topologies, and synapse locations.

E

GAC
906

GAC
906

r

r

CBa2
424

F

GAC
906

GAC
27011

CBa2w
478

G

ON-OFF GC 18693

GAC
906

H

ON-OFF GC 18693

GAC
5575

I

ON-OFF GC 18693
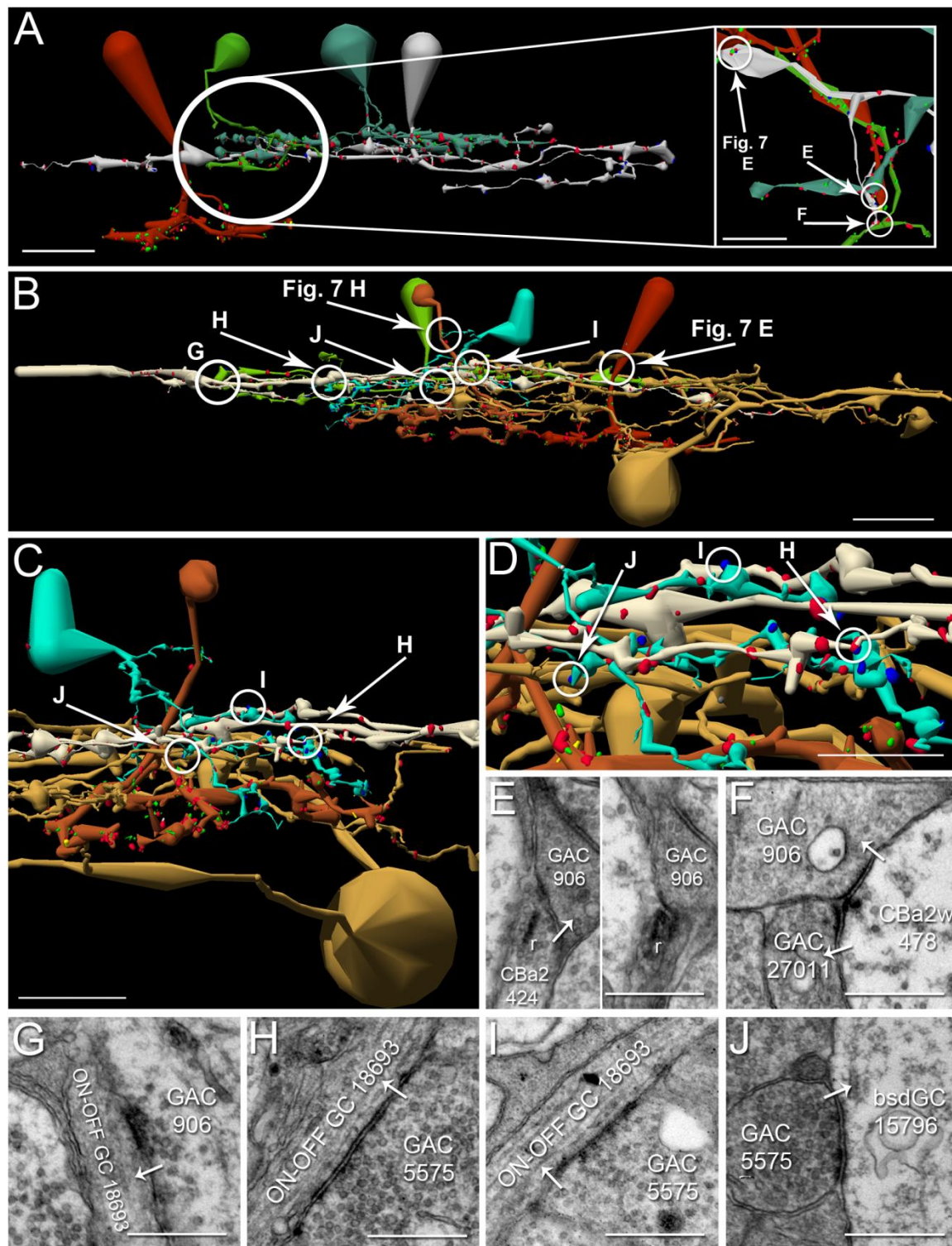
GAC
5575

J

GAC
5575

bsdGC
15796

Figure 2.10. CBb axon tangency to potential targets without axonal synapses. **A-B.** Renderings of CBbs with contact, but not synapses onto ganglion cells, vertical orientation. Circles, locations of synapses shown in C-D; scale bars, 20 µm. **C-D.** TEM of synapses indicated by circles in A-B. White arrows indicate synapse directionality; GC, ganglion cell; scale bars, 0.5 µm. **A,C.** CBb3 5513's (copper) axon is tangent (adjacent with no intervening muller glia) to OFF ganglion cell 13858 (sand), yet does not form a synapse. **B,D.**CBb4 3116 (silver) forms an axonal ribbon dyad onto bsdGC 15796 (D, Fig. 2.6 A & E) and an unknown target (D), whereas CBb4 4569 (dark mustard) does not form an axonal ribbon onto the same unknown target despite being tangent to it. Incidently, CBb4 3116 and CBb4 4569 are gap junctionally coupled (data not shown).
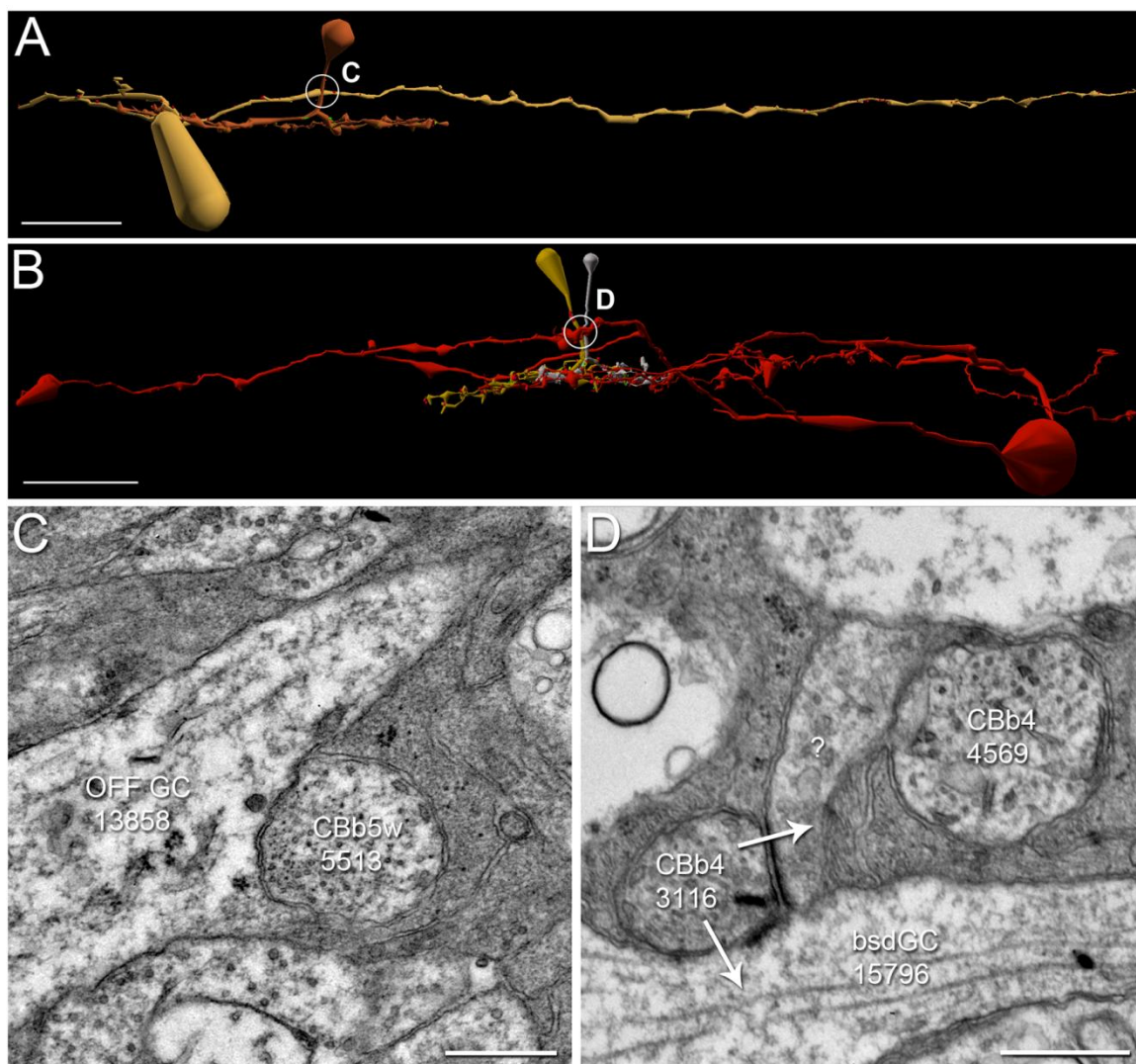
Figure 2.11. Interaction between sparse network topologies and joint distributions. **A.** An array of bipolar cell axons (white) traverses the image plane of the retina. In the top field, a cell class with high coverage is shown in different colors for every instance of the class. Each bipolar cell axon is contacted several times for an average contact of 2.4. **B.** Two different classes of ganglion cells (yellow, blue) form part of their tiling by sampling from the bipolar cell array. Most bipolar cells are missed, for an average outflow contact of 0.375, which is meaningless. Six circled bipolar cells are contacted by the ganglion cells (none twice), and the ganglion cells are errorless in contacting encountered bipolar cells. As ganglion cells are not space filling cells, further inputs would be superfluous.
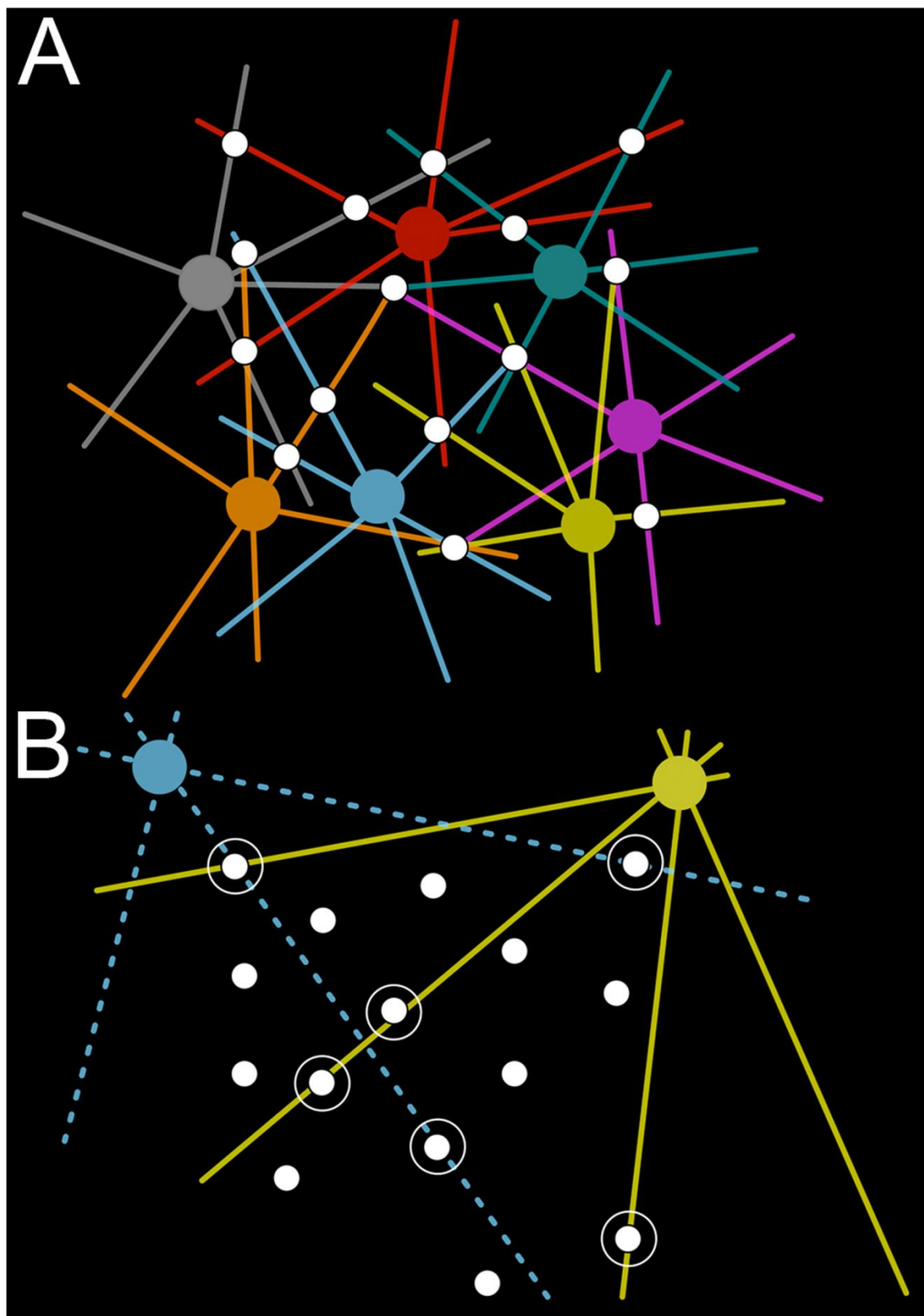
Figure 2.12. Axonal ribbon motifs summary semischematic. Wiring diagram for axonal ribbon motifs discovered across all cone bipolar cell classes in RC1 collapsed onto one representative cell. Spatial distributions of axonal ribbons have been preserved as best as possible to represent actual axonal ribbon locations. The axonal branch in sublamina 2 and the bifurcated descending axon are included for completeness, though both occur in a minority of cone bipolar cells.   Note that in addition to abundant axonal ribbon output, cone bipolar descending axons are frequently postsynaptic to amacrine cell inputs. S1-S6, IPL sublaminae 1-6; orange arrows, excitatory ribbon synapses; green flathead arrows, inhibitory GAC- or γAC-mediated synapses; GC, ganglion cell.
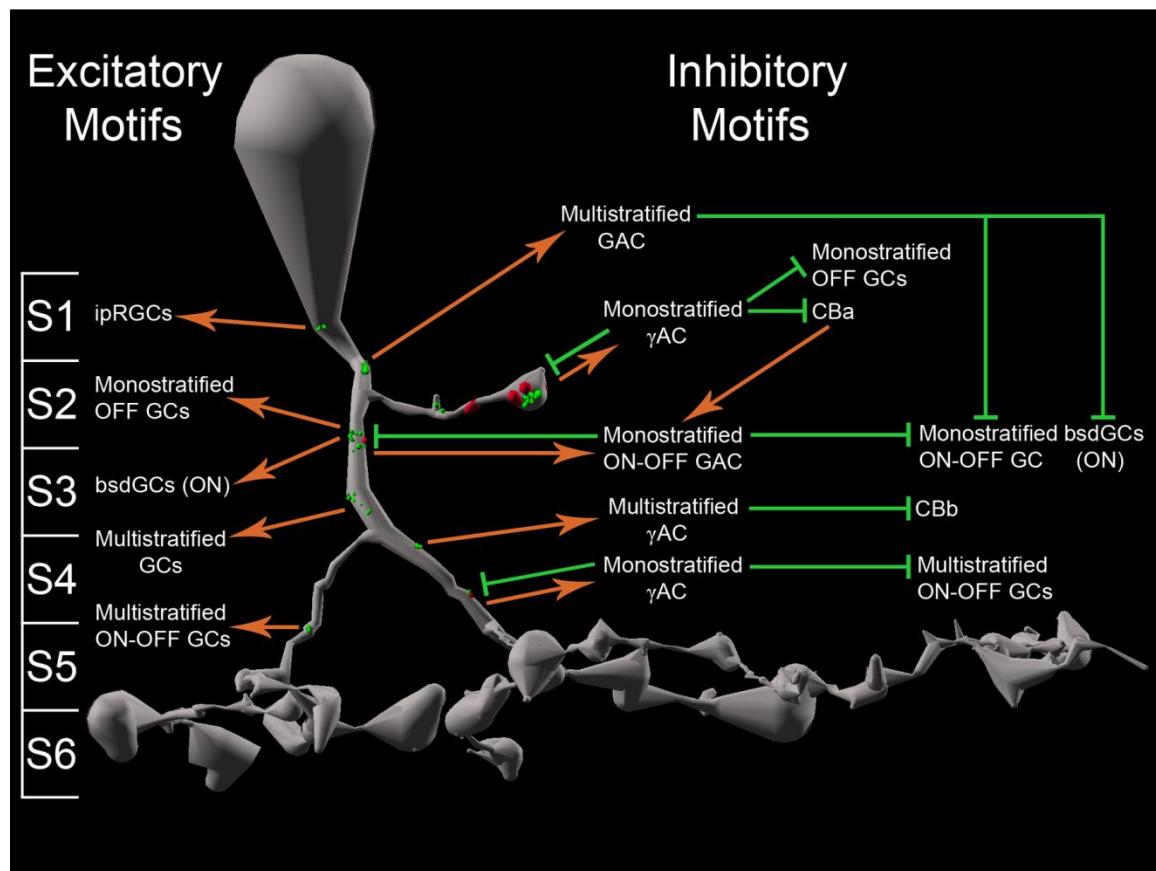
References

Aggelopoulos NC, Meissl H. 2000. Responses of neurones of the rat suprachiasmatic nucleus to retinal illumination under photopic and scotopic conditions. J Physiol 623:211-222.

Anderson JR et al. 2011a. Exploring the retinal connectome. Mol Vision 17:355-379.

Anderson JR et al. 2009. A computational framework for ultrastructural mapping of neural circuitry. PLoS Biol 7(3):e1000074.

Anderson JR et al. 2011b. The Viking viewer for connectomics: scalable multi-user annotation and summarization of large volume data sets. J Microscopy 241:13-28.

Briggman KL, Bock DD. 2011. Volume electron microscopy for neuronal circuit reconstruction. Curr Opin Neurobiol 22:1-8.

Calkins DJ et al. 1998. Microcircuitry and mosaic of a blue-yellow ganlion cell in the primate retina. J Neurosci 18(9):3373-3385.

Chavez AE, Diamond JS. 2008. Diverse mechanisms underlie glycinergic feedback transmission onto rod bipolar cells in the rat retina. J Neurosci 28:7919-7928.

Chen X et al. 2011. Amacrine-to-acacrine cell inhibition: Spatiotemporal properties of GABA and glycine pathways. Vis Neurosci 28:193-204.

Chun MH et al. 1993. Electron microscopic analysis of the rod pathway of the rat retina. J Comp Neurol 332:421-432.

Dacey DM et al. 2005. Melanopsin-expressing ganglion cells in primate retina signal colour and irradiance and project to the LGN. Nature 433:749-754.

Dumitrescu ON et al. 2009. Ectopic retinal ON bipolar cell synapses in the OFF inner plexiform layer: contacts with dopaminergic amacrine cells and melanopsin ganglion cells. J Comp Neurol 517:226-244.

Eggers E, Lukasiewicz P. 2011. Multiple pathways of inhibition shape bipolar cell responses in the retina. Vis neurosci 28:95-108.

Eggers ED, Lukasiewicz PD. 2006a. GABA(A), GABA(C), and glycine receptor-mediated inhibition differentially affects light-evoked signaling from mouse retinal rod bipolar cells. J Physiol 572:215-225.

Eggers ED, Lukasiewicz PD. 2006b. Receptor and transmitter release properties set the time course of retinal inhibition. J Neurosci 26:9413-9425.

Eggers ED, Lukasiewicz PD. 2010. Interneuron circuits tune inhibition in retinal bipolar cells. J Neurophysiol 103:25-37.

Eggers ED et al. 2007. Presynaptic inhibition differentially shapes transmission in distinct circuits in the mouse retina. J Physiol 582:569-582.

Famiglietti EV. 1981. Functional architecture of cone bipolar cells in mammalian retina. Vision Res 21:1559-1563.

Famiglietti EV et al. 1977. Neuronal Architecture of on and off pathways to ganglion cells in carp retina. Science 198(4323):1267-1269.

Famiglietti EV, Kolb H. 1976. Structural basis for ON- and OFF-center responses in retinal ganglion cells. Science 194(4261):193-195.

Fatima-Shad K, Barry PH. 1992. A patch-clamp study of GABA- and strychnine-sensitive glycine-activated currents in post-natal tissue-cultured hippocampal neurons. Proc Biol Sci 250(1328):99-105.

Ghosh KK et al. 2001. Glutamate receptors in the rod pathway of the mammalian retina. J Neurosci 21:8636-8647.

Gold MR, Martin AR. 1984. Gamma-Aminobutyric acid and glycine activate Cl-channels having different characteristics in CNS neurones. Nature 308(5960):639-641.

Graham D et al. 2008. Melanopsin Ganglion Cells: A bit of fly in the mammalian eye. Webvision: The Organization of the Retina and Visual System [Internet] Salt Lake City (UT): University of Utah Health Sciences Center; 1995-2008 Aug 01.

Hoshi H et al. 2009. ON inputs to the OFF layer: bipolar cells that break the stratification rules of the retina. J Neurosci 29(28):8875-8883.

Jeon CJ, Masland RH. 1995. A population of wide-field bipolar cells in the rabbit retina. J Comp Neurol 360:403-412.

Kolb H. 1982. The morphology of the bipolar cells, amacrine cells and ganglion cells in the retina of the turtle Pseudemys scripta elegans. Philos Trans R Soc Lond B Biol Sci 298(1092):355-393.

Kolb H et al. 1990. The synaptic organization of the dopaminergic amacrine cell in the cat retina. J Neurocytol 19(3):343-366.

Kolb H et al. 1992. Neurons of the human retina: a Golgi study. J Comp Neurol 318(2):147-187.

Liang Z, Freed M. 2010. The ON pathway rectifies the OFF pathway of the mammalian retina. J Neurosci 30(16):5533-5543.

Linberg KA et al. 1996. Retinal neurons of the California ground squirrel, Spermophilus beecheyi: a Golgi study. J Comp Neurol 365:173-216.

MacNeil M et al. 2004. The population of bipolar cells in the rabbit retina. J Comp Neurol 472:73-86.

Manookin MB et al. 2008. Disinhibition combines with excitation to extend the operating range of the OFF visual pathway in daylight. J Neurosci 28:4136-4150.

Marc RE. 1986. Neurochemical stratification in the inner plexiform layer of the vertebrate retina. Vision Res 26(2):223-238.

Marc RE, Jones BW. 2002. Mjolecular phenotyping of retinal ganglion cells. J Neurosci 22:413-427.

Marc RE et al. 2012. Building Retinal Connectomes. Current Opinion in Neurobiology.

Marc RE, Liu WL. 2000. Fundamental GABAergic amacrine cell circuitries in the retina: nested Feedback, concatenated inhibition, and axosomatic synapses. J Comp Neurol 425:560-582.

Marc RE et al. 1995. Pattern recognition of amino acid signatures in retinal neurons. J Neurosci 15:5106-5129.

Mariani AP. 1982. Biplexiform cells: ganglion cells of the primate retina that contact photoreceptors. Science 216:1134-1136.

Masland RH. 2001. Neuronal diversity in the retina. Curr Opin Neurobiol 11(4):431-436.

McGuire B et al. 1984. Microcircuitry of bipolar cells in cat retina. J Neurosci 4(12):2920-2938.

Molnar A et al. 2009. Crossover inhibition in the retina: circuitry that compensates for nonlinear rectifying synaptic transmission. J Comput Neurosci 27:569-590.

Molnar A, Werblin F. 2007. Inhibitory feedback shapes bipolar cell responses in the rabbit retina. J Neurophysiol 98(6):3423-3435.

Ostergaard J et al. 2007. Synaptic contact between melanopsin-containing retinal ganglion cells and rod bipolar cells. Invest Ophthalmol Vis Sci 48:3812-3820.

Pang JJ et al. 2004. Stratum-by-stratum projection of light response attributes by retinal bipolar cells of Ambystoma. J Physiol 558:249-262.

Ramon y Cajal SR. 1892. La rétine des vertébrés. Cellule 9:121-225.

Roska B et al. 2006. Parallel processing in retinal ganglion cells: how integration of space-time patterns of excitation and inhibition form the spiking output. J neurophysio 95:3810-3822.

Roska B, Werblin F. 2003. Rapid global shifts in natural scenes block spiking in specific ganglion cell types. Nature Neurosci 6:600-608.

Scholes J. 1975. Colour receptors, and their synaptic connexions, in the retina of a cyprinid fish. Philos Trans R Soc Lond B Biol Sci 270(902):61-118.

Scholes J, Morris J. 1973. Receptor—bipolar connectivity patterns in fish retina. Nature 241(5384):52-54.

Sherry DM, Yazulla S. 1993. Goldfish bipolar cells and axon terminal patterns: a Golgi study. J Comp Neurol 329(2):188-200.

Strettoi E et al. 1990. Synaptic connections of rod bipolar cells in the inner plexiform layer of the rabbit retina. J Comp Neurol 295(3):449-466.

Tian N. 2008. Synaptic activity, visual experience and the maturation of retinal synaptic circuitry. J Physiol 586(18):4347-4355.

Tsukamoto Y et al. 2001. Microcircuits for night vision in mouse retina. J Neurosci 21:8616-8623.

Umino O et al. 1994. The network properties of bipolar-bipolar cell coupling in te retina of teleost fishes. Vis Neurosci 11(3):533-548.

Wagner HJ, Wagner E. 1988. Amacrine cells in the retina of a teleost fish, the roach (Rutilus rutilus): a Gogi study on diferentiation and layering. Philos Trans R Soc Lond B Biol Sci 321(1206):263-324.

Wässle H et al. 2009. Cone contacts, mosaics, and territories of bipolar cells in the mouse retina. J Neurosci 29(1):106-117.

Wässle H et al. 1991. The rod bipolar cell of the mammalian retina. Visual Neuroscience 7(1-2):99-112.

Werblin F. 2010. Six different roles for crossover inhibition in the retina: Correcting the nonlinearities of synaptic transmission. Vis Neurosci 27:1-8.

Werblin F, Dowling JE. 1969. Organization of the retina of the mudpuppy, Necturus maculosus. II. Intracellular recording. J Neurophysiol 32(3):339-355.

Wong KY, Dowling JE. 2005. Retinal bipolar cell input mechanisms in giant danio. III. ON-OFF bipolar cells and their color-opponent mechanisms. J Neurophysiol 94:265-272.

Wong KY et al. 2007. Synaptic influences on rat ganglion-cell photoreceptors. J Physiol 582:279-296.

Zhang J et al. 2002. Confocal analysis of reciprocal feedback at rod bipolar terminals in the rabbit retina. J Neurosci 22(24):10871-10882.

CHAPTER 3

DIFFUSELY-STRATIFIED OFF CONE BIPOLAR CELL

INPUTS TO AMARINE CELLS IN THE

ON INNER PLEXIFORM LAYER

Abstract

Analysis of the rabbit retinal connectome RC1 reveals a class of diffusely-stratified OFF cone bipolar cells (dsOFF CBCs) that synaptically target amacrine cells in the ON inner plexiform layer (IPL). This network architecture constructs a large zone of comingled ON and OFF cells in IPL sublaminae 3-5, indicating that the mammalian inner plexiform layer is not as discretely segmented as previously thought. Current tenets assert that the monostratified bipolar cells of the mammalian retina require multistratified amacrine cells to mediate ON-OFF crosstalk, since ON and OFF cone bipolar cell axonal arbors putatively occupy distinct domains in the inner plexiform layer. Nonetheless, recent studies demonstrated the capacity of ON cone bipolar cells to violate the mammalian IPL stratification rules with axonal synapses in the OFF IPL, and a subset of OFF CBCs with primary axons longer than some ON CBC primary axons (Anderson et al., 2011a; Dumitrescu et al., 2009; Hoshi et al., 2009; Lauritzen et al., 2013). Our goal was to confirm the comingling of ON and OFF CBC synapses in the ON IPL with automated transmission electron microscopy (ATEM), and identify the targets of the dsOFF CBC synapses in ON territory.

Introduction

A canon of the mammalian retinal research community is that ON and OFF channels occupy discrete domains within the mammalian inner plexiform layer (IPL), with OFF cells that depolarize to light decrements stratified in the distal 40% of the IPL and ON cells that depolarize to light increments stratified in

the proximal 60% of the IPL (Famiglietti et al., 1977; Famiglietti and Kolb, 1976; MacNeil et al., 2004a; Wässle et al., 2009; Werblin and Dowling, 1969). For nearly forty years, this paradigm stood. Nevertheless, examples of nominal CBCs breaking the mammalian IPL stratification rules were recently reported (Anderson et al., 2011a; Dumitrescu et al., 2009; Hoshi et al., 2009; Lauritzen et al., 2013). Indeed, many nonmammalian BC classes multistratify, with axonal outputs in both the OFF and ON sublayers (Kolb, 1982; Pang et al., 2004; Ramon y Cajal, 1892; Scholes, 1975; Scholes and Morris, 1973; Sherry and Yazulla, 1993; Wong and Dowling, 2005). Moreover, axonal ribbons were occasionally reported by researchers, but never systematically qualified and quantified (Famiglietti, 1981; Jeon and Masland, 1995; Kolb et al., 1990; Kolb et al., 1992; Linberg et al., 1996; Mariani, 1982; McGuire et al., 1984). Finally, the existing bipolar cell classification scheme developed by MacNeil et al. (2004b) illustrates that CBa1-2n OFF bipolar cells marginally encroach on the ON IPL. As such, there is motivativation to further investigate the extent to which other classes of bipolar cells might violate the canonical IPL stratification rules. These results impelled us to comprehensively classify a suspected cohort of OFF CBCs that synapse in the ON sublayer of the IPL.

All retinal cells discovered with distinct morphologies have thus far proven to possess distinct physiological properties (Masland, 2001b). On this basis, the gross morphologies of cells have routinely served as the means by which to classify different retinal cell types, with level of IPL arborization purposing the cells' physiological roles. Scientists have used these methods to create lists of

candidate cells that may or may not have synaptic connections, based on the presence or absence of costratification within the IPL. Nonetheless, light microscopy lacks the resolution to resolve functional synapses and the finest neural processes, and previous anatomical methods (including serial section approaches) underreport synapses; thus, much of the connectivity within the retina has been missed.

With new connectomics approaches, using automated transmission electron microscopy (ATEM) at 2.18 nm resolution, metabolic fingerprinting, synaptic connectivity analyses, and 3D renderings of cells, it is possible to reconstruct functional anatomical networks that were impossible to see before. Synaptic connections are often assumed to exist between cells that costratify within the IPL. Yet Anderson et al. (2011a) showed neural apposition without synaptic contact to be the dominant mode in the IPL, so costratification can only provide locations of possible, not guaranteed, connectivity between and two cells. The ability to resolve functional synapses and fine neural processes at the ultrastructural level to obtain absolute network groundtruth allows us to solve this problem.

Here, we confirm that a subset of OFF cone bipolar cells indeed multistratify across the traditional IPL boundary, and establish functional synapses at the same IPL depth as nearest neighbor ON CBCs, constituting a new OFF cone class. To consistently extend the MacNeil et al. (2004a) bipolar cell classification scheme, we name these cells CBabs. A major role of these CBabs is to provide OFF input synapses to ON layer monostratified amacrine

cells, thus constructing ON-OFF amacrine cells in the nominal ON IPL. These CBabs further scaffold γAC- and GAC-based network motifs capable of passing ON-OFF inhibition to polarity-matched and polarity-opposite bipolar and ganglion cells. These motifs are consistent with within and crosschannel feedback as well as within- and crosschannel feedforwad. Since unique neural morphology typically represents unique physiological properties ((Masland, 2001b), these diffusely-stratified CBabs likely represent a discrete functional component of ON-OFF signaling in the mammalian retina.

Methods

Tissue

Connectome volume RC1 was assembled from a light-adapted female Dutch Belted rabbit (Oregon Rabbitry, OR) after *in vivo* excitation mapping as described in Anderson et al. (2011a) in accord with Institutional Animal Care and Use protocols of the University of Utah, the ARVO Statement for the Use of Animals in Ophthalmic and Visual Research, and the Policies on the Use of Animals and Humans in Neuroscience Research of the Society for Neuroscience.

Computational Molecular Phenotyping (CMP)

Retinal neurons in RC1 were classified by CMP per Marc and Jones (2002) by using an array of small-molecule signatures (4-aminobutyrate [GABA], glycine , L-glutamate, L-glutamine, taurine, and the activity marker 1-amino-4-guanidobutane [AGB]). Briefly, the isolated rabbit eye was hemisected and

immersion-fixed overnight in 1% paraformaldehyde, 2.5% glutaraldehyde, 3% sucrose, 0.01% CaCl2, in 0.1 M phosphate buffer, pH 7.4. Tissues were then dehydrated in graded methanols and acetone and embedded in epoxy resin. Tissues were then serial sectioned at 70-90 nm onto 12-spot Teflon-coated slides (Cel Line, Fisher Scientific, Waltham, MA). Antibody exposure and silver intensification is described below under antibody characterization. Incubation of all antibodies generated against small-molecular targets was performed overnight at room temperature, and visualization was with goat anti-rabbit secondary IgG coated with 1.4 nm gold (Amersham, Arlington Heights, IL) and silverintensified (Kalloniatis and Fletcher, 1993).

Small-Molecular Antibody Characterization

Anti-hapten IgGs from Signature Immunologics (Salt Lake City, UT; Table 2.1) have been extensively characterized in prior publications (Marc et al., 1995; Marc, 1999a,b; Marc and Cameron, 2002; Marc and Jones, 2002). Each is an IgG isotype (determined by affinity chromatography and immunoblotting) produced in rabbit hosts immunized with glutaraldehyde-amino acid conjugates to bovine serum albumin (BSA) as described in Marc et al. (1995). Five analysis types were used to characterize the specificity and detectivity of each anti-hapten IgG: 1) dependence on target molecule trapping; 2) immunodot assays against cognate small molecule–protein conjugates; 3) competition assays against free and bis-conjugates of small molecules (Table 2.2); 4) binding curves on quantitative artificial antigen stacks; and 5) cluster analysis (Marc et al., 1995).

RC1 Assembly, Analysis, and Sharing

Bipolar cell networks in the ultrastructural rabbit retinal connectome RC1 (Anderson et al., 2011a) were annotated with the Viking viewer (Anderson et al., 2011b), and explored via 3D rendering and graph visualization of connectivity (Anderson et al., 2011b). Small molecule signals embedded in RC1 for computational molecular phenotyping (CMP) include 4-aminobutyrate, glycine, L-glutamate, L-glutamine, taurine, and the activity marker 1-amino-4-guanidobutane (AGB). Combined with morphological reconstruction, CMP permits robust bipolar cell classification (Anderson et al., 2011a). RC1 was acquired by ATEM at 2.18 nm resolution and assembled into a volume with the NCRToolset (Anderson et al., 2009). Molecular-ultrastructural registrations were generated with ir-tweak (Anderson et al., 2011a; Anderson et al., 2009; Anderson et al., 2011b). 3D renderings are built from disk annotations in Vikingplot (Anderson et al., 2011b), allowing rendering of surfaces and characterization of areas and volumes. All cells rendered in this paper are publicly available as Google Collada *.dae files via the Connectome Viz application. These can be imported into 3D visualization tools such as Collada or Blender (http://www.blender.org). One defect in converting disk topologies to volumes for rendering of tapered processes sometimes led to somas or varicose neurites with vertically peaked shapes. These anomalies will be repaired in future code sets. Networks were visualized as directed multigraphs with Connectome Viz, and topologies explored with Structure Viz (Anderson et al., 2011b). The RC1 dataset and these associated analytical tools are publically available at

connectomes.utah.edu. Quantitative features of connections (numbers of synapses, axon dimensions, etc.) can be queried within these various tools and with Microsoft SQL.

Identification of IPL layers

The ON-OFF border of the IPL is not absolute and we adopted a structural reference to define the transition between zones dominated by OFF and ON cone bipolar cells. In practice, the axial location of the ON-OFF border was set as most proximal surface of the A_{II} AC lobule nearest a given bipolar cell. The OFF layer was defined as the region between the most distal GABA+ (γ+) processes and the ON-OFF border. Similarly, the ON layer was defined as the region between the most proximal γ+ processes and the ON-OFF border. For simplicity, we refer to these regions as the ON and OFF layers, corresponding to the older but less descriptive sublamina a and sublamina b, respectively. As in previous work, we define the amacrine cell layer - IPL border as level 0 and the ganglion cell layer - IPL border as level 100 (Marc, 1986).

Cell Classification

All cells were classified using three criteria: molecular signatures, synaptic connectivity, and morphology. Bipolar cells were further subclassified according to their stratifications within the IPL, compared to the rabbit bipolar cell classification scheme outlined by MacNeil et al. (2004a). An itemization of the rules required for cell identity follows. Table 2.4 lists abbreviations used throughout this chapter.

<u>Rules for bipolar cells</u>. Virtually all bipolar cells possess ribbon synapses. Their somas reside in the inner nuclear layer (INL) and they are glutamate-positive. Glycine-positive (G+) bipolar cells coupled to A_{II} AC arboreal dendrites via gap junctions and stratified in the proximal 60% of the IPL were classified as ON cone bipolar cells with their precise level of stratification used to further refine their class memberships (CBb3, CBb3n, CBb3-4, CBb4, CBb5, CBb6, wide-field cone bipolar cell, and rod bipolar cell). Anderson et al. (2011a) showed that quantitative G+ signatures are an absolute discriminator of bipolar cell :: A_{II} AC coupling. Glycine-negative (G-) bipolar cells that stratified in the distal 40% of the IPL and were both presynaptic and postsynaptic to A_{II} AC appendages were defined as OFF cone bipolar cells, with their precise level of stratification used to further refine their class (CBa1, CBa1w, CBa1-2, CBa1-2n). Bipolar cells with G-signatures stratified in most proximal IPL, presynaptic to A_{II} AC arboreal dendrites, neither postsynaptic nor coupled to them, and presynaptic and postsynaptic to $\gamma+$ A_I ACs were classified as rod bipolar cells. There are 104 rod bipolar cells in RC1. These independent classifiers are, collectively, errorless (Anderson et al., 2011a). There are instances where CBa and CBb terminals (never rod bipolar cells) make synaptic contacts lacking classical synaptic ribbons. We call these bipolar cell conventional synapses, and they occur in terminals with numerous ribbons at other sites. One glutamate-positive bipolar cell class (CBa1w) is presynaptic and postsynaptic to A_{II} ACs but lacks ribbons and only makes bipolar cell conventional synapses. These cells are not

discussed in this paper as they are not involved with the characterization of axonal synapses.

Rules for CBabs. CBabs satisfy the molecular and network criteria for CBas (glycine-negative and chemical synapses with A_{II} AC lobular appendages in the most distal 40% of the IPL), yet deviate morphologically from canonical OFF cone bipolar cells by diffusely arborizing alongside CBb processes in the proximal 60% of the IPL.

Rules for amacrine cells. Amacrine cells possessed conventional synapses only (not ribbon synapses) with somas residing in the INL, except for ON starburst amacrine cells whose somas reside in the ganglion cell layer. G and γ signals further refined their classification as GACs and γACs. Cells with moderate glycine signals, presynaptic lobular appendages in the OFF IPL, and coupled and postsynaptic arboreal dendrites in the ON IPL were defined as A_{II} ACs.

Rules for ganglion cells. Ganglion cells discussed in this paper were glutamate-positive, lacked presynaptic specializations, were never postsynaptic to rod bipolar cells and had somas placed in the GCL or processes that traversed the entire volume. Based on cone bipolar cell input patterns they were further classified as ON, OFF, or ON-OFF. Some classes were also γ+ to differing extents (Marc and Jones, 2002) due to amacrine cell coupling.

Image Preparation

As described in our prior papers on connectomics (Anderson et al., 2009), display TEM images in this paper were produced by remapping RC1 volume tiles to gamma 1.3. Optical and TEM overlays used the TEM greyscale brightness combined with the hue, and saturation from the optical image as described in Anderson et al. (2011a). 3D versions and network maps of annotated cells were generated in Vikingplot and Viz applications (Anderson et al., 2011b).

Results

We mined the axonal arbors of all OFF bipolar cells, identified those that comingle with ON bipolar cell telodendria, and reconstructed the synaptic connectivity of said OFF arbors in ON territory. Table 2.3 contains a legend for the color scheme used to represent synapse types in all 3D reconstructions displayed throughout this manuscript. All cell identification numbers used in this manuscript are identifiers that can be invoked in Viking, VikingPlot, and Viz tools (Anderson et al., 2011a) to validate all of the ultrastructural features, network motifs, and statistics we report here. RC1 is an open-source, open-access, open-data resource.

CBabs Arborize More Proximally in the IPL than Their

OFF CBC Cohorts

One hundred four of 400 CBCs (26%) in the RC1 volume are OFF CBCs, four of which are semicomplete traces as their processes exit the volume, thus

preventing more refined classification. Of the remaining 100 OFF CBCs, 10 have yet to be classified, 21 are CBa1s, 1 is a CBa1w, 2 are CBa1-2s, 1 is a CBa1-2n, 26 are CBa2s, 4 are CBa2ws, and 35 diffusely arborize more proximally into the IPL than their OFF CBC cohorts, where they comingle with ON CBC axonal arbors and synaptically target GACs and YACs. For consistent extension of the McNeil et al., 2004 rabbit BC classification scheme, we hereafter refer to these dsOFF CBCs as CBabs. Subsets of CBabs establish multitiered territories across OFF and ON layers, as deep as layer 6; thus, we identify these as CBab 2-3, CBab2-4, CBab2-5, and CBab2-6.

CBabs Exit the Canonical OFF IPL

When viewed against each other (Figure 3.1), the telodendria of the 35 CBabs in RC1 can be seen to clearly extend more proximally into the IPL than their OFF CBC cohorts. Laminae 1 and 2 are visible by plotting CBa1s, CBa1ws, and CBa2s against each other. Collectively, these cells establish the nominal OFF IPL (Figure 3.1 A-B). This demonstrates that the CBab axonal processes exit the canonical OFF IPL, and form synapses in territories inaccessible to other OFF CBCs. A zoom of some of these processes (Figure 3.1 C) shows clearly that CBab telodendria extend more proximally into the IPL than the other classes of CBas, thus exiting the canonical OFF IPL. This yields opportunities for synaptic partnership with a greater variety of cell classes than that which is possible by the other CBas.

CBabs Enter the Canonical ON IPL

By viewing the CBabs against all CBbs, it becomes clear that not only are the OFF CBCs exiting canonical OFF territory, they enter canonical ON territory (Figure 3.2). The axonal arbors, rife with ribbon synapses and postsynaptic densities, comingle with CBb axonal arbors. The CBabs can be seen to ramify at different depths throughout the ON IPL (Figure 3.2 A). A zoom of some of these processes shows clearly that CBab telodendria costratify with CBbs, often extending as deep as sublamina 6 (Figure 3.2 B-C). Thus, they are *bona fide* multistratified OFF bipolar cells that span both OFF and ON IPL laminae.

CBabs Costratify with Nearest Neighbor CBbs

How can we be certain that these multistratified bipolar cells are functionally OFF (hyperpolarizing to light increments)? As described in the methods section, we verified that all CBas are glycine negative, chemically synaptic to A_{II} AC lobules, and stratify in the outer 40% of the IPL. The CBabs satisfy the first two criteria, but their morphology deviates from the defined criteria. Indeed, that is precisely how we discovered the CBabs; they satisfy all criteria for a CBa cell except morphology. The glycine signatures and chemical synapse with A_{II} AC lobules of three representative CBabs are shown in Figure 3.3 D-F, H-J, L-N. Despite satisfying the glycine signature and A_{II} AC connectivy criteria for CBa identity, the CBabs costratify with CBbs and establish functional synaptic contacts in the ON IPL. We show both the three-dimensional reconstructions (Figure 3.3 A-C) as well as TEM sections displaying functional

synapses formed by CBabs in the same plane of section as nearest-neighbor ON CBCs (Figure 3.3 G, K, O).

γAC Targets

CBabs form ribbon synapses onto both mono- and multistratified wide-field γACs in the nominal ON IPL. The γACs often form reciprocal conventional synapses, creating feedback inhibition motifs (Figure 3.6). Three γAC targets of CBabs in the ON IPL are presented here. Each of the γAC targets forms only conventional synapses, and is confirmed as both GABA-positive and glycine-negative (Figure 3.4 D-O).

First, CBab2-5 3928, CBab2-5 458, and CBab2-5 359 all form reciprocal synapses with multistratified, ON-OFF γAC 115 in the ON IPL (Figure 3.4 A, Figure 3.6 E-G). It is worth note that despite the multistratification of γAC 115 in both the OFF and ON laminae, it only intersects with the three CBabs in the ON laminae where it forms the synaptic contacts. It is, however, presynaptic to two other CBabs in the nominal OFF IPL. Thus, this ON-OFF γAC receives its OFF input from both the OFF and ON layers.

Second, monostratified ON-OFF wide-field γAC 5453 possesses a reciprocal synapse with CBab2-5 5543 deep in the ON layer at the lamina 5-6 region (Figure 3.4 B, Figure 6 J-K). The synaptic topology is interesting, as γAC 5453 actually receives two ribbon monadic inputs from CBab 5543. γAC 5453 participates as one half of a ribbon dyad recipient to CBab 5543 input twice in the

same plane of section. Furthermore, the other target for one of these two dyads is a GAC described more fully in the "GAC targets" section.

Third, monostratified ON-OFF wide-field γAC 16073 receives synaptic input from two CBabs in the mid-IPL. CBab2-4 6046 and CBab2-4 each form ribbon synapses onto γAC 16073 in ON sublamina 3 (Figure 3.4 C, Figure 3.6 L-M). This γAC communicates with both the ON and OFF lamina via monostratification in the mid-IPL, an architecture also discovered in GACs involved in CBb axonal ribbon crossover inhibition motifs (Lauritzen et al., 2013).

GAC Targets

CBabs are both pre- and postsynaptic to GACs in the ON IPL (Figure 3.5). CBabs form synapses with ON layer monostratified ON-OFF GACs and multistratified ON-OFF GACs. Each GAC target was verified as both glycine-positive and GABA-negative (Figure 3.5, D-O). CBabs 458 and 5543 form reciprocal synapses with multistratified GAC 7703. Three examples are describe here.

First, CBab2-5 5504 makes a reciprocal synapse with ON layer monostratified ON-OFF GAC 8035 (Figure 3.5 A; Figure 3.7 A, E). The tight monostratification of GAC 8035 deep in lamina 5 of the ON IPL emphasizes the point that the OFF input to this ON-OFF cell could not arise from CBa1s or CBa2 restricted to the traditional OFF IPL. Unfortunately, the soma for GAC 8035 did not cross a section in the volume with a glycine label, so the glycine signature

obtained for this cell was obtained from its ON layer process with a small diameter and therefore less reliable.

Second, CBab 2-4 6046 forms a reciprocal synapse with ON layer 3-4 monostratified ON-OFF GAC 7134 (Figure 3.5 B; Figure 3.7 H). GAC 7134 is a distinct class of narrow-field GAC from GAC 8035, as evidenced by the smaller arbor and dense branching pattern. Thus, at least two classes of ON layer monostratified GACs are synaptically targeted by CBabs.

Third, multistratified ON-OFF GAC 7703 forms reciprocal synapses with CBab2-6 458 and CBab2-6 5543 (Figure 3.5 C; Figure 3.6 J; Figure 3.7 C, J-L). Of note is the fact that neither CBab forms synapses with GAC 7703 in the OFF layer. Rather, they only synaptically connect in the ON IPL. CBab 458 and GAC 7703 processes contact each other repeatedly throughout both the OFF and ON laminae and form several synapses in both layers. The synapse highlighted here is the deepest between the two cells, and resides in the ON IPL.

CBab-Driven Within- and Crosschannel Inhibition Motifs

Amacrine cells targeted by CBabs mediate feedback and feedforward, within- and crosschannel inhibition motifs consistent with the electrophysiological literature yet achieved via unpredicted architectures, including synaptic contacts in the ON IPL. They construct ON-OFF amacrine cells, create within channel (OFF>OFF) feedback and feedforward motifs, and create crosschannel (OFF>ON and ON>OFF) feedback and feedforward motifs. Often, they achieve

these motifs by breaking the canonical stratification rules to gain access to monostratified amacrine cells. Detailed descriptions of specific motifs follow.

γAC-Mediated Within- and Crosschannel Feedback

Inhibition Motifs

First, multistratified ON-OFF γAC 115 forms reciprocal synapses with CBab2-5 3928, CBab2-5 458, and CBab2-4 359 (Figure 3.6 A, E-G) between ON sublayers 3-5. This constitutes a CBab within-channel inhibition motif. γAC 115 also receives ribbon drive from CBb5 5608 (Figure 3.6 A, D), thus forming a CBb $>_i$ ON-OFF γAC ≥ CBab crosschannel inhibition motif.

Second, monostratified γAC 5453 makes reciprocal synapses with CBb6 6129 and CBab-2-5 5543 (Figure 3.6 B, H-K). This creates a bidirectional CBb ≤ $>_i$ ON-OFF γAC $_i$< ≥ CBab crosschannel inhibition motif. Since γAC 5453 monostratified in ON sublaminae 5-6, it is inaccessible to other CBas. Only CBabs have the possibility of synaptic contact.

Finally, CBab 6046 and CBab 5538 drive wide-field ON-OFF γAC 16073 with ribbon synapses (Fig 3.7 C, L-M). γAC 16073 is further presynaptic to CBb3 909, CBb5 1021, and CBb5 307, and postsynaptic to CBb5 307 (data not shown due to steric limitations and for clarity of 3D rendering). The combination of ON and OFF ribbon inputs classify γAC 16073 as an ON-OFF cell that constructs CBab $>_i$ ON-OFF γAC ≥ CBb crosschannel inhibition motifs. It is further interesting that γAC 16073 diverges its output to at least two distinct classes of CBb, CBb3 and CBb5, respectively.

GAC-Mediated Within- and Crosschannel Feedback

Inhibition Motifs

First, ON layer monostratified ON-OFF GAC 8035 makes a reciprocal synapse with CBab2-5 5504 in IPL sublamina 5 (Figure 3.7 A, E). CBb5 6118 also provides a ribbon input in lamina 5, thus GAC 8035 is an ON-OFF GAC which constructs a CBb >ᵢ ON-OFF GAC ≥ CBab crosschannel feedback motif.

Second, ON layer monostratified ON-OFF GAC 7134 forms reciprocal synapses with CBb4 5501 and CBab 6046; thus, it is an ON layer monostratified ON-OFF GAC (Figure 3.7 B, H-I). Due to the reciprocal synapses, GAC 7134 mediates a bidirectional CBab ≤ >ᵢ ON-OFF γAC ᵢ< ≥ CBb crosschannel feedback inhibition motif.

Third, narrow-field GAC 7703 makes reciprocal synaptic contacts with CBab 458, CBab 5543, CBb 440, and CBb 6129 (Figure 3.6 J; Figure 3.7 C, J-O). CBb 440 is gap junctionally coupled to CBb 431. This constitutes both within- and crosschannel feedback motifs. Importantly, despite the multistratification of GAC 7703, the synapses between the CBabs and the GAC occur in IPL strata 5 rather than in the OFF IPL. Furthermore, ON layer monostratified YAC 5453 constructs parallel within and crosschannel inhibition motifs via reciprocal synapses between CBab 5543 and CBb 6129. Note that the CBab could not access the monostratified YAC were it not multistratified deep into canonical ON territory. Finally, it is interesting that CBb6 440 participates in a chain of twenty-four coupled CBbs (data not shown). This chain spans all CBb classes, which are coupled in a tiered fashion across the RC1 volume. This

could spread the otherwise narrow-field ON-OFF inhibition from GAC 7703 to a larger patch of retina to extend its functional range.

γAC-Mediated Within- and Crosschannel Feedforward

Inhibition Motifs

In addition to the CBab ribbon input described above, monostratified ON-OFF wide-field γAC 16073 forms conventional synapses onto multistratified ON-OFF ganglion cell 8575 and bsdGC 15796 (Figure 3.6 C, N-O). Thus, γAC 16073 forms a divergent feedforward ON-OFF inhibition motif to two classes of ganglion cell. This means that γAC 16073 could provide parallel copies of its ON-OFF inhibition to two classes of ganglion cell.

GAC-Mediated Within- and Crosschannel Feedforward

Inhibition Motifs

ON-OFF GAC 7703 described in the within- and crosschannel inhibitory feedback motifs above also feeds forward to ON-OFF ganglion cell 8575 (Figure 3.7 D, P). Thus GAC 7703 is capable of integrating convergent differential cone bipolar cell drive from multiple classes of bipolar cell, and distributing this complex ON-OFF inhibition to ON-OFF ganglion cells. The two GAC-mediated feedforward motifs above demonstrate narrow-field ON-OFF inhibition distributed to ON and ON-OFF ganglion cells.

CBabs Provide Direct Ganglion Cell Drive in the ON IPL

CBabs directly drive at least one class of ganglion cell in the nominal ON IPL. For instance, CBab2-5 5543 and CBab2-5 5543 each form ribbon synapses onto multistratified ON-OFF ganglion cell 8575 in IPL sublayer 5 (Figure 3.8 A-C, F). Furthermore, CBab 5543 and CBab 458 drive narrow-field feedforward inhibition to ganglion cell 8575 via GAC 7703, shown above. This demonstrates that individual CBabs, not simply members of the same class, both excitatorily drive targets and regulate the postsynaptic membrane of the same targets via feedforward inhibition motifs in the ON IPL. Finally, It is interesting that ganglion cell 8575 multistratifies across the canonical OFF and ON IPL, but receives OFF input in the ON layers. This is addressed in the discussion section.

Convergent and Divergent Feedforward Inhibition

to Ganglion Cells

By isolating points of synaptic interconnectivity, we can concatenate subnetworks into larger networks. Interestingly, the CBab-driven narrow-field GAC and wide-field γAC described in feedback inhibition motifs above converge synapses onto multistratified ON-OFF ganglion cell 8575 (Figure 3.7 P; Figure 3.6 N; Figure 3.8 A, F). Additionally, γAC 16073 diverges its output across ON-OFF ganglion cell 8575 and bsdGC (ON) 15796 (Figure 3.6 N-O; Figure 3.8 A, F). This combination of narrow-field GAC-mediated inhibition and wide-field γAC -mediated inhibition illustrates the complexity of the feedforward inhibition controlling individual ganglion cell postsynaptic membrane potential, and

illustrates that individual γACs diverge their inhibitory outputs to multiple classes of ganglion cell. Thus, CBabs provide OFF excitatory drive in the ON IPL to amacrine cells that inject ON-OFF inhibition to multiple classes of ganglion cell.

CBab-Driven Nested Feedback Inhibition

In addition to the simple feedback inhibition motifs described above, CBab-driven GACs and γACs construct nested feedback inhibition motifs. In the context of the IPL, biologically nested feedback manifests as excitatory drive from one bipolar cell to two amacrine cell targets, A1 and A2. A1 and/or A2 provide direct simple feedback inhibition to the bipolar cell, and A1 or A2 also provides inhibition to the other amacrine cell. This is exactly the motif we find. Specifically, both CBabs and CBbs provide direct ribbon synapses to GAC 7703, γAC 5453, and γAC 115 (Figure 3.8 F). All three amacrine cells form reciprocal conventional synapses onto the bipolar cells presynaptic to them. Additionally, GAC 7703 forms conventional syanpses onto both γAC 5453 and γAC 115 (Figure 3.8 D-F), thus completing parallel nested feedback motifs.

Discussion

The routine appearance of mixed signaling strata combined with precise source-target synaptic pairings, regardless of lamination, suggests that rules of proper connectivity override stratification of plexiform layers. The discovery of diffusely-stratified OFF cone bipolar cells in the ON IPL extends new organizational concepts regarding neural architectures underlying ON and OFF

signaling, thereby generating a refactoring of the IPL. We here review key signaling features of specific CBab motifs, the joint incidence of source-target processes, the erosion of our classical notion of segregated ON-OFF processing streams in the IPL, and discuss the functional implications. Bipolar cell nomenclatures differ across species and we will now be discussing several; we periodically depart from the McNeil et al. (2004) rabbit scheme for the discussion and simply refer to cone bipolar cells as ON cone bipolar cells and OFF cone bipolar cells. We often describe CBabs more generally as diffusely-stratified OFF cone bipolar cells.

Throughout vertebrate evolution, every nonmammalian class possessed multistratified ON and OFF bipolar cells (Kolb, 1982; Pang et al., 2004; Ramon y Cajal, 1892; Scholes, 1975; Scholes and Morris, 1973; Sherry and Yazulla, 1993; Wong and Dowling, 2005). The ON and OFF layers were never completely segregated, but the overt branching patterns of ON and OFF cone bipolar cells in polarity-opposite strata became subdued for reasons unknown. Now, the recent discovery of routine ON cone bipolar cell axonal synapses in the OFF IPL (Lauritzen et al., 2013) combined with dsOFF CBC synaptic communication in the ON IPL explicate the importance of mixed strata. However, more concretely, functional mixing reflects important network access properties. CBab ribbons in the proximal 60% of the IPL provide OFF inputs to ON-OFF ganglion cells and unique ON layer monostratified amacrine cells, facilitating ON-OFF crosstalk. Ultimately, there is no unique proximal ON stratum in the IPL. Indeed, all but the most proximal 20% of the ON IPL is a stack of mixed ON-OFF strata with CBab

synaptic contacts distributed throughout (Figure 3.9). We propose that OFF signals in the ON layer provide unique network opportunities for crossover signaling and loci for mixing OFF excitation with polarity-matched ON inhibition.

Not all CBas invade the ON territory. Source-target neurite analyses for CBabs and other synaptic pairings suggests that the retina routinely invokes partial motifs. The concept of joint distributions of source-target incidence described in detail by (Lauritzen et al., 2013) provides a geometric proof that cells with different space filling properties (e.g., dense/overlapping arbors versus sparse/tiled arbors) will not always yield smooth statistics. Simply stated, the important statistics describe *target* sampling from a given potential supply of sources. It is not possible to optimize a complex biological system to provide 100% source contacts for all cells, given that the copy numbers for each class (i.e., each *ultimate* cell class, Marc and Jones (2002)) varies, as do their coverages and Hausdorff dimensions. Therefore, the only metric that matters is the efficiency of *target* sampling. This is critical for understanding connectivity between cells with different space filling and coverage properties, such as bipolar cells, amacrine cells, and ganglion cells. Their target sampling is perfect. Not all axons are hit because there is an oversupply of sources. The target does not "know" that there are excess source axons since they are not needed. Thus, participation of a subset of OFF cone bipolar cell synapses in ON territory represents the synaptic requirement of targets cells, not the sources. It does not reflect imprecision. The key descriptor for such networks is the joint density

distribution of source and target, expressed as a metric of signal transfer sites per unit area or volume of neural space.

Source-Target Pairings Regardless of Lamination

Why would a multistratified ON-OFF ganglion with processes in the OFF IPL need to collect OFF input in the ON layers? We do not completely understand, but we believe it is likely a matter of contact incidence between correct synaptic partners (i.e., correct partners will form synapses anywhere they contact, regardless of stratification).

It is worth note that despite the multistratification of γAC 115 in both the OFF and ON laminae, it only intersects with the three CBabs in the ON laminae where it forms the synaptic contacts. It is, however, presynaptic to two other CBabs in the nominal OFF IPL. Taken together with the OFF layer CBa2 synaptic communication, this suggests that this γAC will form synapses with OFF bipolar cells anywhwere it contacts them regardless of lamination.

CBabs Constitute a New Morphological Bipolar Cell Class

CBabs clearly adopt multistratified territories, that cross the canonical IPL ON-OFF boundary. Given the decades of literature supporting structure-function relationships, it is justifiable to expect that this subset of OFF cone bipolar cells possesses unique physiological response properties. Whether or not other mammalian retinas contain a similar class remains to be seen. Unique markers for this cell class could help distinguish this, but ultimately, comparative

neuroanatomy should be perfomed as connectome volumes for additional species are created. The first retinal connectome in mouse is currently being assembled which will allow us to directly recapitulate and extend findings discovered with light microscopy in genetically engineered mice.

It is clear that these OFF cone bipolar cells can access monostratified amacrine cells in the canonical ON IPL that are inaccessible by the OFF cone bipolar cell classes. The motifs reported in this manuscript demonstrate repeatedly that multistratified OFF cone bipolar cells can facilitate ON-OFF crosstalk by contacting monostratified amacrine cells, though multistratified amacrine cells are synaptically engaged in this process as well. This yields a new host of possible network architectures that mediate ON-OFF crosstalk that are not currently considered when interpreting physiological data.

CBabs May Be Identical to CBa1-2ns

It is likely that many of these CBabs are the same as the CBa1-2n cells identified by MacNeil et al. (2004a), which are illustrated with arbors as proximal as lamina 3. The processes that extend more proximally into laminae 4-5 may have been missed due to the lower resolution of light microscopy. The degree of axonal arbor diffusion should correlate with response property complexity. Regardless of incomplete annotations of CBas (i.e., fine processes may have been missed, 10 cells not fully classified), the transition from lamina 2 to lamina 3 is clearly distinguishable (Figure 3.1; Figure 3.2) via CBa2 and CBb3 arbors. CBa2 telodendria end and CBb3 telodendria begin at the canonical ON-OFF

boundary (40% IPL depth). Also, total IPL thickness is measurable by plotting nearest neighbor CBa1s-CBb6s and ro bipolar cells in any given region for calibration. Due to partial annotation, our estimate of CBab/CBb comingling is necessarily and underestimate. This motif is more prevalent than we report here.

Parallel Glycinergic and GABAergic Inhibition

The repeated finding of parallel GAC- and γAC-mediated inhibition (Figure 3.6, 3.7, 3.8) indicates not only redundancy in the system, it suggests a design that capitalizes on the differential kinetics of GABAA, GABAC, and glycine receptors. Synaptic targets that receive presynaptic input from both GACs and γACs, and also possess receptors for both of these neurotransmitters could create more complex response properties in their postsynaptic membrane potentials than cells with responses mediated exclusively by one of these neurotransmitter/receptor combinations. This could mediate more faithful representations of the photic input in the retinal sector stimulated, increase the range of stimuli capable of affecting the postsynaptic cell, or control selective filtering of the photic signals passed to ganglion cells and deeper into the central visual pathways.

CBab-Driven Convergent and Divergent, Simple and Nested,

Feedback and Feedforward Inhibition Motifs

Cases of synaptic convergence involving multiple classes of presynaptic cells (Figure 3.6, 3.7, 3.8) indicate the combining of multiple parallel pathways

into one postsynaptic membrane potential. Given that every tested class of retinal cell identified based on unique morphology has proven to possess unique physiological responses (Masland, 2001b), we can derive some basic functional implications from the network motifs discovered in RC1. For instance, when multiple classes of cell converge synaptic input to a common target, this presumably constructs a postsynaptic cell with more complex response properties than a cell that receives convergent drive from cells of the same class. Conversely, divergent output from one cell class to multiple postsynaptic targets establishes parallel processing streams. When the postsynaptic cells are of the same class, this creates parallel pathways carrying the same signal. When the postsynaptic cells are of more than one class, then presumably they extract different components of the presynaptic input, such as transient versus sustained, depending on which receptor types they express on the postsynaptic membrane immediately opposite the presynaptic input (Awatramani and Slaughter, 2000; Devries, 2000; Freed, 2000; Masland, 2001a).

Analysis of RC1 reveals CBab-driven networks that scaffold ON-OFF cross inhibitory processes via feedback and feedforward motifs. Alternating synaptic chains of GACs and γACs arranged in nested feedback motifs emerge. Long chains of amacrine-amacrine synapses were previously discovered in RC1 (Anderson et al., 2011a), but the precise network motifs remained to be discovered, and modeling has shown that nested feedback can improve the fine-tuning of bipolar cell presynaptic frequency-response characteristics (Marc and Liu, 2000). Here, we take the analysis one step forward by identifying specific

functional (crossover) motifs constructed by GACs and γACs involved in refinement of the input signal ultimately passed to ON-OFF ganglion cells. The narrow-field and wide-field components of the GAC and γAC feedback may represent spatially fine-grain and course-grain tuning of the ganglion cell input. As other local networks constructed, these data can help parse out the source of unique ganglion cell response properties.

CBabs Are Routine Network Elements Throughout the

Canonical ON IPL

CBabs synapse with amacrine cells throughout IPL sublaminae 3-5, emphasizing their routinity and potential impact on all ON cone bipolar cell classes. The dominant CBab theme is construction of ON-OFF amacrine cells in the ON IPL that are inaccessible to other OFF cone bipolar cells. The excitatory motifs provide direct ribbon drive to at least one class of ganglion cell. The inhibitory motifs comprise both feedback and feedforward as they target GACs and γACs, which in turn form synapses onto CBas, CBbs, and at least two classes of ganglion cell. It seems that by breaking the classical stratification rules of the IPL the CBabs facilitate specific ON-OFF subnetworks that could not otherwise be constructed. These unpredicted network topologies can facilitate interpretation of electrophysiological results, and introduce testable hypotheses for future inquiry.

Refactoring the IPL Functional Strata

Lauritzen et al. (2013) indicated mixed ON-OFF processing in the distal 40% of the rabbit IPL. The data presented here extend mixed ON-OFF strata proximally into the IPL by another 40% from the canonical ON-OFF boundary, creating mixed ON-OFF strata in the distal 80% of the IPL, consistent with BC stratification patterns in nonmammalians. The same ON-OFF CBC excitatory drive is partitioned into GAC and γAC-mediated parallel channels that target the same ganglion cells, which presumably defines the transiency and sustainability of the response properties of the ganglion cell targets. γAC -mediated ON-OFF inhibition is distributed to multiple classes of ganglion cell (ON-OFF and ON (bsdGCs)), distributing common signals to differentially specialized targets. The establishment of bipolar cell axonal arbors in polarity opposite territory increases the potential source-target combinations, and may be necessary for efficient sampling of presynaptic signals by ganglion cells in order to develop correct response properties. Collectively, these results erode current concepts of segmented ON-OFF processing in the IPL strata, with promise to improve interpretation of electrophysiological results. Future analyses will focus on mapping the complete input cohort for specific classes of amacrine and ganglion cells to more accurately account for their physiological response properties. Ultimately, connectomics on multiple volumes is needed to conduct comparative neuroanatomy across species and better understand the corrupt networks of pathological states.

Acknowledgments

Figure 3.1. CBabs exit the OFF IPL. **A.** Vertically oriented renderings of 35 CBabs (bright green) with telodendria in the ON IPL plotted against 32 CBas (cool colors). Cone bipolar cell color corresponds to depth of IPL stratification as follows: CBa1, sage; CBa2, green; CBab, bright green. **B.** Same cells as in A, except all CBa1s and CBa2s are collapsed to mustard color to enhance contrast against CBabs. **C.** Zoom in of the division between CBa1 and CBa2 depth versus CBab depth. CBab processes can be clearly seen to extend more proximally into the IPL than their CBa1 and CBa2 cohorts. Scale bar (A-B), 25 μm. Scale bar (C), 5 μm.
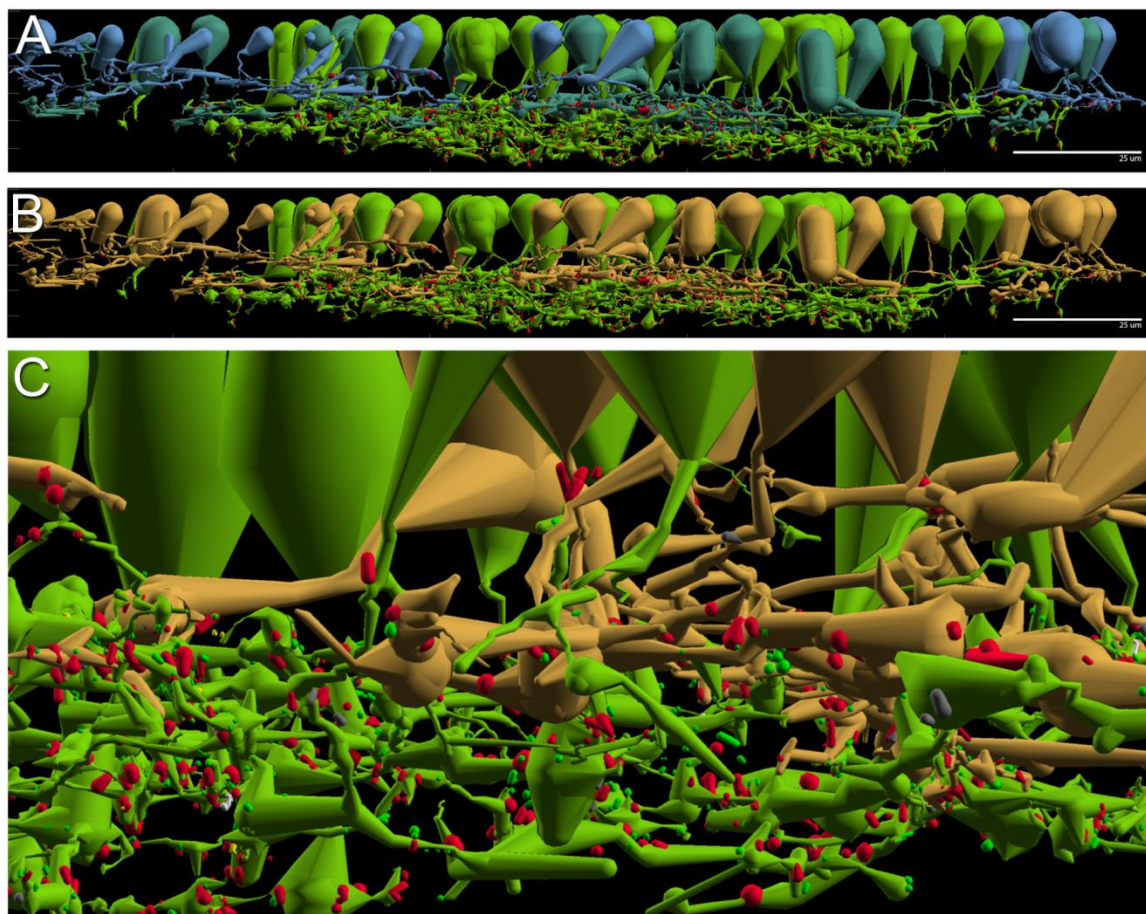
Figure 3.2. CBabs enter the ON IPL. **A.** Vertically oriented renderings of 35 CBabs (bright green) with telodendria in the ON IPL plotted against 71 CBbs (neutral and warm colors). Cone bipolar cell color corresponds to depth of IPL stratification as follows: CBab, bright green; CBb3, tan; CBb3-4, dark mustard; CBb4, silver; CBb5, mustard; CBb6, bright red; wide-field cone bipolar cell, deep red. **B.** Same cells as in A, except all CBbs are collapsed to copper color to enhance contrast against CBabs. The upper (distal) edge of CBb telodendria demarcates the canonical OFF-ON division of the IPL. **C.** Zoom in of the CBab versus CBb telodendria for clarity of CBab depth. CBab processes can be clearly seen to comingle with CBb arbors in the ON IPL. Scale bar (A-B), 25 μm. Scale bar (C), 5 μm.
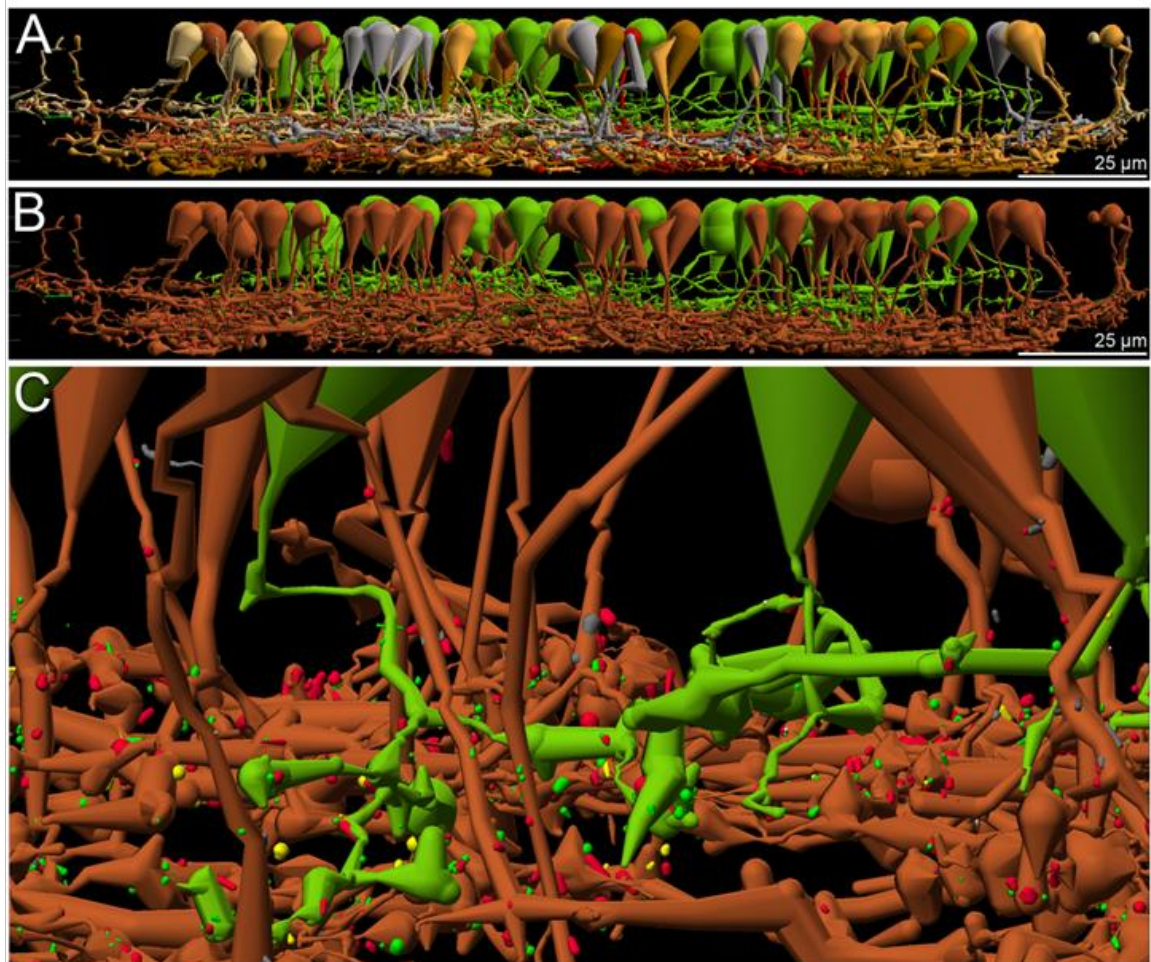
Figure 3.3. CBabs costratify with nearest neighbor ON CBCs. **A-C.** Vertically oriented renderings of 3 CBabs against their nearest neighbor CBbs. Cone bipolar cell color corresponds to depth of IPL stratification as follows: CBab, bright green; CBb3, tan; CBb3-4, dark mustard; CBb4, silver; CBb5, mustard; CBb5w, copper; CBb6, deep red (B) for contrast against CBb5ws, & brown (C). **D-E,H-I,L-M.** Glycine-negative molecular signatures and corresponding TEM of CBab somas, for CBabs shown in A-C. F,J,N. Chemical synapses between A$_{II}$ ACs and CBabs shown in A-C. **G,K,O.** TEM of CBab processes and CBb processes with forming synapses in the same IPL plane of section. Sections thickness, 70nm. **A.** CBab2-4 181 costratifies with CBb4 arbors, and marginally with the distal portion of CBb5 arbors. **B.** CBab2-5 458 costratifies with CBb5w arbors, and marginally with the distal portion of CBb6 arbors. **C.** CBab2-5 5543 costratifies with the distal portion of CBb6 arbors. Zoom in of the CBab versus CBb telodendria for clarity of CBab depth. CBab processes can be clearly seen to comingle with CBb arbors in the ON IPL. White arrows indicate synapse directionality. r, ribbons. Scale bars (A-C), 10 µm. Scale bars (D-E, H-I, L-M), 5 µm. Scale bars (F,J,N), 0.5 µm. Scale bars (G), 0.5 µm. Scale bars (J), 1 µm. Scale bars (N), 2.5 µm.
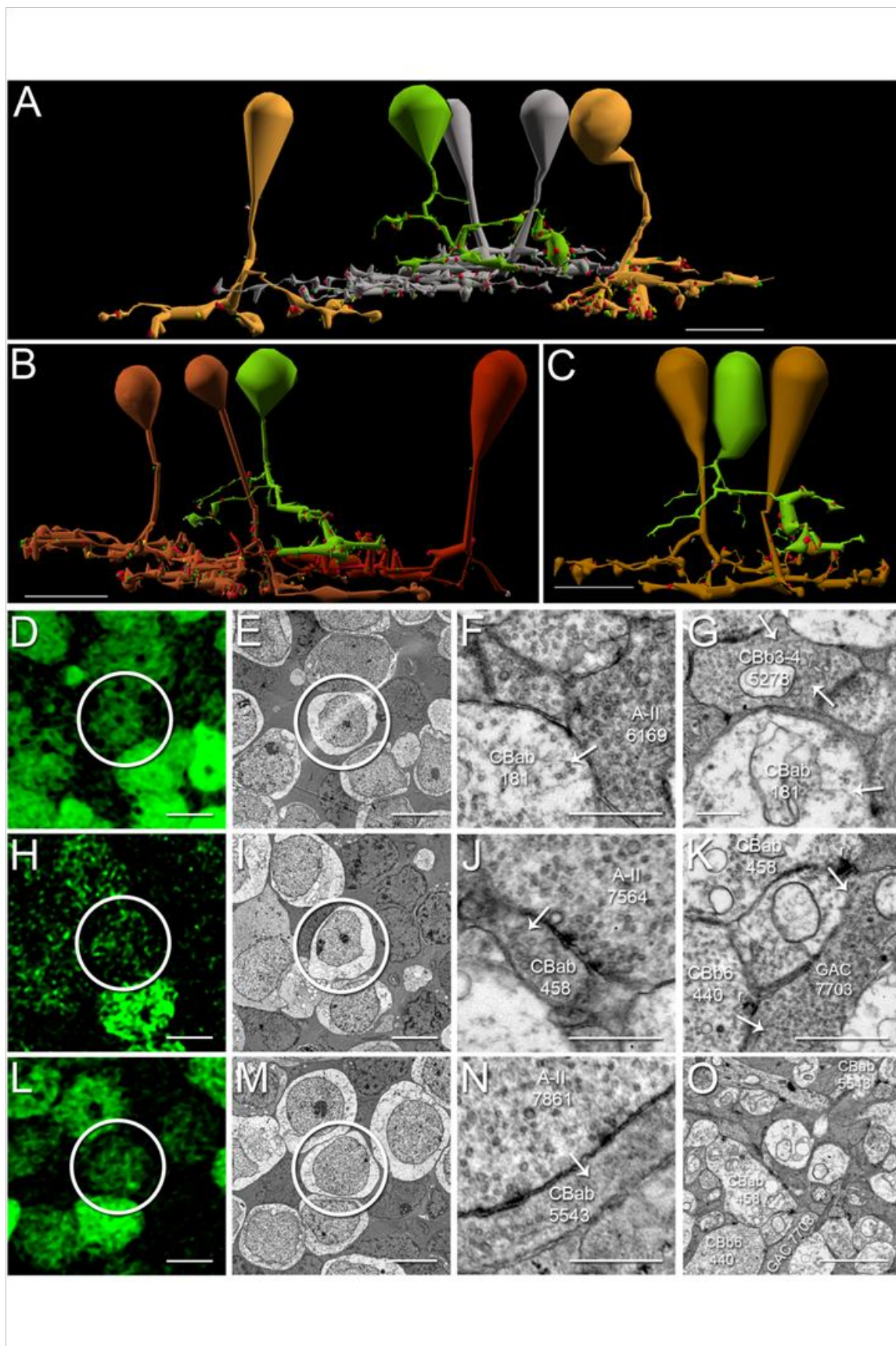
Figure 3.4. CBabs target γACs in the ON IPL. **A-C**. Vertically oriented renderings of CBabs targeting both mono- and multistratified γACs in the ON IPL. Circles, locations of synapses between CBabs and γAC s. Arrows, locations from which GABA and glycine signatures were obtained for D-O. **D-E,H-I,L-M.** GABA-positive signatures and corresponding TEM of somas or processes for γAC<u>s</u> shown in A-C. **F-G,J-K,N-O.** Glycine-negative signatures and corresponding TEM of somas or processes for γAC<u>s</u> shown in A-C. G. γAC 115 displays moderate glycine levels. Scale bars (A-C), 10 μm**.** Scale bars (D-K), 5 μm**.** Scale bars (L-O), 1 μm**.**
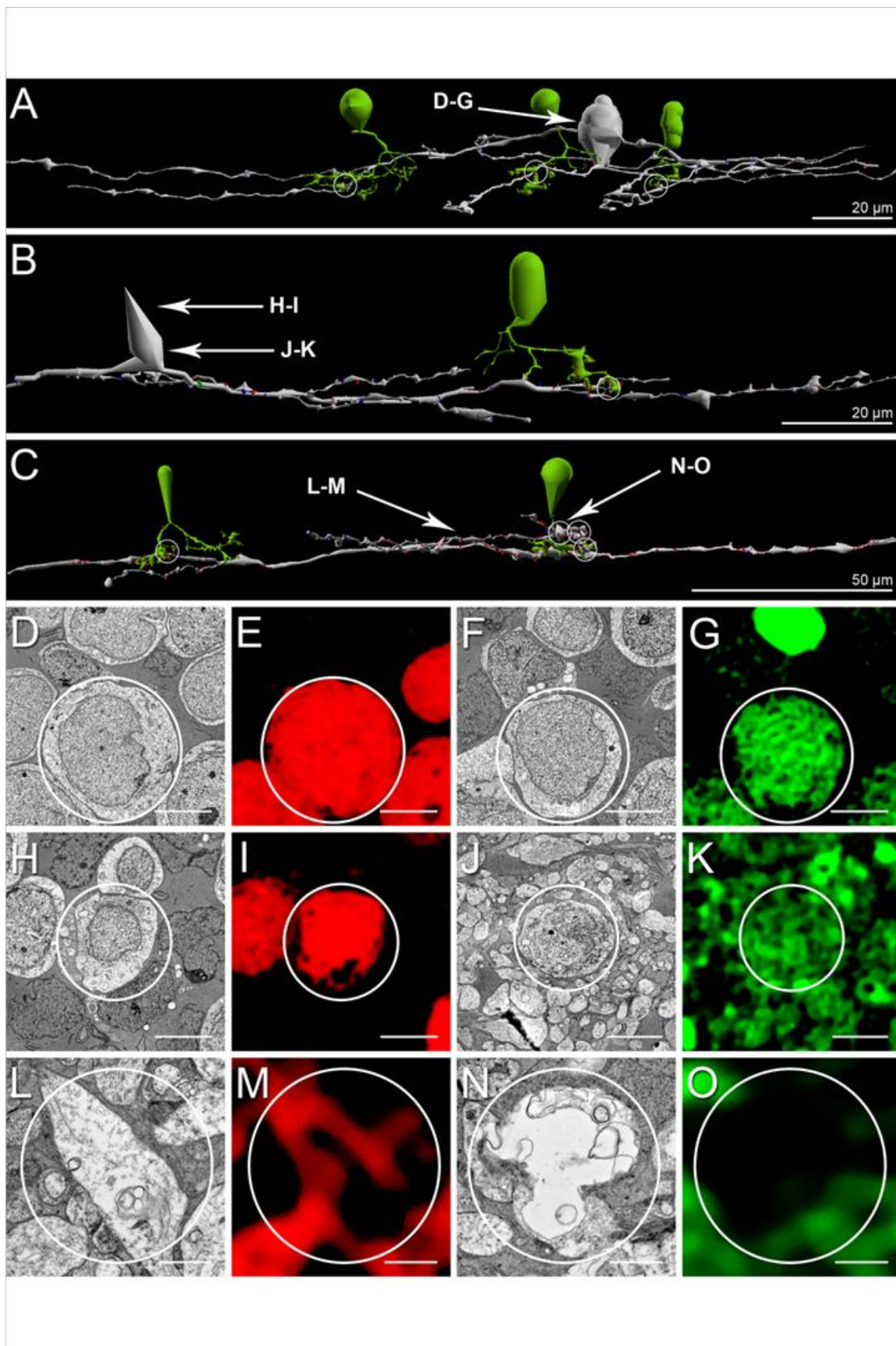
Figure 3.5. CBabs target GACs in the ON IPL. **A-C**. Vertically oriented renderings of CBabs targeting both mono- and multistratified GACs in the ON IPL. Circles, locations of synapses between CBabs and GACs. Arrows, locations from which GABA and glycine signatures were obtained for D-O. **D-E,H-I,L-M.** Glycine-positive signatures and corresponding TEM of somas or processes for GAC<u>s</u> shown in A-C. **F-G,J-K,N-O.** GABA-negative signatures and corresponding TEM of somas or processes for GAC<u>s</u> shown in A-C. Scale bars (A-C), 10 µm**.** Scale bars (D-K, N-O), 5 µm**.** Scale bars (L-M), 1 µm**.**
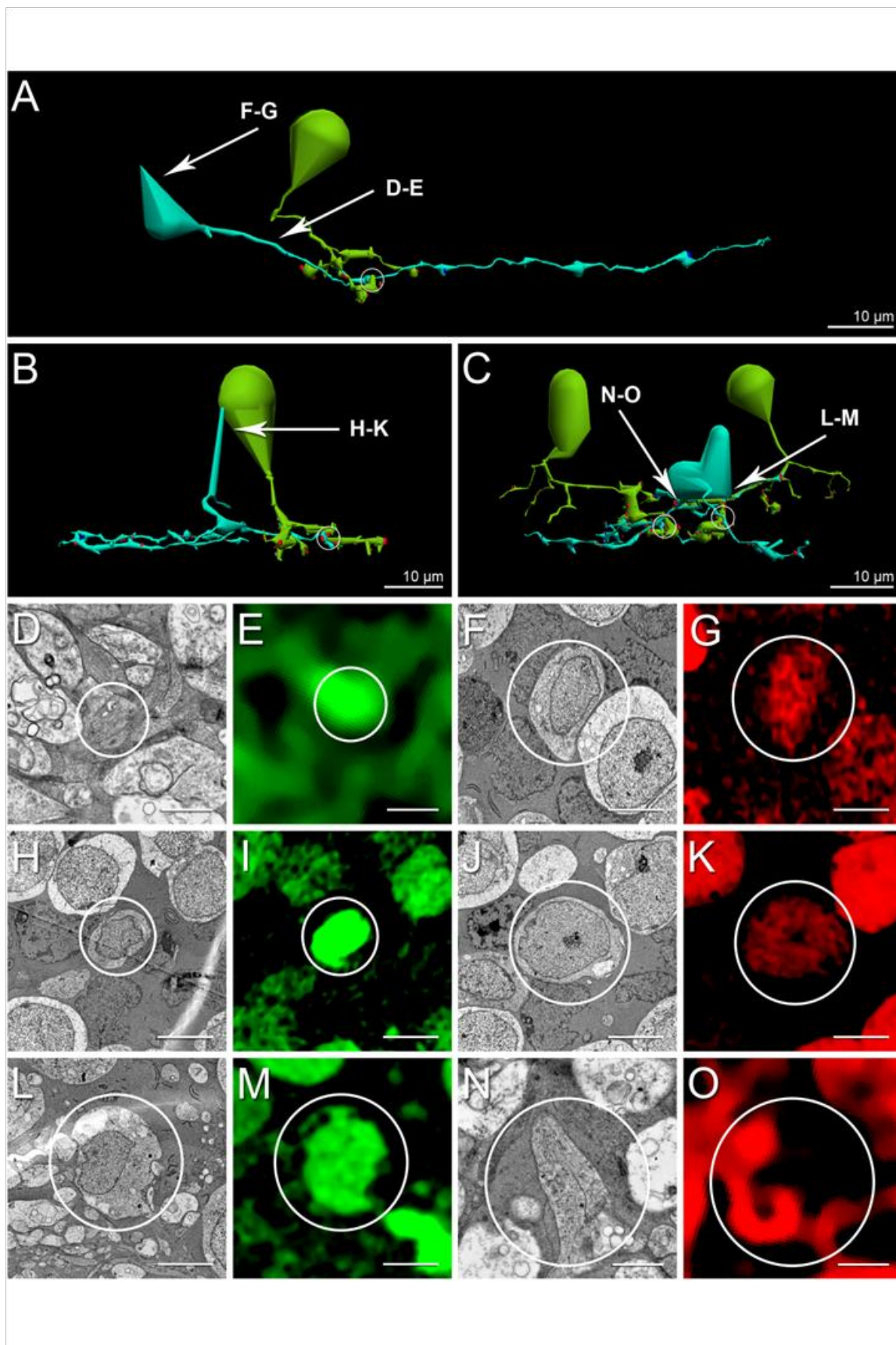
Figure 3.6. CBab-driven γACs mediate inhibition in the ON IPL. **A-C**. Vertically oriented renderings of CBabs targeting both mono- and multistratified γACs in the ON IPL. Circles, locations of synapses shown in D-O. **D-O.** TEM of synapses indicated by circles in A-C. **D-G.** γAC 115 shown in A (silver) is postsynaptic to a ribbon from CBb5 5608 (D), and possesses reciprocal synapse with CBabs 3928, 458, and 359 (E,F,G, respectively). H-K. γAC 5453 shown in B (silver) possesses reciprocal synapses with CBb6 6129 and CBab 5543 (H-I, J-K, respectively). L-O. γAC 16073 shown in C (silver) receives ribbon synapses from CBab 5538 (L) and CBab 6046 (M), and forms conventional synapses with ON-OFF GC 8575 (N) and bsdGC (O). Abbreviations. GC, ganglion cell; bsdGC, bistratified diving ganglion cell. White arrows indicate synapse directionality. r, ribbons. Scale bars (A-C), 10 µm. Scale bars (D-K), 5 µm. Scale bars (L-O), 1 µm.
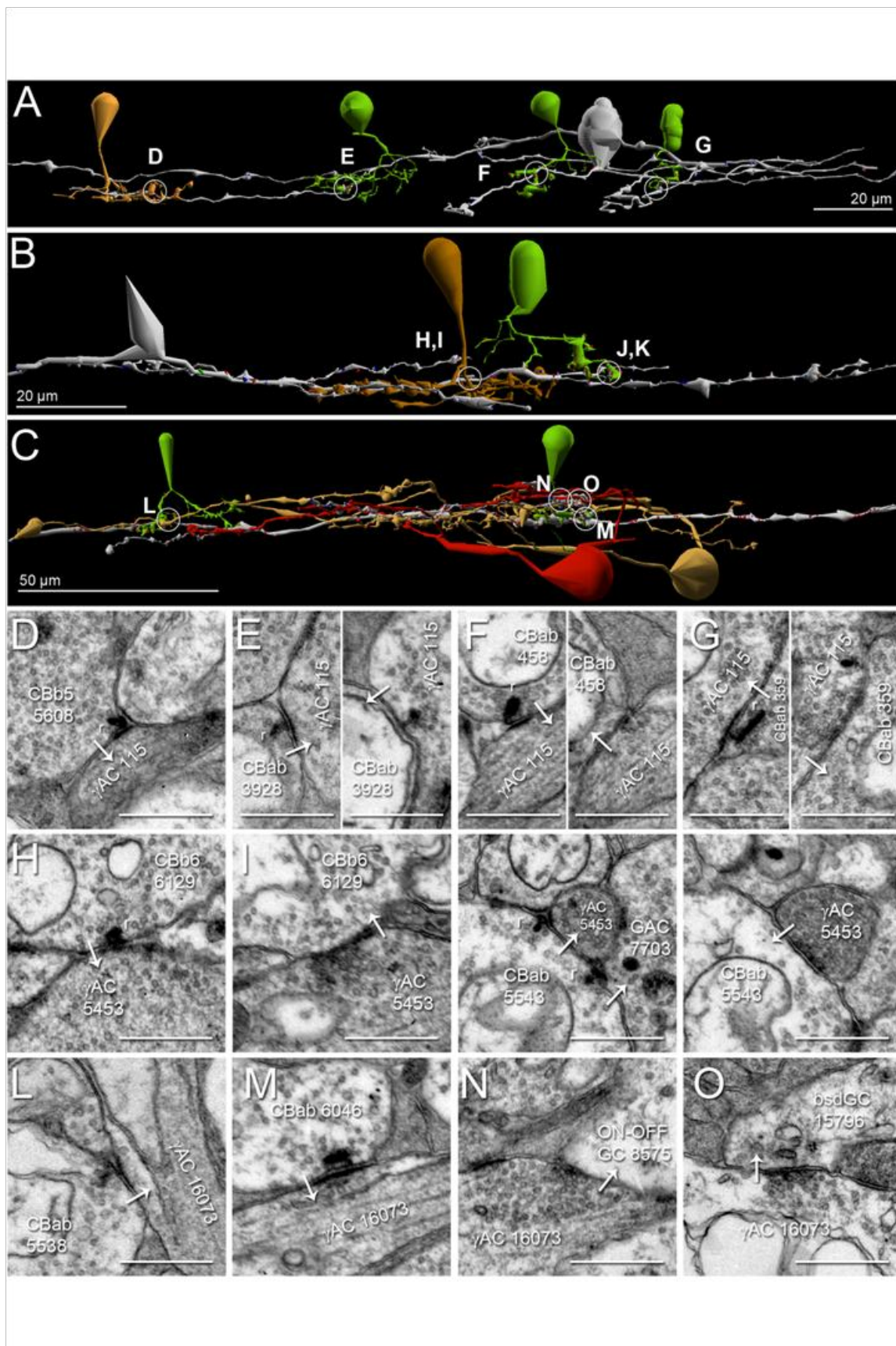
Figure 3.7. CBab-driven GACs mediate inhibition in the ON IPL. **A-C**. Vertically oriented renderings of CBabs targeting both mono- and multistratified GACs in the ON IPL. Circles, locations of synapses shown in E-P. **E-P.** TEM of synapses indicated by circles in A-C. **E-G.** GAC 8035 shown in A (patina) forms reciprocal synapses with CBab 5504 (E) and CBb5 6118 (F-G). **H-I.** GAC 7134 shown in B (patina) forms reciprocal synapses with CBab 6046 (H) and CBb4 5501 (I). **J-O.** GAC 7703 shown in C (patina) forms reciprocal synapses with CBab 5543 (J; Fig. 3.6 J-K), CBab 458 (K-L), CBb6 440 (M-N), and CBb6 6129 (O). **P.** GAC 7703 forms a conventional synapse onto ON-OFF GC 8575. Abbreviations. GC, ganglion cell. White arrows indicate synapse directionality. r, ribbons. Scale bars (A-C), 10 µm**.** Scale bars (D-O), 5 µm**.**
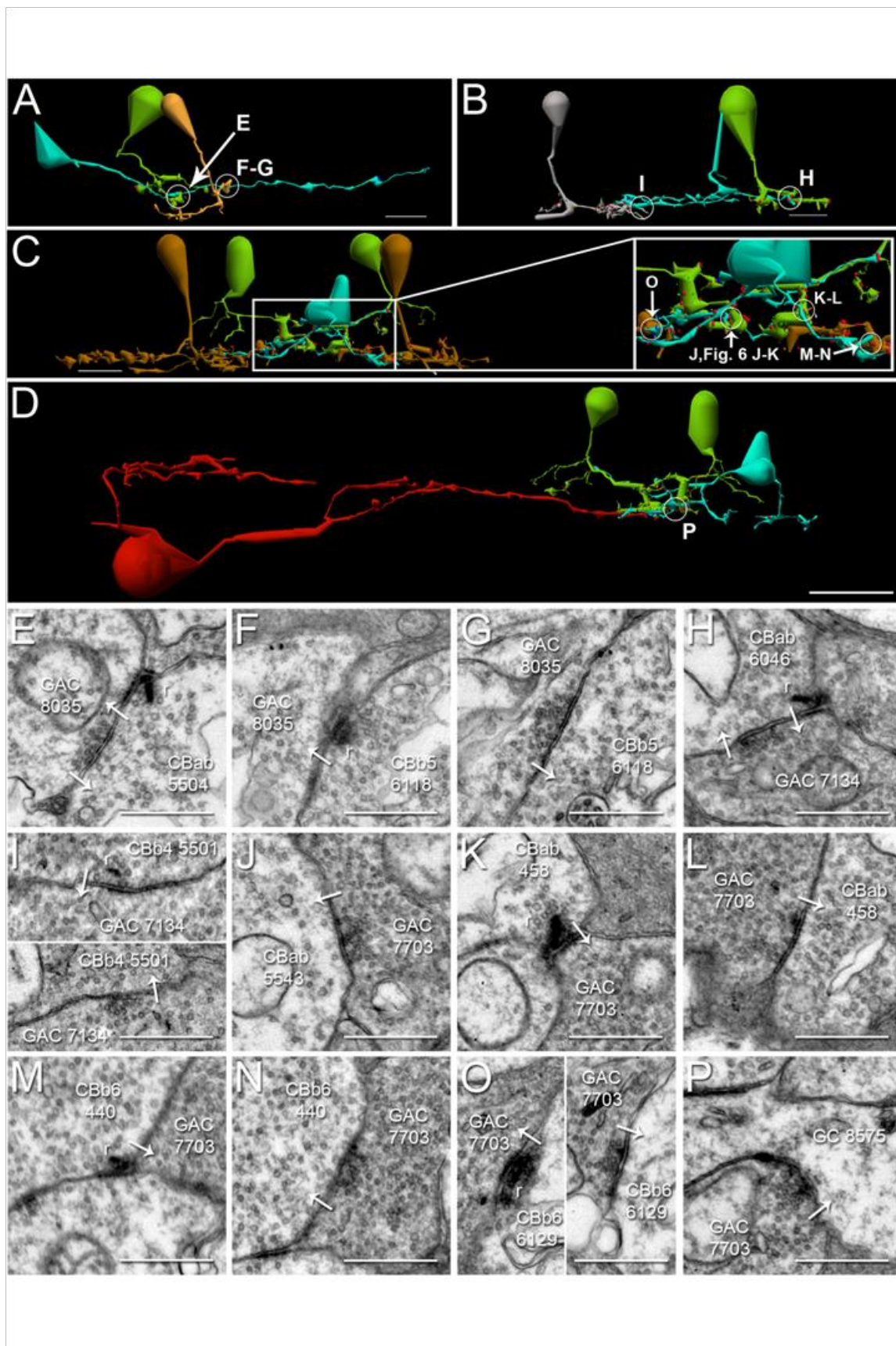
Figure 3.8. CBab-driven ON-OFF crossover inhibition. **A**. Horizontally-oriented rendering of nested CBab-driven feedback and feedforward subnetworks concatenated to form a larger network. Circles, locations of synapses shown in B-E. **B-E.** TEM of synapses indicated by circles in A. CBab 5543 and CBab 458 converge ribbon synapses onto ON-OFF GC 8575 (B,C,respectively). GAC 7703 forms conventional synapses onto γAC 5453 (D) and γAC 115 (E). White arrows indicate synapse directionality. r, ribbons. **F.** Wiring diagram for the rendering shown in A. CBab 5543 (B) and CBab 458 (C) directly drive ON-OFF GC 8575 and GAC 7703. GAC 7703, γAC 5453, and γAC 115 each provides simple feedback inhibition to the CBabs and CBbs that directly drive them with ribbon synapses. GAC 7703 further mediates nested feedback inhibition to CBab 5543 and CBab 458 via γAC 5453 (D) and γAC 115 (E). GAC 7703 also provides feedforward inhibition to ON-OFF GC 8575 (Fig. 3.7 P), which receives convergent γAC-mediated feedforward inhibition from γAC 16073, also driven by CBabs. γAC 16073 diverges CBab-driven feedforward inhibition ON-OFF GC 8575 (Fig. 3.6 N) and bsdGC 15796 (Fig. 3.6 O). Vertices. Green ellipses, CBab; cyan ellipses, CBb; brown ellipses, ganglion cell; red triangle, γAC; green inverted triangle, GAC. Edges. Green arrows, excitatory ribbon synapses; red flathead arrows, inhibitory conventional synapses. Abbreviations. GC, ganglion cell; bsdGC, bistratified diving ganglion cell. Scale bars (A), 50 μm**.** Scale bars (B-E), 0.5 μm**.**
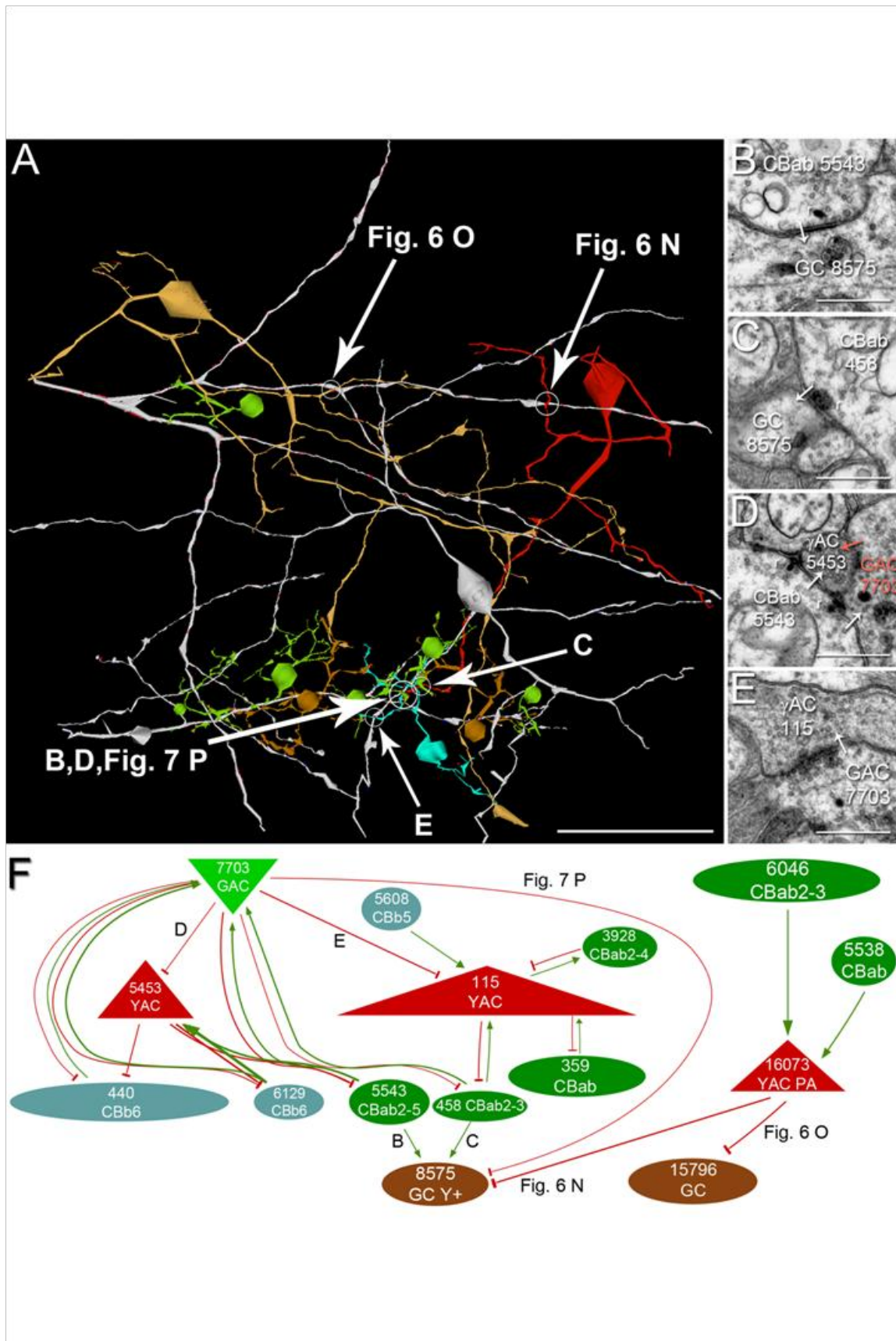
Figure 3.9. The ON and OFF IPL are not discretely organized. **A.** The canonical division of ON and OFF IPL laminae. A dividing line is standardly drawn at 40% IPL depth, demarkating the OFF (most distal 40%) from the ON (most proximal 60%) IPL layers. CBas are thought to constrain their axonal arbors to the OFF layer, while CBbs constrain their axonal arbors to the ON layer. Spatial relationships are conserved. **B.** Renderings of the 15 distinct morphological classes of BC discovered thus far in RC1. These recapitulate the 13 classes describe by MacNeil et al. (2004a), and add two new classes, CBab and CBb6. Inside the circle on the left side of the panel, a CBb6 (brown) and CBab (bright green) are seen breaching the canonical ON-OFF boundary by branching and forming synapses in polarity-opposite territory. **C.** Since both CBbs and CBabs form functional synapse in polarity-opposite territory, mediating ON-OFF crosstalk, we refactor the distal 80% of the functional IPL as mixed ON-OFF strata.

References

Anderson, J.R., Jones, B.W., Watt, C.B., Shaw, M.V., Yang, J., DeMill, D., Lauritzen, J.S., Lin, Y., Rapp, K., Mastronarde, D., Koshevoy, P., Grimm, B., Tasdizen, T., Whitaker, R., Marc, R.E. 2011a. Exploring the retinal connectome. Mol Vision 17:355-379.

Anderson, J.R., Jones, B.W., Yang, J.-H., Shaw, M.V., Watt, C.B., Koshevoy, P., Spaltenstein, J., Jurrus, E., Kannan, U.V., Whitaker, R., Mastronarde, D., Tasdizen, T., Marc, R.E. 2009. A computational framework for ultrastructural mapping of neural circuitry. PLoS Biol 7: e1000074.

Anderson, J.R., Mohammed, S., Grimm, B., Jones, B.W., Koshevoy, P., Tasdizen, T., Whitaker, R., Marc, R.E. 2011b. The Viking viewer for connectomics: scalable multi-user annotation and summarization of large volume data sets. J Microscopy 241:13-28.

Awatramani, G.B., Slaughter, M.M. 2000. Origin of transient and sustained responses in ganglion cells of the retina. Journal of Neuroscience 20:7087-7095.

Devries, S.H. 2000. Bipolar cells use kainate and AMPA receptors to filter visual information into separate channels. Neuron 28:847-856.

Dumitrescu, O.N., Pucci, F.G., Wong, K.Y., Berson, D.M. 2009. Ectopic retinal ON bipolar cell synapses in the OFF inner plexiform layer: contacts with dopaminergic amacrine cells and melanopsin ganglion cells. J Comp Neurol 517:226-244.

Famiglietti, E.V. 1981. Functional architecture of cone bipolar cells in mammalian retina. Vision Res 21:1559-1563.

Famiglietti, E.V., Kaneko, A., Tachibana, M. 1977. Neuronal Architecture of on and off pathways to ganglion cells in carp retina. Science 198:1267-1269.

Famiglietti, E.V., Kolb, H. 1976. Structural basis for ON- and OFF-center responses in retinal ganglion cells. Science 194:193-195.

Freed, M. 2000. Parallel cone bipolar pathways to a ganglion cell use different rates and amplitudes of quantal excitation. Journal of Neuroscience 20:3956-3963.

Hoshi, H., Liu, W.-L., Massey, S.C., Mills, S. 2009. ON inputs to the OFF layer: bipolar cells that break the stratification rules of the retina. J Neurosci 29:8875-8883.

Jeon, C.J., Masland, R.H. 1995. A population of wide-field bipolar cells in the rabbit retina. J Comp Neurol 360:403-412.

Kolb, H. 1982. The morphology of the bipolar cells, amacrine cells and ganglion cells in the retina of the turtle Pseudemys scripta elegans. Philos Trans R Soc Lond B Biol Sci 298:355-393.

Kolb, H., Cuenca, H., Wang, Dekorver, L. 1990. The synaptic organization of the dopaminergic amacrine cell in the cat retina. J Neurocytol 19:343-366.

Kolb, H., Linberg, K.A., Fisher, S.K. 1992. Neurons of the human retina: a Golgi study. J Comp Neurol 318:147-187.

Lauritzen, J.S., Watt, C.B., Anderson, J.R., Jones, B.W., Marc, R.E. 2013. ON Cone Bipolar Cell Axonal Ribbons in the OFF Inner Plexiform Layer of the Rabbit Retina. J Comp Neurol 521:977-1201.

Linberg, K.A., Suemune, S., Fisher, S.K. 1996. Retinal neurons of the California ground squirrel, Spermophilus beecheyi: a Golgi study. J Comp Neurol 365:173-216.

MacNeil, M., Heussy, J., Dacheux, R., Raviola, E., Masland, R. 2004a. The population of bipolar cells in the rabbit retina. J Comp Neurol 472:73-86.

MacNeil, M.A., Heussy, J.K., Dacheux, R.F., Raviola, E., Masland, R.H. 2004b. The population of bipolar cells in the rabbit retina. Journal of Comparative Neurology 472:73-86.

Marc, R.E. 1986. Neurochemical stratification in the inner plexiform layer of the vertebrate retina. Vision Res 26:223-238.

Marc, R.E., Jones, B.W. 2002. Mjolecular phenotyping of retinal ganglion cells. J Neurosci 22:413-427.

Marc, R.E., Liu, W. 2000. Fundamental GABAergic amacrine cell circuitries in the retina: nested feedback, concatenated inhibition, and axosomatic synapses. Journal of Comparative Neurology 425:560-582.

Mariani, A.P. 1982. Biplexiform cells: ganglion cells of the primate retina that contact photoreceptors. Science 216:1134-1136.

Masland, R.H. 2001a. The fundamental plan of the retina. Nature Neuroscience 4:877-886.

Masland, R.H. 2001b. Neuronal diversity in the retina. Curr Opin Neurobiol 11:431-436.

McGuire, B., Stevens, J., Sterling, P. 1984. Microcircuitry of bipolar cells in cat retina. J Neurosci 4:2920-2938.

Pang, J.J., Gao, F.F., Wu, S.M. 2004. Stratum-by-stratum projection of light response attributes by retinal bipolar cells of Ambystoma. J Physiol 558:249-262.

Ramon y Cajal, S.R. 1892. La rétine des vertébrés. Cellule 9:121-225.

Scholes, J. 1975. Colour receptors, and their synaptic connexions, in the retina of a cyprinid fish. Philos Trans R Soc Lond B Biol Sci 270:61-118.

Scholes, J., Morris, J. 1973. Receptor—bipolar connectivity patterns in fish retina. Nature 241:52-54.

Sherry, D.M., Yazulla, S. 1993. Goldfish bipolar cells and axon terminal patterns: a Golgi study. J Comp Neurol 329:188-200.

Wässle, H., Puler, C., Müller, F., Haverkamp, S. 2009. Cone contacts, mosaics, and territories of bipolar cells in the mouse retina. J Neurosci 29:106-117.

Werblin, F., Dowling, J.E. 1969. Organization of the retina of the mudpuppy, Necturus maculosus. II. Intracellular recording. J Neurophysiol 32:339-355.

Wong, K.Y., Dowling, J.E. 2005. Retinal bipolar cell input mechanisms in giant danio. III. ON-OFF bipolar cells and their color-opponent mechanisms. J Neurophysiol 94:265-272.

CHAPTER 4

THE CONNECTOMICS OF ROD-CONE

INTERACTION NETWORKS

Abstract

Crossover suppression between mammalian rod and cone pathways has been demonstrated psychophysically for many decades, but its supporting synaptic architecture has remained cryptic. Connectomics analysis of the rabbit retina reveals eight primary rod-cone crossover motifs. Rod pathway suppression originates in all ON and OFF cone bipolar cells and targets rod bipolar cells via inhibitory amacrine cells. Wide-field GABAergic and narrow-field glycinergic amacrine cells effect spatially coarse and fine rod pathway suppression for both ON and OFF channels. Cone pathway suppression originates in rod bipolar cells and targets all classes of cone bipolar cells. Such crossover systems likely drive winner-take-all operations, analogous to brain decision networks, mediating fast switching between rods and cones, and maintaining bias for the winner network.

Introduction

Vertebrates experience two protracted mesopic periods daily (Fig. 4.1 A) during which rod and cone signaling events coexist (Buck, 2004; Stabell and Stabell, 1998, 2002). Many animals exploit this visual regime, but mammals navigate it with exceptional facility, differing from most other vertebrates by segregating rod and cone signal flow into separate bipolar cell (BC) channels (Fig. 4.1 B, C) and by inserting an additional amplification stage in the pathway (Dacheux and Raviola, 1986; Strettoi et al., 1990; Strettoi et al., 1992) collected by ganglion cells (GCs). This somehow permits rapid switching between rod and

cone vision under clouds, canopies or open skies, in caves or burrows. While the switch seems perceptually smooth, psychophysical dissection has long documented that it is accompanied by strong rod-cone crossover suppression (Buck, 2004) and complex chromatic interactions (Goldberg et al., 1983; Ingling et al., 1977; Stabell and Stabell, 1998, 2002; Thomas and Buck, 2006; Trezona, 1970). No validated network models exist for crossover suppression.

Visualizing individual functional network motifs is virtually impossible with conventional methods due to the large spatial scales and complex topologies of real networks (Marc et al., 2012). The difficulty is greater with crossover networks as they transfer signals between different subnetworks that can be widely spaced and sparsely connected. Indeed, inhibitory crossover networks between rod and cone channels have never been documented despite decades of electron microscopy. Visualizing retinal crossover networks (Werblin, 2010; Molnar et al., 2009) requires large-scale 3D connectomics tracing at synaptic resolution (Anderson et al., 2009; Anderson et al., 2011b; Briggman and Denk, 2006; Briggman et al., 2011; Bock et al., 2011). Connectomics provides tools to parse networks by tracing cellular partners over many synaptic transfers (Marc et al., 2012). We searched for rod-cone pathway interactions by starting at individual rod BC axon terminals and tracing their networks outward across wide fields of the inner plexiform layer in rabbit retinal connectome RC1, a 0.25 mm diameter cylinder of the inner retina built at 2 nm resolution (Anderson et al., 2011). All cells in this paper are indexed in volume RC1 to their location maps, network associations, and shapes and all resources are publicly accessible. We

performed wide analysis (querying many copies of a cell class for shared features) on 104 adjacent rod BCs (Fig. 4.2 A), and deep analysis (mapping all connections of a cell) on a central patch of 5 rod BCs to define their connectivities with amacrine cells (ACs). All cells were classified within independent molecular, shape, and network feature spaces as detailed in the methods (*20*) and previous publications (Anderson et al., 2011a; Lauritzen et al., 2013). Specifically, we traced GABAergic ACs (γACs) and glycinergic ACs (GACs) that form directed cone BC to rod BC networks (Fig. 4.2, 4.3) and directed rod BC to cone BC networks (Fig. 4.4).

Methods

The Connectome Volume RC1

RC1 is an open-source, open-access ultrastructural data volume. The acquisition, construction, navigation, analysis, and access procedures for RC1 are detailed in previous papers (Anderson et al., 2011b; Anderson et al., 2011a; Anderson et al., 2009; Lauritzen et al., 2013; Tasdizen et al., 2010). In brief, volume was built from mid-ventral retina of a light-adapted female Dutch Belted rabbit (Oregon Rabbitry, OR), with *in vivo* excitation mapping using 1-amino-4-guanidobutane (AGB) and fixation for automated transmission electron microscope (TEM) imaging as described in Anderson et al. (2011a). All procedures are in accord with Institutional Animal Care and Use protocols of the University of Utah, the ARVO Statement for the Use of Animals in Ophthalmic and Visual Research, and the Policies on the Use of Animals and Humans in

Neuroscience Research of the Society for Neuroscience. The physical volume itself is a collection of 370 data sections (341 ATEM sections with 29 intercalated optical molecular sections, all at ≈70 nm), imaged at a resolution of 2.18 nm/pixel, producing a collection of over 350,000 images with synaptic / gap junction resolving capacity. The computational assembly of the image slices has been previously published (Tasdizen et al., 2010), as has a detailed description of the server / client architecture of Viking, our open-source navigation and annotation tool (Anderson et al., 2011b). Tracing has been carried out by a team of trained annotators (see Acknowledgements).

Mining Cells

RC1 contains > 600 annotated neuronal cell bodies. A few hundred cells have been fully traced: mostly bipolar cells (BCs), A_I and A_{II} amacrine cells (ACs), and some ganglion cells (GCs). RC1 currently contains >600,000 individual annotations and ≈10,000 individual processes have been classified. Candidate rod-cone crossover networks in RC1 were visualized and annotated with the Viking viewer by starting at every one of the 104 mapped 3D rod bipolar cells (BCs) in RC1 and tracing outwards from individual amacrine cell (AC) synapses on the rod BC axon and axon terminal, to determine the synaptic identity of the process (e.g., exclusively rod BC or cone BC-driven) and explored via 3D rendering and graph visualization of connectivity (Anderson et al., 2011b). Each cell referenced in this manuscript possesses a unique index number that can be entered into one of six tools (Viking, Network Viz, Structure Viz, Statistics

Viz, Motifs Viz, and Vikingplot) to explore connectivity. In Viking, each index opens a dialogue containing all the structure locations (annotations) that make up a cell's shape and a list of all its child structure locations (synapses, gap junctions, adherens junctions). In Network and Motif Viz, the index accesses the associated network of the cell from immediately-connected (1 hop) up to 8 synaptic hops distant. Individual connection tip links contain child structure indices for navigation in Viking. In Structure Viz, the index accesses a fast 3D skeleton of the cell with its various contacts denoted. Clicking on a contact loads its location into the system clipboard and direct navigation to the site is then made in Viking. Every image capture used in this manuscript is indexed and available as a Viking XML bookmark file that allows the user to navigate to the locations from which all images were acquired. Finally, Vikingplot is a MatLab® application (Natick, MA) that renders cell shapes in 3D using customizable lighting models. All renderings produced for this manuscript are available as *.tiff and native MatLab® scalable 3D *.fig files. These tools are described in more detail in Anderson et al. (2011a; 2011b) and their extensive application demonstrated in Lauritzen et al. (2013).

Cell Classification

Identification of each cell is based on independent domain classifiers: form (shape, stratification), network connectivity, molecular metrics (Anderson et al., 2011a; Anderson et al., 2009; Lauritzen et al., 2013). RC1 contains both capstone and intercalated optical sections that provide small molecule signals for

cell classification: L-aspartate, 4-aminobutyrate, glycine, L-glutamate, L-glutamine, taurine, and the activity marker 1-amino-4-guanidobutane (AGB). These molecular markers are detected with small molecule-specific antibodies provided by Signature Immunologics, Inc (Torrey, UT): product number B100 anti-1-amino-4-guanidobutane IgG, D100 anti-L-aspartate IgG, E100 anti-glutamate IgG, G100 anti-glycine IgG, Q100 anti-L-glutamine IgG, TT100 anti-taurine IgG, YY100 anti-GABA IgG. Visualization uses archival silver immunogold methods (Marc et al., 1995). Detailed characterization of these IgGs is provided in Marc and Jones (2002), Anderson et al. (2011a), and Lauritzen et al. (2013). Using the molecular signature set alone, every neuron in RC1 can be classified without error as a horizontal cell, OFF cone BC, ON cone BC, rod BC, GAC, γAC, or GC. More importantly, each molecular classifier uniquely maps onto the distinctive morphologies of each class of cells in 3D (including fine-scale stratification in the inner plexiform layer) and unique collections of network motifs accessed by each (Anderson et al., 2011a; Lauritzen et al., 2013). Rod BCs have a unique cluster of strong glutamate signals and weak photopic activity signals; axon terminals deep in the proximal inner plexiform layer; unique synaptic drive from both A_I and A_{II} ACs; lack gap junctions; and do not drive retinal ganglion cells (GCs). In contrast, all ON cone BCs (CBb cells) have a distinctive glutamate-glycine signature and varied activity signals according to class; arborize in several tiers of the proximal inner plexiform layer with much wider axonal fields than rod BCs; and engage in networks that exclude A_I ACs and include GCs as targets; and are heavily coupled to A_{II} ACs and other CBb cells.

OFF cone BCs (CBa cells) have high glutamate, glycine-free signatures; varied activity according to class, including the strongest light responses; arborize in several tiers of the distal inner plexiform layer with wide fields; engage in networks that exclude A_I ACs and include GCs as targets; are presynaptic and postsynaptic to A_{II} ACs; and are extensively coupled to other CBa cells. Similar distinctive feature spaces classify ACs and GCs in RC1 (Lauritzen et al., 2013). Finer discrimination of 17 distinct BCs was based on complete 3D reconstructions of over 200 CBb and CBa cells in RC1. The details of these methods and stratification analysis are available in Lauritzen et al. (2013).

<u>Image Preparation</u>

Most display TEM images in this paper were produced from raw RC1 screen captures or by remapping the TEM tile lookup tables tiles to gamma 1.3 (Anderson et al., 2011a). Optical and TEM overlays used the TEM greyscale brightness channel combined with the hue, and saturation from the optical image as described in Anderson et al. (2011a).

Results

We identified eight primary rod-cone crossover motifs (Table 4.1, Fig. 4.5). Every rod BC receives suppressive AC input from multiple cone BCs and every cone BC receives extensive AC suppression from surrounding rod BCs. Light absorbed by cones can thus inject antagonistic signals into rod BCs by five network motifs (C1-5), and light absorbed by rods can inject antagonistic signals into cone BCs by three network motifs (R1-3). These motifs converge on target

BCs with algebraic signal polarities of antagonistic surrounds: hyperpolarizing for ON and depolarizing for OFF BCs (Table 4.1). While the physiological profiles of different BC classes are far more complex than we describe here, we characterize the nominal gains (amplifications) of these motifs by their serial glutamatergic cationic (n), GABAergic or glycinergic anionic (p), and coupling (c) transfer functions, expressing a chain's gain as their product (npc). For example, the cone $\rightarrow$ BC $\rightarrow$ AC $\rightarrow$ BC signaling chain has a net gain of n^2p. We assume that most excitatory gains are > 1 (Copenhagen et al., 1990; Yang and Wu, 2004) and that most inhibitory (Maltenfort et al., 1998; Wu, 1991) or coupling networks have gains < 1.

Cone Pathway ON Motifs Suppressing Rod Pathways

ON cone BCs (CBb cells) inhibit rod BCs by two pathways using one-stage inhibition. Motif C1 (Cone 1) is the most common cone ON pathway crossover network for suppressing rod BCs: wide-field ON γAC processes driven by and presynaptic to CBb cells (Fig. 4.2 B-D, 4.5 A) are also presynaptic but never postsynaptic to rod BC descending axons and axon terminals (Fig. 4.2 E), forming a cone-biased rod suppression network. Over 100 instances of motif C1 have been mapped. Figure 4.2 C displays one of many possible minimum spanning subgraphs for motif C1: a subset of C1 motifs that delivers at least one suppressive synapse to every rod BC in the graph. In Fig. 4.2 C, some processes were traced completely across the volume, while others are intentionally displayed as fragments to show the minimum distance between a cone BC and

the nearest rod BC target for that process. The distance between a given CBb driver cell and its nearest target rod BC along a single wide-field γAC neurite can be as small as 10 μm or can span the full width of the RC1 volume (Fig. 4.2 B-D). As every rod BC receives 14-38 such synapses, the total C1 suppression path is dense. Motif C1 γACs are driven by ON cone BCs (CBb cells) and form widespread CBb feedback networks (Fig. 4.2 F, G). RC1 is 0.25 mm wide, and many wide-field γAC classes have dendritic fields > 0.5 mm wide (MacNeil et al., 1999). Though many wide-field ACs that target BCs in RC1 necessarily have somas *outside* the volume, most can be identified as γACs since they traverse GABA labeled reference slices in RC1 (Anderson et al., 2011a). Every rod BC is thus embedded in a millimeter-scale GABAergic inhibitory field (Fig. 4.2 C, D; 4.5 A). We have identified eight classes of CBb cells in rabbit (Lauritzen et al., 2013) and all drive motif C1. CBb cells also display extensive in-class and tiered cross-class coupling (data not shown), permitting shared rod suppression across the spatial and temporal response domains of all CBb classes. Motif C1 processes are also nested, i.e., presynaptic to each other (data not shown). Given that wide-field γACs are likely spiking neurons with large receptive fields (Bloomfield, 1992), nesting may temporally shape signaling. However, nesting is common among γACs (Anderson et al., 2011a; Marc and Liu, 2000) and is not unique to rod-cone crossover.

Motif C2 uses narrow-field ON GACs, e.g., cell 178 in Fig. 4.2B, embedding rod BCs in a small field (≈ 0.1 mm) of CBb-initiated glycinergic inhibition. Motif C2 also inhibits A_{II} ACs (data not shown). Notably, motif C2

roughly matches the sizes of peripheral cone-rod suppression domains seen in human psychophysics (Buck, 2004; Thomas and Buck, 2006), although short range C1 motifs are also abundant.

Cone Pathway OFF Motifs Suppressing Rod Pathways

OFF cone BCs (CBa cells) inhibit rod BCs by three pathways using two-stage inhibition, largely initiating in wide-field CBa-driven γACs (Fig. 4.3; Fig. 4.5 C-E). In motif C3, CBa cells drive a nominal OFF γAC inhibitory field whose synapses target the somas and proximal dendrites of a bistratified γAC class in the OFF layer (Fig. 4.3 A, B). This is the only synaptic drive this cell class receives: it receives no BC input. One instance of motif C3 (γAC 5281) is presynaptic to four rod BCs, three CBbs (Fig. 4.3 A, C), and several ACs and GCs in the ON layer. These bistratified γACs are likely ON cells, but lack excitatory inputs. Some γAC classes in the rabbit retina do lack AMPA or NMDA receptor-mediated drive, arborize in the distal OFF layer, and are candidates for motif C3 cells.

Motif C4 is a massive inhibitory path originating in CBa cells via OFF wide-field γACs that target the distal dendrites of A_I ACs (Fig. 4.3 A, D-F). All traced C4 motifs (n>20) are driven by CBa cells, and every class of CBa cells (we have tabulated 8 distinct classes) can initiate a C4 motif. We were also able to tabulate every synapse on A_I AC 4943, showing that suppression synapses outnumber rod BC inputs by ≈10:1 in the RC1 volume. Every one of the five A_I ACs we mapped receives > 100 inhibitory synapses on its proximal dendrites in a ring-like

cluster (Fig. 4.3 A) and this include the largest GABAergic inhibitory synapses ever found in the retina (Fig. 4.3 F) with diameters reaching 2 µm. High synapse number and large postsynaptic area weighting may make the C4 pathway effective despite its lower gain of n^2p^2 (Table 4.1, Fig. 4.5 D). There is also a parallel motif C4a via the CBa →A_{II} AC → OFF γAC → A_I AC chain (Fig. 4.5 D). Finally, motif C5 is the narrow-field glycinergic OFF layer paramorph of motif C2, originating with CBa drive and targeting A_I ACs (Fig. 4.5 E). Thus, both fine-grain and coarse-grain suppression converges on A_I ACs.

Rod Pathway Motifs Suppressing Cone Pathways

The flow of suppressive signals from rod BCs to cone BCs largely engages the well-known A_{II} AC (Fig. 4.4 A) and, via directly connected CBb and CBa cells, accesses all classes of cone BC inhibitory pathways in high gain suppression chains. Motifs R1 and R2 use heterocellular A_{II} AC :: CBb coupling (Fig. 4.4 B) and A_{II} AC $>_i$ CBa (Fig. 4.4 C) glycinergic signaling, respectively, to access cognate cone γAC pathways (Fig. 4.4 D, E). We have mapped >100 processes mediating these motifs and while some are the same wide-field γACs that mediate cone BC suppression of rod BCs, the majority are cone pathway feedback γAC processes that do not target rod BCs at all. Cone BC-specific narrow-field glycinergic ACs are also accessed by these motifs, but we have not yet fully traced them nor given them separate codes. These two motifs are powerful, with gains of n^3 (Table 4.1, Fig. 4.5). Finally, motif R3 involves distinct CBb-dominated wide-field feedback γACs that capture sparse ribbon inputs from

rod BCs (Fig. 4.2 F, G). Their processes span the entire RC1 volume and their fields likely reach 1 mm in diameter (data not shown). A single process can contact 15 cone BCs for each rod BC. If such wide-field feedback γACs in motif R3 are spiking interneurons (Bloomfield, 1992), a few rod BCs could suppress 60-100 cone BCs over a square millimeter of retina.

Discussion

Physiological Implications of Rod-Cone Crossover Suppression

The eight rod-cone crossover motifs could clearly mediate direct rod-cone crossover suppression. Other signal mixing architectures such as rod-cone coupling, low levels of rod-cone mixing at the BC level (Pang et al., 2010), and targeting of cones and rods to different horizontal cell compartments are known, but it is unclear how these could mediate rod-cone suppression. It is certain that additional crossover motifs will be identified: we have some instances of ON-OFF motifs that may be C1/C4 hybrids, as well as abundant cone BC-driven inhibition of A_{II} cells. More complete definitions of these will require deeper tracing than we have been able to achieve, but are all consistent with extensive rod-cone crossover at every level of the inner plexiform layer.

Cone suppression of rod sensitivity is most effective with transient rather than steady stimuli (Ingling et al., 1977), consistent with the fast ionotropic attributes of AC-mediated inhibition (Eggers and Lukasiewicz, 2006a). We propose that retinal rod-cone suppression motifs operate as archetypal $GABA_A$ receptor-mediated winner-take-all networks, similar to cortical sensory fields

(Kurt et al., 2008). If such networks did not exist, concurrent activation of rods and cones in complex scenes might elicit additive rather than opponent sensitivity envelopes. Such networks may be developmentally sensitive. For example, monocular form deprivation in juvenile macaques prevents maturation of photopic spectral sensitivity curves into a normal trichromatic opponent envelope (Sperling and Harwerth, 1971), instead producing a simple achromatic rod-dominated envelope even at photopic levels (Harwerth et al., 1990). Human amblyopia leads to a milder defect where red-green lateral inhibition in spectral sensitivity curves is attenuated (Harwerth and Levi, 1977). As rods are evidently operational at photopic levels (Harwerth et al., 1990), rod-cone crossover suppression may be critical in stabilizing perception. Some crossover networks may serve hue and contrast tuning as well. Rabbits are photopic dichromats with short wave system 1 (SWS1) blue cones and long wave system (LWS) green cones; humans have LWS green and red cones. Psychophysically, the addition of rod signals to cone pathways often mimics a blue channel (Buck, 1997; Trezona, 1970) and, in principle, the field of rod BC inhibition surrounding cone BCs could form *de facto* LWS cone / short-wave-mimicking rod opponent networks. All CBb BCs engage in crossover suppression, so SWS1 / rod opponency should also exist, consistent with the observation that rod interactions can lead to a wide range of hue percepts in humans (Stabell and Stabell, 2002; Thomas and Buck, 2006). These chromatic percepts can even be enhanced in blue cone monochromacy (Young and Price, 1985), where the only possible opponent pigment is presumed to be rhodopsin, yielding pure SWS1 / rod

opponent systems. The rod-cone interaction architectures of rabbit are likely relevant for primate chromatic, spatial, and temporal percepts, as human rod-cone interactions clearly involve peripheral retina (Buck, 2004; Thomas and Buck, 2006; Trezona, 1973), a region stereotyped across mammals (Jeon et al., 1998). Though the human foveola is rod free (Curcio et al., 1987) and lacks rod-biased neurons such as A_{II} ACs (Kolb et al., 2002), the rod-free zone is so small (≈ 0.2 mm) that wide-field γAC crossover motifs could easily bridge the foveola and surrounding rod networks, permitting concurrent rod suppression of foveal cone signals and foveal suppression of nearby rod signals. A definitive proof will require assembly of a primate retinal connectome.

Rod-cone crossover suppression resembles sparsely instantiated, densely convergent winner-take-all (Kurt et al., 2008) networks. Psychophysical evidence shows that human mutual rod-cone suppression can operate in a winner-take-all mode (Buck, 2004; Stabell and Stabell, 1998, 2002), which must have a crossover design (Oster et al., 2009). Ultimately, physiological biasing must provide the switching features that distinguish simple opponent outcomes from winner-take-all outcomes. A more detailed assessment of molecular tuning at each signaling stage is essential to determine how rod-cone crossover chains are refined by differential glutamate, GABA, and glycine receptor subunit expression, or other switching schemas (Eggers and Lukasiewicz, 2006a). The similarity of retinal and cortical cross-channel suppression in perceptual, pharmacologic, and network domains argues that the retina may be an

exceptional model for exploring general mechanisms in the development, maintenance, and dysfunction of decision networks.

Acknowledgments

Table 4.1. Synaptic chains mediating rod-cone cross-channel suppression

Motif	Gain	Chain
C1	n^2p	C $>_m$ CBb > wf γAC $>_i$ RB
C2	n^2p	C $>_m$ CBb > nf GAC $>_i$ RB
C3	n^2p^2	C > CBa > wf γAC $>_i$ wf "ON" γAC $>_i$ RB
C4	n^2p^2	C > CBa > wf γAC $>_i$ A$_l$ γAC $>_i$ RB
C4a	n^2p^3	C > CBa > A$_{ll}$ GAC wf $>_i$ γAC $>_i$ A$_l$ γAC $>_i$ RB
C5	n^2p^2	C > CBa > nf GAC $>_i$ A$_l$ γAC $>_i$ RB
R1	n^3pc	R $>_m$ RB > A$_{ll}$ GAC :: CBb > wf ON γAC $>_i$ CBb
R2	n^3p^2	R $>_m$ RB > A$_{ll}$ GAC $>_i$ CBa > wf OFF γAC $>_i$ CBa
R3	n^2p	R $>_m$ RB > wf ON γAC $>_i$ CBb

Legend. We characterize the nominal gains (amplifications) of these motifs by their serial glutamatergic cationic (n), GABAergic or glycinergic anionic (p), and coupling (c) transfer functions, expressing a chain's gain as their product (npc). For example, the cone → BC → AC → BC signaling chain has a net gain of n^2p. We assume that most excitatory gains are > 1 (*22, 23*) and that most inhibitory (*24, 25*) or coupling networks have gains < 1. We argue that concatenated excitatory gains (n, n^2, n^3) play a major role in setting the sensitivity of networks and that contatenated inhibitory gains and coupling are likely attenuating (p, cp, p^2). This vastly oversimplifies the likely nonlinearities, cable attenuations, synaptic fatigue, synaptic desensitization, and timing events associated with each network (*45*), but should be a dominant weighting factor in any model.

Figure 4.1. Rod-cone transitions and networks.   **A**. Visual threshold (VT, black line) varies over the daily cycle. The cusps are transitions between rod and cone dominated vision. Variations in threshold (dotted lines) are driven by skylight and canopy factors. **B**. In mammals, rod signals collected by rod bipolar cells are aggregated by A_{II} amacrine cells (ACs) and redistributed into the cone bipolar cell chain, resulting in three-stage excitatory amplification (n^3). **C**. Other vertebrates use mixed rod-cone bipolar cells that drive ganglion cells directly, achieving only two-stage amplification (n^2).

A

mesopic   mesopic

overcast

cones

VT↑
time

rods

sunset   moonrise   sunrise

B. Mammals

rods $\xrightarrow{\quad n \quad}$ rod bipolar cells $\xrightarrow{\quad n^2 \quad}$ A_{II} amacrine cells

cones $\longrightarrow$ cone bipolar cells $\xrightarrow{\quad n^3 \quad}$ ganglion cells

C. Other Vertebrates

rods $\xrightarrow{\quad n \quad}$ mixed bipolar cells $\xrightarrow{\quad n^2 \quad}$ ganglion cells

cones $\longrightarrow$ cone bipolar cells $\longrightarrow$ ganglion cells
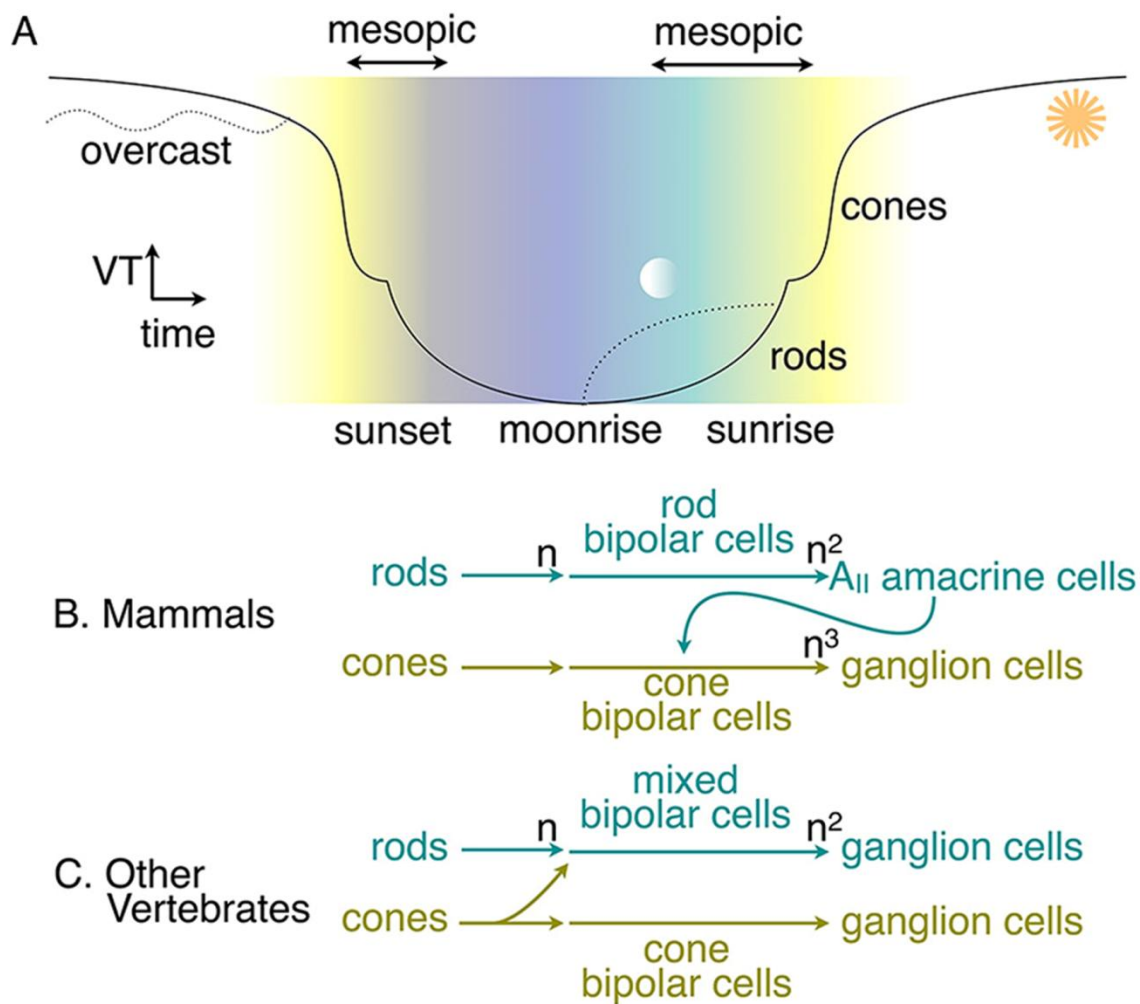
Figure 4.2. Motifs C1 and C2. **A**. A rendering of all rod BC axon terminals in volume RC1. Rod BC 5923 is circled. Each color is a single rod BC terminal. **B**. Wide-field γAC 598 (red) and narrow-field GAC 278 (green) engaged in motifs C1 and C2 respectively. **C**. A minimum spanning graph that provides crossover cone inhibition to every rod BC using γAC (red, orange) and GAC (green) processes, including γAC 598 (up arrow) and GAC 278 (down arrow). CBb5 6120 is circled. The smallest distance between a CBb and its target rod BC is marked by the small square and a large CBb → RB path is marked by the rectangle. **D**. The inhibitory field of processes superimposed on the rod BC field (magenta). Motif C1 γAC process 32477 (white process, arrows) spans rod BC 5923 and CBb5 6120. The field of γAC 18282 that drives motif R3 is superimposed in blue. **E**. γAC 32477 is presynaptic (the arrow indicates signal flow) to rod BC 5293, which receives input from another motif C1 cell (γAC 39982) and a classical A_I AC (γAC 39986). **F**. CBb5 6120 provides excitatory input via a synaptic ribbon (r) onto γAC 32477. **G**. γAC 32477 provides reciprocal inhibition (arrow) to CBb5 6120. **H**. Motif C2 GAC 278 collects signals from two nearby CBb cells (CBb5 277, CBb6 344) and delivers glycinergic inhibition to two adjacent rod BCs (RB 334, RB 342). **I**. CBb5 synapses onto GAC 278. Inset, ribbon viewed at a different tilt, revealing the uniform synaptic cleft. **J**. Motif C2 synapse from GAC 278 onto RB 342, which also collects three C1 synapses from ACs 31700, 39998, 31702. Scales: A, C, D 100 µm; B 69 µm ; H 50 µm; E, F, G, I, J 500 nm.
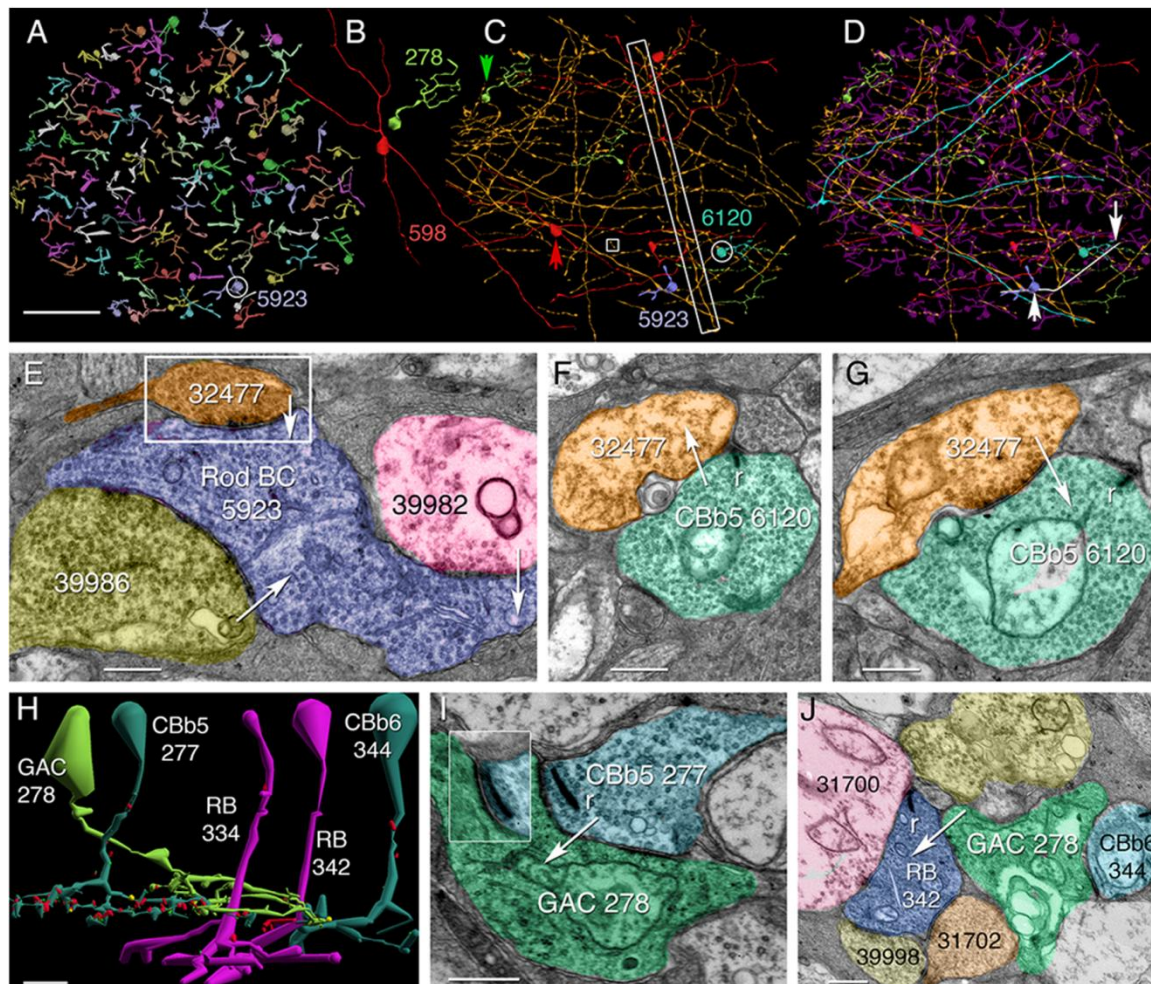
Figure 4.3. Motifs C3 and C4. **A**. Motif C3 γAC 5281 and its target rod BCs (dark magenta), and motif C4 A$_I$ AC 4943 with elements of its source C4 crossover chain (CBab 5542, CBa2 5532, OFF γAC 5441) and its target rod BCs (bright magenta). Synapses on the proximal dendrites of A$_I$ AC 4943 are marked with circles. Scale, 50 µm. **B**. A composite γAC 5281 with four of its six somatic AC inputs marked. Inset, enlargement of AC 43117. **C**. γAC 5281 targeting CBbw 483 in the ON layer. Inset, enlargement of the synapse. **D**. γAC 5281 targeting rod BC 10960 in the ON layer. **E**. CBab 5538 driving motif C4 γAC 8551. **F**. Motif C4 γAC 13448 driving A$_I$ AC 4943. Asterisks delimit a 2.1 µm synaptic arc. **G**. A$_I$ AC 4943 presynaptic to rod BC 469. **H**. A$_I$ AC 4943 postsynaptic to rod BC 8586. Scales in panels B-H, 500 nm.
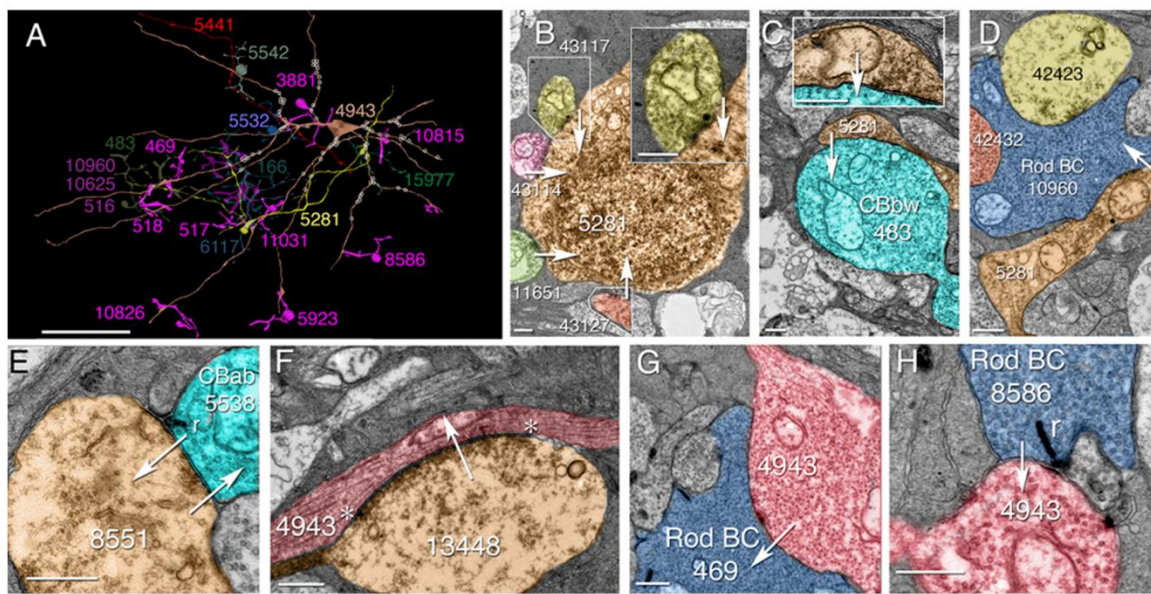
Figure 4.4. Motifs R1 and R2. **A**. A$_{II}$ AC 514 with motif R1 and R2 partners. The vertical view displays AC 514, rod BC 471, CBb 1724, and CBab 4568. The horizontal below shows the same cell, motif R1 process 23512 that targets CBb4 4569, and motif R2 process 43404 that targets CBab 181. The signaling chain is shown for R1 and R2. Scales, 10 μm. **B**. One of six gap junctions (arrowheads) between AC 514 and CBb1724. **C**. CBb 1724 synapse onto motif R1 γAC 23512. **D**. Motif R1 γAC 23512 targeting CBb4 4569. **E**. AC 514 synapses onto CBab 4658. **F**. CBab 4568 forms a synapse onto motif R2 γAC 43404. Inset, enlargement of the 122 nm long ribbon. **G**. Motif R2 γAC 43404 targets CBab 181. Scales B-G, 500 nm; Scale for inset F, 250 nm.
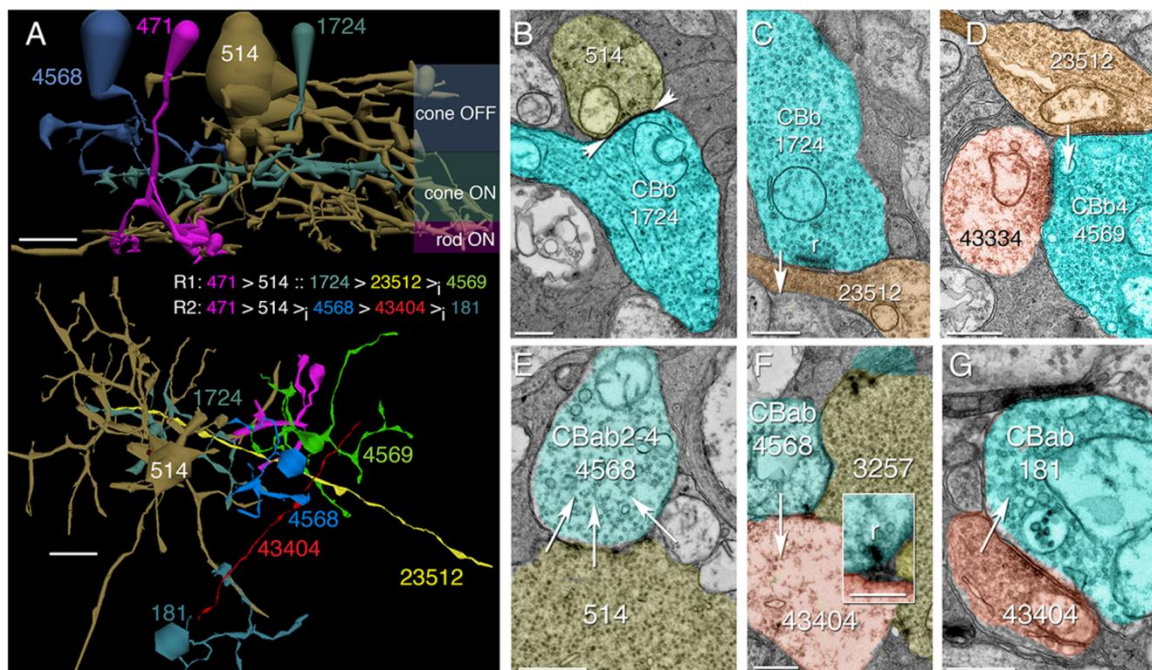
Figure 4.5. Crossover motifs. **A**. Motif C1. Coupled CBb cells (tan honeycomb) are presynaptic to wide-field ON γACs that target single rod BCs (RB, white circle) in a chain synapses for a total gain of n^2p (see text and Table S1). **B**. Motif C2. CBbs are presynaptic to narrow-field ON GACs that target single rod BCs. **C.** Motif C3. CBa cells (gold honeycomb) are presynaptic to wf OFF γACs that target bistratified wf ON γACs in the OFF layer by somatic synapses, which in turn target rod BCs. **D**. Motif C4/C4a. CBa cells are presynaptic to wf OFF γACs that target A_I γACs in the OFF layer by GABAergic synapses on the proximal dendrites, which in turn target rod BCs. Some OFF γACs are also targeted by A_{II} ACs in the chain. **E**. Motif C5. CBa cells drive narrow-field GACs that synapse on the proximal dendrites of A_I γACs. **F**. Motif R1. Rod BCs drive A_{II} ACs coupled to CBb cells. CBb cells are presynaptic to ON γACs that inhibit nearby and distant CBb cells. **G**. Motif R2. Rod BCs drive A_{II} ACs that are presynaptic to CBa cells, which drive OFF γACs to inhibit nearby and distant CBa cells. **H**. Motif R3. Sparse rod BCs drive mixed rod-cone γACs that are presynaptic to large numbers of CBb cells.
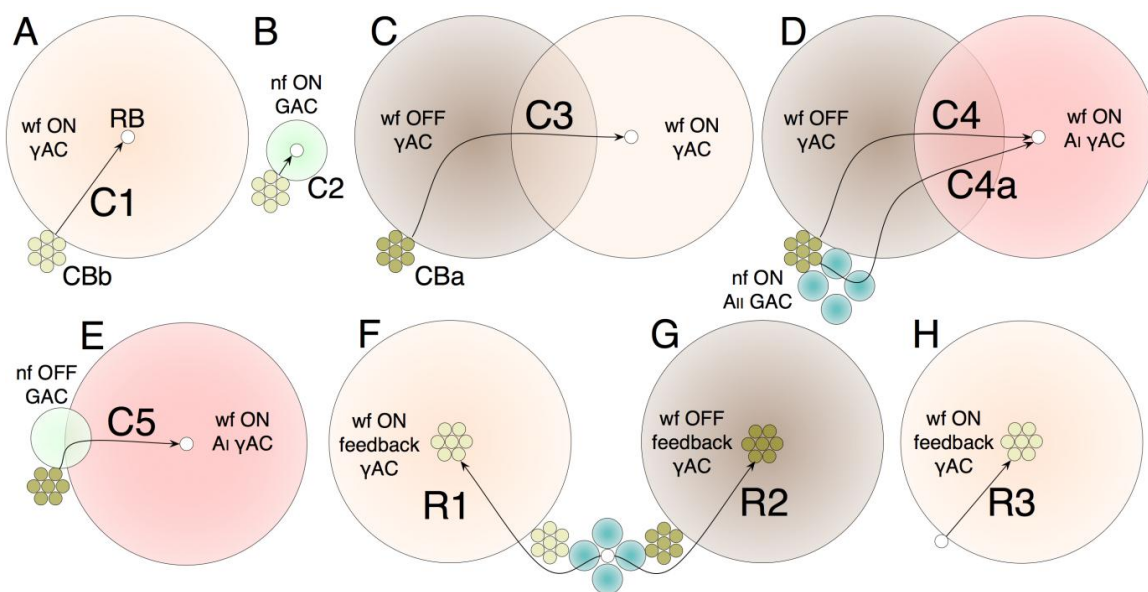
References

Anderson JR et al. 2009. A computational framework for ultrastructural mapping of neural circuitry. PLoS Biol 7(3):e1000074.

Anderson JR et al. 2011a. Exploring the retinal connectome. Mol Vision 17:355-379.

Anderson JR et al. 2011b. The Viking viewer for connectomics: scalable multi-user annotation and summarization of large volume data sets. J Microscopy 241:13-28.

Bloomfield SA. 1992. Relationship between receptive and dendritic field size of amacrine cells in the rabbit retina. J Neurophysiol 68:711-725.

Bock DD et al. 2011. Network anatomy and in vivo physiology of visual cortical neurons. Nature 471(7337):177-182.

Briggman KL, Denk W. 2006. Towards neural circuit reconstruction with volume electron microscopy techniques. Current Opinion in Neurobiology 16:562-570.

Briggman KL et al. 2011. Wiring specificity in the direction-selectivity circuit of the retina. Nature 471:138-188.

Buck SL. 1997. Influence of rod signals on hue perception: evidence from successive scotopic contrast. Vision Res 37:1295-3101

Buck SL. 2004. Rod-cone interactions in human vision. In: Chalupa LM, Werner J, editors. Visual Neurosciences. Cambridge, MA: MIT Press. pp. 863-878.

Copenhagen DR et al. 1990. Signal transmission through the dark-adapted retina of the toad (Bufo marinus). Gain, convergence, and signal/noise. J Gen Physiol 95:717-732.

Curcio CA et al. 1987. Distribution of cones in human and monkey retina: individual variability and radial asymmetry. Science 236:579-582.

Dacheux RF, Raviola E. 1986. The rod pathway in the rabbit retina: a depolarizing bipolar and amacrine cell. J Neurosci 6:331-345.

Eggers ED, Lukasiewicz PD. 2006a. GABA(A), GABA(C), and glycine receptor-mediated inhibition differentially affects light-evoked signaling from mouse retinal rod bipolar cells. J Physiol 572:215-225.

Goldberg SH et al. 1983. Inhibitory influence of unstimulated rods in the human retina: evidence provided by examining cone flicker. Science 221:180-182.

Harwerth RS, Levi DM. 1977. Increment threshold spectral sensitivity in anisometropic ambylopia. Vision Res 17:585-590.

Harwerth RS et al. 1990. Behavioral studies of the sensitive periods of development of visual functions in monkeys. Behav Brain Res 41:179-198.

Ingling CRJ et al. 1977. Cones change rod sensitivity. Vision Res 17:555-563.

Jeon CJ et al. 1998. The major cell populations of the mouse retina. Journal of Neuroscience 18(21):8936-8946.

Kolb H et al. 2002. A new look at calretinin-immunoreactive amacrine cell types in the monkey retina. J Comp Neurol 453:168-184

Kurt S et al. 2008. Auditory cortical contrast enhancing by global winner-take-all inhibitory interactions. PLoS ONE 3:e1735.

Lauritzen JS et al. 2013. ON Cone Bipolar Cell Axonal Ribbons in the OFF Inner Plexiform Layer of the Rabbit Retina. J Comp Neurol 521(5): 977-1201. doi: 10.1002/cne.23244 [Epub ahead of print].

MacNeil MA et al. 1999. The shapes and numbers of amacrine cells: matching of photofilled with Golgi-stained cells in the rabbit retina and comparison with other mammalian species. Journal of Comparative Neurology 413(2):305-326.

Maltenfort MG et al. 1998. Decorrelating actions of Renshaw interneurons on the firing of spinal motoneurons within a motor nucleus: a simulation study. J Neurophysiol 80:309-323.

Marc RE et al. 1995. Pattern recognition of amino acid signatures in retinal neurons. J Neurosci 15:5106-5129.

Marc RE, Liu WL. 2000. Fundamental GABAergic amacrine cell circuitries in the retina: nested Feedback, concatenated inhibition, and axosomatic synapses. J Comp Neurol 425(4):560-582.

Marc RE, Jones BW. 2002. Mjolecular phenotyping of retinal ganglion cells. J Neurosci 22:413-427.

Marc RE et al. 2012. Building Retinal Connectomes. Current Opinion in Neurobiology 22(4):568-574.

Molnar A et al. 2009. Crossover inhibition in the retina: circuitry that compensates for nonlinear rectifying synaptic transmission. J Comput Neurosci 27:569-590.

Oster M et al. 2009. Computation with Spikes in a Winner-Take-All Network. Neural Computation 21:2437-2465.

Pang JJ et al. 2010. Direct rod input to cone BCs and direct cone input to rod BCs challenge the traditional view of mammalian BC circuitry. Proc Natl Acad Sci U S A 107:395-400.

Sperling HG, Harwerth RS. 1971. Red-green cone interactions in the increment-threshold spectral sensitivity of primates. Science 172:180-184.

Stabell B, Stabell U. 1998. Chromatic rod-cone interaction during dark adaptation. J Opt Soc Am A Opt Image Sci Vis 15:2809-2815.

Stabell B, Stabell U. 2002. Effects of rod activity on color perception with light adaptation. J Opt Soc Am A Opt Image Sci Vis 19:1249-1258.

Strettoi E et al. 1990. Synaptic connections of rod bipolar cells in the inner plexiform layer of the rabbit retina. J Comp Neurol 295(3):449-466.

Strettoi E et al. 1992. Synaptic connections of the narrow-field, bistratified rod amacrine cell (AII) in the rabbit retina. J Comp Neurol 325:152-168.

Tasdizen T et al. 2010. Automatic mosaicking and volume assembly for high-throughput serial-section transmission electron microscopy J Neuroscience Methods 193:132-144.

Thomas LP, Buck SL. 2006. Foveal and extra-foveal influences on rod hue biases. Vis Neurosci 23:539-542.

Trezona PW. 1970. Rod participation in the 'blue' mechanism and its effect on colour matching. Vision Res 10:317-332.

Trezona PW. 1973. The tetrachromatic colour match as a colorimetric technique.
.   Vision Res 13:9-25.
Werblin FS. 2010. Six different roles for crossover inhibition in the retina: correcting the nonlinearities of synaptic transmission. Vis Neurosci 27:1-8.

Wu SM. 1991. Input-output relations of the feedback synapse between horizontal cells and cones in the tiger salamander retina. J Neurophysiol 65:1197-1206.

Yang XL, Wu SM. 2004. Signal transmission from cones to amacrine cells in dark- and light-adapted tiger salamander retina. Brain Res 1029:155-161.

Young RS, Price J. 1985. Wavelength discrimination deteriorates with illumination in blue cone monochromats. Invest Ophthalmol Vis Sci 26:1543-1549.

CHAPTER 5

DISCUSSION

Refactoring the Inner Plexiform Layer

Over four decades of research has indicated that the mammalian retina is structurally and functionally segregated into ON and OFF domains (Famiglietti et al., 1977; Famiglietti and Kolb, 1976; MacNeil et al., 2004; Wässle et al., 2009; Werblin and Dowlin, 1969a, b), yet nonmammalian bony vertebrates (reptiles, avians, amphibians, teleost fishes) possess multistratified bipolar cells that overtly arborize and form synapses in opposite-polarity IPL layers (Pang et al., 2004; Sherry and Yazulla, 1993). Researchers have infrequently reported ribbon sites in mammalian ON cone bipolar cell axons, though these were never quantified and their functional significance remained unknown. The first two chapters demonstrate repeatedly that the ON and OFF neural retina are not discrete. Rather, neural multistratification is more subtle than in other vertebrates, but not evolutionarily lost. Chapter 3 reveals photopic-scotopic inhibitory crosstalk at the level of the neural retina. Decades of psychophysical data indicates mutual rod-cone pathway suppression, but previous techniques failed to capture the substrate, and it was largely suspected to arise from cortical processing. This discovery suggests that the neural retina can behave as a winner-take-all network analogous to those found in cortex, expanding our functional view and validating the neural retina as an excellent model system for understanding plexiform layers throughout the brain. The following four sections discuss specific results presented in Chapters 1-3 and a common principle of joint distributions of source-target neurites that evolves from this work and reframes our statistical interpretations of neural networks.

ON Cone Bipolar Cells Break the IPL Stratification Rules

The existence of mixed ON/OFF signaling has been dismissed or ignored for mammalians until recent optical evidence of ON BC axonal ribbon output in the OFF layer of the IPL was reported by several groups (Dumitrescu et al., 2009; Hattar et al., 2002; Hoshi et al., 2009). Ultrastructural connectomics now recapitulates (Anderson et al., 2011a) and extends (Lauritzen et al., 2013) these findings to demonstrate all classes of ON cone bipolar cells (CBbs) form input and output synapses throughout the OFF IPL. Specifically, ON cone bipolar cells target intrinsically photosensitive GCs (ipGCs) and bistratified diving GCs (bsdGCs) in the nominal OFF IPL, both of which are pure ON cells (Dumitrescu et al., 2009; Hoshi et al., 2009) with OFF layer-stratifying dendrites. CBbs also synapse with discrete sets of glycinergic ACs (GACs) and GABAergic ACs (γACs) to construct ON $>_i$ OFF and OFF $_{i<}$ ON crossover inhibition motifs (Lauritzen et al., 2013). It remains unclear why ipGCs and bsdGCs arborize in the OFF layer to harvest CBb cell inputs when those are also available in the ON layer, yet connectomics shows that these cells also capture massive input from OFF γACs but not OFF cone (CBa) bipolar cells, providing wide-field ON polarity input via OFF synaptic chains: [cone > CBa BC > γAC $>_i$ ipGC/bsdGC] with a gain of n^2p (see np notation from Chapter 3). Why they obtain a low-gain ON signal in the OFF layer is not clear, but certain OFF ACs appear to be preferred targets. Furthermore, since most inhibitory gains (p) could be fractional (Wu, 1991), the direct ON input from CBb axons should have a higher sensitivity than the polarity-matched input via the CBa-driven amacrine cells by a factor of p^{-1}.

The immediate interpretation is that targets of such differentially amplified, kinetically distinct, yet polarity matched input signals can finesse their spatial sampling and postsynaptic membrane potential responses with such input arrays. Simply, these ON-OFF crosstalk architectures could afford greater spatiotemporal control of the responses of the target cells, allowing them to increase or decrease transiency over varied photic capture regions, for instance.

OFF Cone Bipolar Cells Break the IPL Stratification Rules

Additional refactoring of the mammalian inner plexiform layer arises from the deep incursion of a subset of CBa cells into the ON layer, where they synaptically construct ON-OFF amacrine cells in concert with comingled CBb syanpses to common targets, and further create ON → OFF and OFF → ON crossover inhibition motifs throughout IPL sublaminae 3-5 (traditionally considered pure ON laminae). Combined with the above discovery of mixed ON-OFF signaling in the distal IPL, this disintegrates the discrete ON-OFF IPL boundary, revealing that 80% of the IPL comprises intermixed ON and OFF signaling motifs. An important outcome of these discoveries is that amacrine and ganglion cell stratification patterns in the inner plexiform layer do not necessarily predict the response properties of a cell. The presence of bistratified ganglion cells with dendrites in the OFF layer but pure ON respnonse properties (Hoshi et al., 2009; Lauritzen et al., 2013), and monostratified ganglion cells in the nominal ON layer with mixed ON-OFF properties (Lauritzen et al., 2013; Tian, 2008) reinforces the idea that cells of a given polarity need to establish opposite-

polarity synaptic partners as routine signaling elements. Moreover, repeating motifs that break our legacy of ON-OFF segregation suggests that appropriate source-target pairing occurs at every joint encounter, regardless of lamination. A complete ultrastructural network mapping is essential to understanding these pathways.

Rod Bipolar Cell-Cone Bipolar Cell Cross Inhibition

The discovery of massive cross inhibition between rod and cone bipolar cells enhances the functional landscape of the retina. The perceptually smooth transition from photopic to scotopic domains demands reconciliation with psychophysical evidence for winner-take-all mutual rod-cone suppression events. Neither physiological nor anatomical approaches have provided accounts for rod-cone cross suppression because they lack the resolution needed for synaptic completeness and the ability to view large networks in the same dataset. We discovered eight rod bipolar-cone bipolar cross inhibitory motifs in RC1, five cone bipolar cell-driven motifs, and three rod bipolar cell-driven motifs. Wide connectomics reveals that *every* cone bipolar cell class receives rod bipolar cell-driven inhibition, and establishes cone bipolar cell class-motif relationships. Deep connectomics proves that *every* rod bipolar cell receives ON cone bipolar cell-driven inhibition and that *every* AI amacrine cell receives OFF cone bipolar cell-driven inhibition. In other words, the retina is not merely a perceptual filter, it appears to operate analogously to decision networks found deeper in the brain.

Joint Distributions of Synaptic Sources and Targets

Synaptic connections at neurite intersections create functional networks. However, differential neurite densities and geometries across cell classes (Reese, 2008) influence the probability of encounter (Lauritzen et al., 2013). Most wide-field γACs cover the retina with extensive in-class overlap with coverages >> 4 (i.e., center to center), whereas narrow-field GACs have modest overlap closer to 4. Many, if not most, ganglion cells tile the same space with low overlap and coverages < 4, often close to 1. BCs have mixed patterning depending on class. Some extensively cover, whereas some tile perfectly. Because some classes are very sparse and others are dense, synaptic encounter rates will depend on joint distributions of synaptic sources and targets. Different cell classes fill the retinal space very differently (formally known as Hausdorff dimensions). The Hausdorff dimensions are typically low for wide-field amacrince cells and α-ganglion cells, and much higher for bipolar cells. These geometries influence how network motifs sample each other. Put simply, it is impossible for every source and target to be optimized to achieve 100% contact or spatially constant contact variance. Chapter 1, Figure 11 provides a geometric proof of this. Because we do not know the sampling volumes for various cell classes, we must discover them by connectomics.

Conventionally scientists attempt to describe the outflow of signals from a given cell class to superclasses of targets (e.g., bipolar cell class X to amacrine cells or ganglion cells) in terms of percentages of targets contacted. Yet the varied topologies discovered via connectomics highlight the importance of joint

distributions (Lauritzen et al., 2013). An example of this is the flow of axonal ribbon signaling from ON cone bipolar cell axons to targets in the OFF layer. The axonal ribbons provide an oversupply of sources relative to targets. Ganglion cells form only a small fraction of postsynaptic targets for ON cone bipolar cell axonal ribbons, due to the ON cone bipolar cells' higher Hausdorff dimensions (the bipolar cells are more space filling) than ganglion cells. However, specific ganglion cells form a synapse with every axonal ribbon encountered, for a sampling efficiency of 100%. Thus, the variance of output patterns of profiles across a given set has little functional meaning.

The Dangers of Inverse Solutions to Complex Networks

New rules governing neural network architectures can now be incorporated into interpretation of physiological observations. For instance, crossover inhibition is currently a contentious area of the physiological literature (Liang and Freed, 2010; Manookin et al., 2008; Werblin, 2010). Two important findings from connectomics have not entered the debate thus far because physiology is incapable of testing them directly. Nonetheless, connectomics reveals their prevalence in crossover networks as detailed below.

First, physiologists assume that the inner plexiform layer (IPL) is divided into discrete ON and OFF layers, with morphologically-defined cell classes constrained to one domain or the other. This often leads to error in interpreting physiological results. They suggest that multistratified amacrine cells which span the ON-OFF boundary must be responsible for the crosstalk, yet connectomics

reveals that other cell classes, such as cone bipolar cells, can multistratify and engage monostratified amacrine cells to construct crossover motifs. This increases the number of possible source-target pairings and teaches us that many additional cells classes may be involved in the crossover inhibition process which have never been considered before. It further carries direct functional consequence, as unique morphological cell classes are believed to possess unique functional properties. Thus, the physiological complexity of these networks is currently underestimated. By identifying the involvement of these new distinct morphological cell classes, we create a list of new cell types to be systematically targeted for future physiological investigation.

Second, crossover inhibition networks have thus far only been discovered to use glycine as the neurotransmitter, but no involvement of GABA. This may initially seem surprising as every cell in the neural retina receives input from GABAergic amacrine cells, yet GABAergic and glycinergic amacrine cells form concatenated and nested feedback and feedforward chains (Marc and Liu, 2000), making it difficult to pharmacologically isolate. Connectomics analyses offer repeated examples of GABA-positive amacrine cells involved in crossover inhibition network motifs, often in parallel and/or nested relationships with glycinergic crossover motifs. These networks appear to pervade the IPL and now become tractable via connectomics analyses.

Collectively, the above results improve our ability to interpret functional data, instruct us in neural synaptic partnering rules, teach us the architectures responsible for complex neural response properties, and create a model for

understanding plexiform layer construction elsewhere in the brain. Functional network analysis presupposes the ability to evaluate canonical networks. Individual cellular recordings cannot decompose the input complexity from which they are created, and models are grossly inadequate without proper parameterization. We assert that the results presented herein provide proof of concept that high resolution ultrastructural connectomics is appropriately scaled to and necessary for effective network analyses.

Conclusion

Completeness

Three central issues must be satisfied to achieve completeness with connectomics approaches. First, 2 nm resolution or better is required to unambiguously mark synapses and gap junctions for complete network mapping (Bourne and Harris, 2011; Kamasawa et al., 2006; Massey, 2008). TEM is optimal for such endeavors. Second, molecular (Anderson et al., 2011a; Shu et al., 2011) or optical (Briggman et al., 2011) tagging to preselect cells of interest in complex neural populations (Bock et al., 2011) need more platforms and the ability to share them effectively (Anderson et al., 2009). Commercial fMRI systems that support macroscale connectomics are indeed established, now the same is needed for high resolution TEM-based connectomics. The next generation of tools should promote comparative neuroanatomy and pathoconnectomics of retinal neurodegenerations by facilitating the creation of multiple connectomes in parallel (Jones et al., 2011; Jones et al., 2003). The

faster we can create and analyze datasets of sufficient size, the greater our potential for discovery. Inexpensive, high-resolution commercial systems must be developed for the scientific community.

Mapping exact contacts and contact patterns across multiple instances of a cell class is required to achieve statistical completeness. We expect that as sampling approaches completeness, some metrics will minimize their variance, but we do not currently know which metrics those are. Some classical statistics may turn out to be useless or even misleading. For example, the mean rod BC ribbon synapse count onto four adjacent A_{II} ACs in RC1 is 74 ± 5 (1 SD) with coefficient of variation (CV) of 0.066. The same cells have a mean rod BC contact count of 11.5 ± 3.7 and a CV of 0.32, a variation fivefold greater for exactly the same sample space. This suggests that neurons normalize synapse number despite varying neurite overlap geometries. On the other hand, there are spatial variances that are clearly meaningless in a physiologic context, such as the percentage of output onto various cells from A_{II} ACs, although they may be useful as classifiers. In network flow, the partitioning of output is not a usable metric, whereas the sampling of an output grid as the input to a spatially complex cell is critical. In that scenario, the sampling of A_{II} ACs by GCs is perfect (i.e., sampling from all encountered opportunities) and likely idempotent. Completeness is also gauged by edge density in network graphs where submotifs can be extracted and quantitatively compared.

The Future of Connectomics

Interpreting the functional role of cells based on electrophysiological properties depends on complete knowledge of their input and output arrays. There are too many possible explanations for observable results to explain with inverse solutions. We need to build connectomes faster and in parallel, with improved management and analysis software to make large-scale datasets tractable in reasonable timeframes.

Currently, advanced customized software is required to build, manage, and analyze terabyte-scale connectome volumes (Anderson et al., 2011a; Fiala, 2005; Jeong et al., 2010). Additionally, expensive TEM platforms with automated stages for high throughput and digital imaging are required, but most TEM scopes currently lack these. If we are to successfully incorporate connectomics approaches as mainstream tools, these obstacle must be surmounted.

To meet this challenge, Marc and colleagues developed an open-source Web-compliant Viking environment (Anderson et al., 2011b) that supports multiuser visualization via dataset conversion to Web-optimized tiles and delivers volume transforms to client devices over the internet. Converting ultrastructure into three-dimensional renderings and network graphs also requires integration of annotation and database architectures. In Viking, disks placed within structural profiles approximate convex hulls which are linked to build three-dimensional representations. Relational elements such as presynaptic complexes (ribbons, densities, vesicle accumulations), postsynaptic densities, gap junctions, and adherens junctions are located and linked to build adjacency matrices.

Additionally, data and metadata queries, and network Web tours can be performed based on annotations.

Analyzing networks requires rendering, graphing, network touring, and informatics. Vikingplot and Viz (Anderson et al., 2011a) are services using Viking databases to allow cell renderings at higher resolutions than optical methods, automated network graphs, navigation between ultrastructural data and network motifs, and automated statistical summaries. Although efforts are being made to achieve automated tracing (Jeong et al., 2010; Jurrus et al., 2010; Luisi et al., 2011; Narayanaswamy, Wang, and Roysam, 2011), currently every connectomes must be validated by human annotation (Anderson et al., 2011a), and none are practical for complex neuropil comprising fine processes. Correcting annotation errors is not an obstacle, as errors become highly salient against repeating themes, completeness in network diagrams ultimately purges errors, and metadata parsing can effectively highlights errors. Errors such as skipping between processes in tracing are flagged as forbidden switches in molecular signatures, associated synapse type, targets, inputs, and network motifs. One of the best methods for error tracking and repair is parsing network graphs for wiring violations (e.g., self-synapse loops). Unexpected network motifs are revisited by experts to determine if they are errors or new discoveries.

To overcome the above obstacles, connectomics datasets must be shared in the future (Amari et al., 2002; Anderson et al., 2011a; Jeong et al., 2010); however, the immense size of these datasets interferes with their distribution. Open-access web services could provide a solution here. Accordingly, we

publicly share our datasets and tools. Viking utilizes open-source tools and common file formats to effectively interface with other widely used applications for viewing, such as Blender or Autodesk® Maya. Intellectual ownership and publication issues become complex and will need to be resolved. Integrating annotated datasets and summary networks with large informatics frameworks is critical for future expansion and sharing as well (Akil et al., 2011; Martone et al., 2008).

The future of neural network discovery must involved cooperative multidisciplinary efforts. Clearly, physiological dissection is needed, as are more accurate models, if we are to understand and repair normal and diseased neural networks. However, complex synaptic chains are difficult to pharmacologically isolate, and models need accurate parameterization to be of any meaning. Connectomics provides the solution to both of these problems with the ability to reconstruct exact complex network architectures such as nested and reentrant motifs and quantify the relative intra- and interclass synaptic weights and directionalities. Targeted symbiotic relationships between these three, and other, disciplines is necessary to understand neural networks. The question of the minimum sufficient solution remains open for now.

References

Akil H et al. 2011. Challenges and opportunities in mining neuroscience data. Science 331:708-712.

Anderson JR et al. 2011b. The Viking Viewer: Scalable multiuser annotation and summarization of large connectomics datasets. J Microscopy 241:13-28.

Anderson JR et al. 2009. A computational framework for ultrastructural mapping of neural circuitry. PLoS Biol 7(3):e1000074.

Bock DD et al. 2011. Network anatomy and in vivo physiology of visual cortical neurons. Nature 471(7337):177-182.

Bourne JN, Harris KM. 2011. Nanoscale analysis of structural synaptic plasticity. Current Opinion in Neurobiology 22:1-11.

Briggman KL et al. 2011. Wiring specificity in the direction-selectivity circuit of the retina. Nature 471:138-188.

Dumitrescu ON et al. 2009. Ectopic retinal ON bipolar cell synapses in the OFF inner plexiform layer: contacts with dopaminergic amacrine cells and melanopsin ganglion cells. J Comp Neurol 517:226-244.

Famiglietti EV et al. 1977. Neuronal Architecture of on and off pathways to ganglion cells in carp retina. Science 198(4323):1267-1269.

Famiglietti EV, Kolb H. 1976. Structural basis for ON- and OFF-center responses in retinal ganglion cells. Science 194(4261):193-195.

Fiala JC. 2005. Reconstruct: a free editor for serial section microscopy. J Microsc 218(Pt 1):52-61.

Hattar S et al. 2002. Melanopsin-Containing Retinal Ganglion Cells: Architecture, Projections, and Intrinsic Photosensitivity. Science 295(5557):1065-1070.

Hoshi H et al. 2009. ON inputs to the OFF layer: bipolar cells that break the stratification rules of the retina. J Neurosci 29(28):8875-8883.

Jeong W et al. 2010. SSECRETT and NeuroTrace: Interactive Visualization and Analysis Tools for Large-Scale Neuroscience Datasets. IEEE Computer Graphics and Applications 30:58-70.

Jones BW et al. 2011. Retinal degenerative disease and remodeling in a large eye model. J Comp Neurol 519:2713-2733.

Jones BW et al. 2003. Retinal remodeling triggered by photoreceptor degenerations. Journal of Comparative Neurology 464:1-16.

Kamasawa N et al. 2006. Abundance and ultrastructural diversity of neuronal gap junctions in the OFF and ON sublaminae of the inner plexiform layer of rat and mouse retina. Neuroscience 142:1093-1117.

Lauritzen JS et al. 2013. ON Cone Bipolar Cell Axonal Ribbons in the OFF Inner Plexiform Layer of the Rabbit Retina. J Comp Neurol 521(5):977-1201.

Liang Z, Freed M. 2010. The ON pathway rectifies the OFF pathway of the mammalian retina. J Neurosci 30(16):5533-5543.

MacNeil M et al. 2004. The population of bipolar cells in the rabbit retina. J Comp Neurol 472:73-86.

Manookin MB et al. 2008. Disinhibition combines with excitation to extend the operating range of the OFF visual pathway in daylight. J Neurosci 28:4136-4150.

Marc RE, Liu WL. 2000. Fundamental GABAergic amacrine cell circuitries in the retina: nested Feedback, concatenated inhibition, and axosomatic synapses. J Comp Neurol 425:560-582.

Martone ME et al. 2008. The cell centered database project: an update on building community resources for managing and sharing 3D imaging data. J Struct Biol 161(3):220-231.

Massey SC. 2008. Circuit functions of gap junctions in the mammalian retina. In: Masland RH, Albright T, editors. The Senses: A comprehensive reference. Amsterdam: Elsevier. p 457-471.

Pang JJ et al. 2004. Stratum-by-stratum projection of light response attributes by retinal bipolar cells of Ambystoma. J Physiol 558:249-262.

Reese B. 2008. Mosaics, tiling and coverage by retinal neurons. In: Masland RH, Albright T, editors. The Senses: A comprehensive reference Vision. Amsterdam: Elsevier.

Sherry DM, Yazulla S. 1993. Goldfish bipolar cells and axon terminal patterns: a Golgi study. J Comp Neurol 329(2):188-200.

Shu X et al. 2011. A genetically encoded tag for correlated light and electron microscopy of intact cells, tissues, and organisms. PLoS Biol 9:e1001041.

Tian N. 2008. Synaptic activity, visual experience and the maturation of retinal synaptic circuitry. J Physiol 586(18):4347-4355.

Wässle H et al. 2009. Cone contacts, mosaics, and territories of bipolar cells in the mouse retina. J Neurosci 29(1):106-117.

Werblin FS. 2010. Six different roles for crossover inhibition in the retina: correcting the nonlinearities of synaptic transmission. Vis Neurosci 27:1-8.

Werblin FS, Dowlin gJE. 1969a. Organization of the retina of the mudpuppy Necturus maculosus: I. Synaptic structure. J Neurophysiol 32:315-338.

Werblin FS, Dowlin gJE. 1969b. Organization of the retina of the mudpuppy Necturus maculosus: II. Intracellular recording. J Neurophysiol 32:339-355.

Wu SM. 1991. Input-output relations of the feedback synapse between horizontal cells and cones in the tiger salamander retina. J Neurophysiol 65:1197-1206.